The University of Adelaide

School of Chemistry and Physics

Experimental Study of Stimulated Brillouin Scattering in Open Cells and Multimode Optical Fibres

By

Allan Chi-Lun Wong

B.Sc. (*Flinders*), B.Sc.(Hons.) (*Adelaide*)

Thesis submitted for the degree of

Master of Science

In

The Discipline of Physics

School of Chemistry and Physics

The University of Adelaide

June 2005

Statement of Originality

This work contains no material which has been accepted for the award for any other degree or diploma in any university or other tertiary institution and, to the best of my knowledge and belief, contains no material previously published or written by another person, except where due reference has been made in the text.

I give consent to this copy of my thesis, when deposited in the university library, being available for loan and photocopying.

Signed: ……

Date: ……

Supervisor: Professor Jesper Munch

Acknowledgements

I sincerely give thanks to my Lord Jesus Christ.

I gratefully thank my supervisor Professor Jesper Munch. He is a very caring supervisor that cared a lot about my progress and how much I learned from the project. He is also an easy to approach teacher who is willing to listen to me and help me immediately when I got hindered from either experimental or conceptual problems.

I would also like to thank Blair Middlemiss for his technical assistance and ideas and Trevor Waterhouse for his help in the Physics Workshop.

Thanks to Dr. Murray Hamilton and Dr. Peter Veitch for their help and guidance while Professor Munch was unavailable or away.

Special thanks to Kwang-Ho Bae for his continuous help and support since my Honours year, Damien Mudge for provision of some equipments, Alex Hemming for the help of the laser.

I would like to thank my parents for their encouragements and endless supports.

Lastly, I would like to thank Professor Munch once again for his tremendous efforts in revising and proofreading my thesis in minute detail. His tireless energy is much admired and appreciated.

Abstract

An experimental study of the stimulated Brillouin scattering (SBS) were performed by performing optical phase conjugation in open cells and multimode optical fibres using a Q-switched, pulsed Nd:YAG laser ($\lambda = 1.064\mu m$). Experiments were done with test tubes that contained two SBS liquids – Fluorinert and Acetone, and multimode optical fibres with 62.5μm core diameter. The three fundamental parameters of SBS: the threshold energy, reflectivity and phase conjugate fidelity were characterised and analysed. In addition, the temporal behaviour of Stokes beam, phase correction, optical breakdown, and pulse compression were investigated.

Table of Contents

List of Figures

List of Tables

Chapter 1

1 Introduction

1.1 Research Objectives

Stimulated Brillouin scattering (SBS) is a third order nonlinear optical phenomenon that occurs when an intense electric field is applied to different nonlinear materials. It was not observed until the advent of the laser in the 1960s, enabled by its ability to produce intense optical fields. Since its first observation in 1964 [1], numerous experimental, theoretical and numerical studies have been undertaken (see Section 1.2). Optical phase conjugation (OPC), also called wavefront reversal (WFR) in some literature, is an optical process that can utilise nonlinear optical effects to reverse precisely both the direction of propagation and the overall phase for an arbitrary beam of light [2]. OPC is most widely implemented using SBS or degenerate four-wave mixing due to their simplicity and effectiveness. Generally, the characteristics and performance of the SBS process can be investigated by performing the OPC using SBS.

In performing SBS experiments, there are a number of parameters that must be investigated, examples are: SBS materials, SBS open cells, pump source conditions, OPC by SBS and SBS applications (see Section 3.1). Among them there are three most important parameters that have been subjects of numerous studies: the SBS threshold, SBS reflectivity and phase conjugate fidelity. Most research aim to reduce the energy threshold, maximise the SBS reflectivity and fidelity using the available SBS materials, waveguides and pump wavelengths. Commercial applications of SBS in open cells are often used in OPC. The most widely used application of OPC is in high power solid-state laser systems [3]. In such laser systems, OPC makes use of a phase conjugate mirror to substitute the highly reflective mirror in the laser cavity to correct the spatial aberrations or phase

distortions of the laser beam introduced by the amplifier medium. The threshold for SBS is usually high (~100kW). But this can be reduced if certain low SBS threshold materials and waveguides such as optical fibres are used [3 – 5]. Some suggested using OPC to correct aberrations in optical pulse trains and atmospheric turbulence [6].

SBS using optical fibres have been studied extensively since its first demonstration in 1972 [7]. There are many applications of SBS in optical fibres. Examples are fibre-Brillouin lasers [8], fibre-Brillouin amplifiers [9], and long-range distributed fibre-optic sensors for remote temperature and strain sensing [10 – 14]. It can also be used in the shifting of the carrier frequency of an optical signal [15]. Applications in communications include: obtaining frequency conversion with amplification, frequency selective amplification in photonic signal transmission (SBS frequency shift is considered small compared to the incident optical frequency) and signal processing systems. In photonic systems, SBS is useful in handling optical carrier signals that are modulated with narrow band, radio frequency analogue signals [16, 17].

This study aimed to gain more insights into the SBS characteristics and to study different SBS parameters in multimode optical fibres. The ongoing and ultimate objective of the research would be to identify the feasibility and the potential problems related to the development of long-range distributed fibre-optic sensors for temperature and strain sensing. This is considered an important military application for remote sensing and industrial application for structural health monitoring. The initial plan was to start with SBS in open cells with two known SBS liquids – Fluorinert and Acetone. The purposes were to gain solid experience and competence in preforming the SBS experiments, to perform simple characterisations and compare with published results to prove whether the results from our experiments were valid and correct. Therefore, the SBS experiments performed in open cells were not planned for detail investigations, but served as preliminaries for performing experiments in optical fibres. The next planned stage was to perform SBS in silica capillary tubes with the diameters comparable to that of optical fibres. It was considered to be a transition and bridging step between SBS in open cells and in multimode optical fibres. The capillary tubes were long waveguides somewhat like the optical fibres but with a hollow core, so that the SBS liquids can be filled in by capillary action. Then the characteristics and behaviour of the SBS liquids in long waveguide could be compared directly with those observed in open cells. However, it was

later found that both SBS liquids that we studied (Fluorinert and Acetone) had refractive indices lower than that of the silica capillary tubes (n = 1.46). This caused the light entered into the capillary tube could not be confined and guided in the core, and that the SBS interaction length could not be established. Due to the problems with capillary tubes, the SBS experiments in optical fibres were performed directly after the open cells experiments were accomplished. As will be mentioned later, because of the time constraints, the SBS experiments in optical fibres were not complete, and more thorough measurements are needed in order to understand the details of the SBS behaviour and characteristics.

The objectives of this research were:

1. **To investigate the characteristics and performance of stimulated Brillouin Scattering (SBS) by performing optical phase conjugation in open cells and multimode optical fibres, using a Q-switched, pulsed Nd:YAG laser. The characteristics that were investigated include: the SBS threshold energy, SBS reflectivity, phase conjugate fidelity and Stokes pulse temporal behaviour.**

2. **To perform preliminary characterisations and comparisons between different stimulated Brillouin Scattering materials, including Fluorinert, Acetone and multimode optical fibres. In addition, to examine the efficiency of SBS threshold reduction in multimode optical fibres by increasing the interaction length, i.e. the fibre length.**

1.2 Overview

Brillouin scattering, the phenomenon of light waves being scattered by acoustic waves (i.e. propagating pressure waves) was first suggested by Brillouin in 1922 [18]. Brillouin scattering (often called spontaneous Brillouin scattering) is a weak optical scattering process, the average scattered intensity is of the order of $10^{-4} – 10^{-11}$. By 1964, sometimes after the invention of laser, the first observation of SBS was reported by Chiao *et al* [1]. They used an intense maser (analogous to laser in microwave region) beam to focus into quartz and sapphire crystals, and detected the scattered light wave due to the amplification and build-up of hypersonic waves (lattice vibrations) in such crystals. Zel'dovich *et al* [19] reported the first observation of WFR by SBS in 1972. Nosach *et al* [5] and Wang *et*

al [6] demonstrated using WFR by SBS to compensate for the phase distortions in a master oscillator/power amplifier (MOPA) laser system. OPC by SBS in optical fibres is an alternative to conventional SBS open cells. Hanisch *et al* [22] used a fibre loop scheme to reduce the SBS threshold and improve reflectivity. But the results showed that it was not very effective and efficient. They observed a maximum reflectivity of only about 50%. Heuer *et al* [21] used an internally tapered optical fibre to reduce the SBS threshold peak power to 500W and had a maximum reflectivity of 92%. Eichler *et al* [20] were able to obtain the SBS power threshold of less than 17kW, with more than 50% reflectivity and 93% fidelity for quartz fibres. They later reduced the power threshold to 300W and improved the reflectivity to over 80% [23]. Other research in OPC by SBS include: using optical feedbacks as external SBS amplifiers [24, 25], pulse compression [26 – 30], beam combination [31 – 34], transient effects [35 – 37], phase conjugate oscillators [38, 39], temporal characteristics [40 – 42] and etc. Comprehensive reviews are given in Refs. [19, 43 – 47].

After the rapid development of optical fibres and the reduction of fibre losses, SBS was first observed in optical fibres in 1972 by Ippen *et al* [7]. Like stimulated Raman scattering, SBS in optical fibres can be useful and detrimental depending on the application one is considering. An example of the detrimental effect is in the communication systems. SBS in optical fibres can occur at very low input powers, once the SBS threshold energy is reached, a backscattered Stokes wave is generated which carries most of the input energy. Hence, the signal power received is greatly depleted and weakened [48]. Since optical fibres play a vital role in modern communications, this problem needed to be addressed. On the other hand, SBS in optical fibres can be useful, as in the case of fibre-Brillouin lasers. In such lasers, the fibre is placed inside the laser cavity to reduce the threshold pump power required for oscillations [8, 48]. In the first observation of SBS in optical fibres, Ippen *et al* [7] were able to achieve SBS with input powers less than 1W, and the threshold for SBS was 40mW, a dramatic reduction in SBS energy threshold when compared to conventional SBS cells. In their paper, they soon realised the drastic effects of SBS in optical fibre transmission. Cotter [49] observed SBS in low-loss silica fibre at 1.32μm using a continuous wave (cw) laser. He found that the input power required to reach the SBS threshold was ~5mW with 65% reflectivity. Agrawal [48] showed that the SBS threshold in low-loss fibres (fibre loss α = 0.2dB/km)

can be as low as ~1mW at 1.55μm. Apart from reducing the SBS threshold and increasing the reflectivity in optical fibres, other research include: OPC using various types of optical fibres [21 – 23, 46, 50], Brillouin linewidth and frequency at low temperatures (80K – 350K) [51], dynamic behaviour [52, 53], periodic oscillations at harmonics of fundamental oscillation frequency [54], short pulses generation [55, 56], polarisation effects [57], inhomogeneous spectral broadening [58], optical amplification [59] etc. Comprehensive reviews of SBS in optical fibres are given in Refs. [46, 48, 60].

1.3 Organisation of the Thesis

This thesis is organised as follows: Chapter 1 gives an introduction of this research, including the research objectives, and a brief overview of the research in SBS and OPC. Chapter 2 gives the basic theories and properties of the SBS and the OPC in ordinary waveguides and optical fibres. Chapter 3 describes the experimental and diagnostics setups, the methods and practices of conducting the experiments. Chapters 4 and 5 discuss and analyse the results obtained from performing SBS experiments in open cells and multimode optical fibres respectively. The characterisations and comparisons between different SBS materials are also included. Chapter 6 concludes and summarises this research, and provides suggestions for future research direction.

Chapter 2

2 Theories of Stimulated Brillouin Scattering and Optical Phase Conjugation

In this Chapter, the theories and principles of stimulated Brillouin scattering (SBS) and optical phase conjugation (OPC) are given in two waveguides, namely the SBS open cells and multimode optical fibres.

2.1 Stimulated Brillouin Scattering

The study of the theory of SBS is broad and diverse, and this Section discusses only the more basic and general case of SBS process: SBS in steady state regime with unfocussed pump source in the SBS open cells and optical fibres.

2.1.1 General Descriptions

SBS is a nonlinear optical effect, that is, the response of a dielectric material to light becomes nonlinear for intense electromagnetic fields. On a fundamental level, the origin of nonlinear response is related to anharmonic motion of bound electrons under the influence of an applied electric field. As a result, the induced polarisation **P** from the electric dipoles satisfies the more general relation [48],

$$\mathbf{P} = \varepsilon_0(\chi^{(1)} \cdot \mathbf{E} + \chi^{(2)} \cdot \mathbf{EE} + \chi^{(3)} \cdot \mathbf{EEE} + ...), \qquad (2.1.0)$$

where ε_0 is the vacuum permittivity and $\chi^{(j)}$, j = 1, 2, … is the jth order susceptibility tensor j+1. Nonlinear optical effects arise from the higher order nonlinear polarisations. For example, second harmonic generation and Pockels effect are second order effects, while third harmonic generation and most nonlinear scatterings are third order effects.

Stimulated scattering, such as SBS, is initiated from the build-up and amplification of random spontaneous scattering, just like stimulated emission is initiated from spontaneous emission. A spontaneous light scattering is caused by the excitation of thermal or quantum mechanical zero-point effects, whereas a stimulated light scattering is caused by an induced intense pump source, and is much more efficient (by many orders of magnitude) than spontaneous scattering. SBS is an optical parametric interaction between the pump wave, Stokes (scattered and Doppler down-shifted frequency) wave and acoustic wave of a nonlinear material, produced by lattice vibrations (or thermal density fluctuations) of the material. It can also be classified as a third order ($\chi^{(3)}$) nonlinear three-wave (pump, Stokes and acoustic waves) mixing process. SBS is initiated from the background thermal fluctuations (i.e. spontaneous Brillouin scattering) in the material. The basic mechanism of SBS process is the generation and amplification of acoustic wave by the pump and Stokes waves via electrostriction. Electrostriction is the density variations of a material system induced by an external force, such as an intense electric field. This in turn, causes a modulation of the refractive index of the material. When a pump wave is incident into a nonlinear material, thermal fluctuations cause the pump wave to scatter randomly. But some waves are backscattered toward the pump wave. The backscattered wave is Doppler shifted. The pump and Stokes waves interfere, produce a periodically moving intensity grating, which is indeed the acoustic wave, according to the Bragg condition. As this process continues, the acoustic wave amplifies, the electrostrictive force drives more pump wave to be backscattered and suppressed all other randomly scattered components. The Stokes wave increases with positive feedback until the process reaches saturation [61].

Quantum mechanically the SBS process is equivalent to the annihilation of one pump photon and a simultaneous creation of one Stokes photon and one phonon (i.e. a quantum energy of lattice vibration). Immediately, the laws of conservations of energy and momentum apply,

$$\omega_p = \omega_s + \omega_A, \tag{2.1.1}$$

and

$$\boldsymbol{k_p} = \boldsymbol{k_s} + \boldsymbol{k_A}, \tag{2.1.2}$$

where ω is the angular frequency, $\mathbf{k} = 2\pi/\boldsymbol{\lambda}$ is the wave vector, the subscripts ***p***, ***s*** and ***A*** represent the pump, Stokes and acoustic wave respectively. The acoustic wave frequency lies in the range of 0.1 – 10GHz, which implies that the frequency is much less than the pump frequency, and that the Stokes frequency is approximately the same as the pump frequency in Eq. (2.1.1). The acoustic wave, with the assumptions that $\omega_p \approx \omega_s$ and $\boldsymbol{k_p} \approx \boldsymbol{k_s}$, satisfies the dispersion relation,

$$\omega_A = 2v_A\left|\boldsymbol{k_p}\right|\sin(\frac{\theta}{2}), \tag{2.1.3}$$

where v_A is the acoustic wave velocity and θ is the angle between pump and Stokes waves. Eq. (2.1.3) shows that the acoustic frequency or the frequency shift of the Stokes wave depends on the scattering angle. The maximum frequency shift is obtained when the Stokes wave is backscattered (i.e. θ = 180º). In this case, the Stokes (or Brillouin) frequency shift f_B is given by,

$$f_B = \frac{\omega_A}{2\pi} = \frac{2nv_A}{\lambda_p} = \frac{n\omega_p v_A}{\pi c}, \tag{2.1.4}$$

where n is the refractive index, λ_p is the pump wavelength, and c is the speed of light.

The basic equations that describe the behaviour of SBS are derived from the Maxwell's equations (for the pump and Stokes waves), and the Navier-Stokes equation (for the acoustic wave) [44, 62, 63],

$$\frac{\partial^2 \tilde{\boldsymbol{E}}_{\boldsymbol{p}}}{\partial z^2} - \frac{n^2}{c^2}\frac{\partial^2 \tilde{\boldsymbol{E}}_{\boldsymbol{p}}}{\partial t^2} = \frac{4\pi}{c^2}\frac{\partial^2 \boldsymbol{P}_{\boldsymbol{NL,p}}}{\partial t^2}, \tag{2.1.5}$$

$$\frac{\partial^2 \tilde{\boldsymbol{E}}_{\boldsymbol{s}}}{\partial z^2} - \frac{n^2}{c^2}\frac{\partial^2 \tilde{\boldsymbol{E}}_{\boldsymbol{s}}}{\partial t^2} = \frac{4\pi}{c^2}\frac{\partial^2 \boldsymbol{P}_{\boldsymbol{NL,s}}}{\partial t^2}, \tag{2.1.6}$$

and $$\frac{\partial^2 \tilde{\rho}}{\partial t^2} - \Gamma \nabla^2 \left(\frac{\partial^2 \tilde{\rho}}{\partial t^2} \right) - v_A{}^2 \nabla^2 \tilde{\rho} = \nabla \cdot \mathbf{L}, \tag{2.1.7}$$

where the subscripts ***p*** and ***s*** represent the pump and Stokes wave, $\tilde{\boldsymbol{E}}$ is the electric field, $\tilde{\boldsymbol{\rho}}$ is the density variation of the medium (i.e. the acoustic field), $\boldsymbol{P_{NL}}$ is the nonlinear polarisation, Γ is the acoustic wave damping parameter, ∇^2 is the Laplacian operator, and $\mathbf{L} = \nabla p_{st} = \nabla\left(-\frac{\gamma}{8\pi} \left\langle \left(\tilde{\mathrm{E}}_\mathrm{p} \tilde{\mathrm{E}}_\mathrm{s}^* \right)^2 \right\rangle \right)$ is the Langevin noise term that describes the thermal excitation of acoustic waves, which leads to the initiation of SBS process. The pump, Stokes and acoustic waves have the form,

$$\tilde{\mathbf{E}}_\mathbf{p}(\mathbf{r},\mathbf{t}) = \mathbf{E}_\mathbf{p}(\mathbf{r},\mathbf{t}) \exp[i(\mathbf{k}_\mathbf{p} \bullet \mathbf{r} - \omega_p \mathrm{t})], \tag{2.1.8}$$

$$\tilde{\mathbf{E}}_\mathbf{s}(\mathbf{r},\mathbf{t}) = \mathbf{E}_\mathbf{s}(\mathbf{r},\mathbf{t}) \exp[i(-\mathbf{k}_\mathbf{s} \bullet \mathbf{r} - \omega_s \mathrm{t})], \tag{2.1.9}$$

and $$\tilde{\boldsymbol{\rho}}(\mathbf{r},\mathbf{t}) = \rho_0 + \boldsymbol{\rho}(\mathbf{r},\mathbf{t}) \exp[i(\mathbf{k}_\mathbf{A} \bullet \mathbf{r} - \omega_A \mathrm{t})], \tag{2.1.10}$$

where $\boldsymbol{E_{p,s}}(\boldsymbol{r},t)$, $\boldsymbol{\rho}(\boldsymbol{r},t)$ are the pump, Stokes and acoustic wave amplitude functions, ρ_0 is the mean density of the medium. Eqs. (2.1.5) – (2.1.7) can be simplified by the following assumptions [64]:

1. Slowly varying amplitudes approximations $\left| \frac{\partial^2 \tilde{\boldsymbol{E}}}{\partial z^2} \right| << \left| \frac{\partial \tilde{\boldsymbol{E}}}{\partial z} \right|$;
2. $\omega_A < \Delta\omega_p$, the acoustic wave frequency is less than the pump bandwidth $\Delta\omega_p = 2\pi c / l_c$, where l_c is the pump coherence length;
3. $\omega_p \approx \omega_s = \omega$, the pump and Stokes frequencies are approximately the same;
4. Wavelength of the acoustic wave is short compared to the change in the length scales of the wave amplitudes $\boldsymbol{E_{p,s}}(\boldsymbol{r},t)$, $\boldsymbol{\rho}(\boldsymbol{r},t)$.

Then, the equations are reduced to [62],

$$\left(\frac{n}{c} \frac{\partial}{\partial t} - \frac{\partial}{\partial z} \right) \boldsymbol{E_p} = i g_1 \boldsymbol{\rho} \boldsymbol{E_s}, \tag{2.1.11}$$

$$\left(\frac{n}{c} \frac{\partial}{\partial t} + \frac{\partial}{\partial z} \right) \boldsymbol{E_s} = i g_1 \boldsymbol{\rho}^* \boldsymbol{E_p}, \tag{2.1.12}$$

and $$-2i\omega_A\frac{\partial \boldsymbol{\rho}}{\partial t}+(\omega_B^2-\omega_A^2-i\omega_A\Gamma_B)\boldsymbol{\rho}-2ikv_A^2\frac{\partial \boldsymbol{\rho}}{\partial t}=g_2\boldsymbol{E}_p\boldsymbol{E}_s^* \tag{2.1.13}$$

where $g_1=\frac{\omega\gamma}{2cn\rho_0}$, $g_2=\frac{k_A^2\gamma}{4\pi}$ are the coupling parameters, $\gamma=\rho_m\frac{\partial\varepsilon}{\partial\rho_m}$ is the electrostrictive constant, ρ_m is the material's mass density, ε is the dielectric constant, ω_B is the angular Brillouin frequency, $\Gamma_B=k_A^2\Gamma=1/\tau_B$ is the Brillouin linewidth and τ_B is the phonon lifetime. Eqs. (2.1.11) – (2.1.13) are the fundamental equations that describe the SBS process.

2.1.2 SBS in Ordinary Cell Geometry

In ordinary cell geometry, such as the cylindrical cell type, it is assumed the SBS process is not affected from its shape. That is, the cell does not impose any constraint or limitation to the interactions of the pump, Stokes and acoustic waves. The theory presented here only considers the SBS in steady state regime with unfocussed pump source. The steady state regime (i.e. the pump wave operates in cw mode) is given by the steady state solutions of Eqs. (2.1.11) – (2.1.13), in which all the time derivatives in the equations equal to zero. The waves are only a function of the distance z in which they travel inside the cell. Assuming the waves travel along the z-axis direction, with the pump wave to the right from $z = 0$ and the Stokes wave to the left from $z = L$, the equations become [62, 63],

$$\frac{dE_p}{dz}=\frac{ig_1g_2|E_s|^2E_p}{\omega_B^2-\omega_A^2-i\omega_A^2\Gamma_B}, \tag{2.1.14}$$

$$\frac{dE_s}{dz}=\frac{-ig_1g_2|E_p|^2E_s}{\omega_B^2-\omega_A^2+i\omega_A^2\Gamma_B}, \tag{2.1.15}$$

and $$\rho(z,t)=\frac{k_A^2\gamma}{4\pi}\frac{E_pE_s^*}{\omega_B^2-\omega_A^2-i\omega_A^2\Gamma_B}. \tag{2.1.16}$$

Note that the SBS process is automatically phase-matched. Define the intensity $I=\frac{nc}{2\pi}|\boldsymbol{E}|^2$, the equations for pump and Stokes intensities are given by,

$$\frac{dI_p}{dz} = -g_B I_p I_s, \tag{2.1.17}$$

and

$$\frac{dI_s}{dz} = -g_B I_p I_s, \tag{2.1.18}$$

where

$$g_B = g_{B,\max} \frac{1}{1+\left(\frac{\omega_B - \omega_A}{\Gamma_B / 2}\right)^2}. \tag{2.1.19}$$

g_B is the Brillouin gain coefficient, which has a Lorentzian profile, and $g_{B,\max} = \frac{\gamma^2 \omega_p^2}{2nc^3 v_A \rho_0 \Gamma}$ is the maximum gain at the Brillouin frequency.

For undepleted pump wave, dI_p / dz can be ignored and assumed the pump wave is constant. The Stokes intensity is solved from Eq. (2.1.18),

$$I_s(z) = I_{s,0} \exp(g_B I_p (L_{eff} - z)), \tag{2.1.20}$$

where $I_{s,0}$ is the initial Stokes intensity and L_{eff} is the SBS effective interaction length, defined to be the shorter of the cell length, three times the coherence length or five times the Rayleigh range of the pump beam [72]. This shows that the Stokes wave is initiated at $z = L$ and grows exponentially as it propagates through the medium.

For depleted pump wave, the pump intensity is affected (depleted) by the growth of the counter-propagating Stokes wave with the intensity comparable to the pump intensity. We can set $dI_p / dz = dI_s / dz$, and so $I_p(z) = I_s(z) + c$, where c is the integration constant that depends on the boundary conditions. Putting the depleted pump intensity into Eqs. (2.1.17) and (2.1.18), and solve the equations with the boundary condition $c = I_p(0) - I_s(0)$. The depleted pump and Stokes intensities are given by [62],

$$I_p(z) = I_s(z) + I_p(0) - I_s(0), \tag{2.1.21}$$

and

$$I_s(z) = \frac{I_s(0)[I_p(0) - I_s(0)]}{I_p(0) \exp[g_B (I_p(0) - I_s(0)) z] - I_s(0)}. \tag{2.1.22}$$

Note that the quantity $I_s(0)$ is not initially known, but can be found by letting $z = L$ in Eq. (2.1.22) and express the ratio $I_s(0)/I_p(0)$ in terms of the known quantities.

2.1.3 SBS in Optical Fibres

SBS in optical fibres only occurs in backward direction, that is, the generation of Stokes wave only. The SBS dynamics in single mode fibres can be described by two coupled intensity equations [65],

$$\left[\frac{n}{c}\left(\frac{\partial}{\partial t}\right)+\frac{\partial}{\partial z}\right]I_p=(-\alpha-g_B I_s)I_p, \tag{2.1.23}$$

$$\left[\frac{n}{c}\left(\frac{\partial}{\partial t}\right)-\frac{\partial}{\partial z}\right]I_s=(-\alpha+g_B I_s)I_p. \tag{2.1.24}$$

where $I_{p,s}$ are the pump and Stokes intensities, g_B is the Brillouin gain coefficient, α is the fibre attenuation coefficient. The steady state coupled intensity equations of SBS in optical fibres describing the pump and Stokes waves for cw operation are then given by,

$$\frac{dI_p}{dz}=-g_B I_p I_s-\alpha I_p, \tag{2.1.25}$$

$$\frac{dI_s}{dz}=-g_B I_p I_s+\alpha I_s, \tag{2.1.26}$$

Here, it is assumed that the Brillouin shift is small such that $\omega_p \approx \omega_s$ and that the fibre loss for the pump and Stokes waves are nearly the same, $\alpha_p \approx \alpha_s \approx \alpha$. Eqs. (2.1.23) and (2.1.24) are derived from the Maxwell and the wave equations describing the electric fields of pump and Stokes waves inside the fibre, and can be solved analytically [48, 65]. The pump and Stokes intensities, with pump depletion and no fibre loss (i.e. $\alpha = 0$), are given by [65, 66],

$$I_p(z)=\left[I_p(0)-I_s(0)\right]\frac{I_p(0)\exp\{g_B[I_p(0)-I_s(0)]z\}}{I_p(0)\exp\{g_B[I_p(0)-I_s(0)]z\}-I_s(0)}, \tag{2.1.27}$$

and $$I_p(z) = \left[I_p(0) - I_s(0)\right] \frac{I_s(0)}{I_p(0)\exp\{g_B[I_p(0) - I_s(0)]z\} - I_s(0)}, \qquad (2.1.28)$$

where $z = 0$ is taken to be at the entrance face of the fibre. Note that these two equations are the solutions to the coupled intensity equations specifically for SBS in single-mode optical fibres. Eqs. (2.1.21) and (2.1.22) are the general solutions for SBS in open cells. The SBS coupled intensity equations for these two conditions are slightly different. The corresponding SBS threshold power is then given by [48],

$$g_{B,peak} P_{th} L_{eff} / A_{eff} \approx 21, \qquad (2.1.29)$$

where A_{eff} is the effective fibre core area and L_{eff} is the effective interaction length due to attenuation. In principle, without any fibre loss the effective interaction length is the entire length of the fibre. $g_{B,peak}$ is the maximum Brillouin gain coefficient at ν_B under quasi-cw pump condition (pulse width >> phonon lifetime) is given by $g_{B,\max}(f_B) = \frac{2\pi n^7 p_{12}^2}{c\lambda_p^2 \rho_0 \nu_A \Gamma_B}$ [66], where n is the refractive index, p_{12} is the longitudinal elasto-optic coefficient, λ_p is the pump wavelength, ρ_0 is the material density, ν_A is the acoustic speed, $\Gamma_B = 1/\pi\tau_B$ is the Brillouin gain linewidth and τ_B is the phonon lifetime. For silica fibres, ν_A = 5.96 × 10^3m/s, n = 1.46, λ_p = 1064nm, and so $f_B \approx$ 16.4GHz. As a numerical example, for a 62.5μm core silica fibre of effective interaction length 5m, $g_{B,\max}$ = 5 × 10^{-11}m/W, and P_{th} ≈ 257.7W. Comparing with the conventional SBS cell, the power threshold in optical fibres is at least 3 orders of magnitude smaller. This is a dramatic reduction of pump power required to initiate SBS process in fibres, and this is the reason that fibre-Brillouin lasers are being developed for efficient, high brightness, and good beam quality output.

If pump depletion is included, which is more realistic for the actual experimental conditions, the solutions to Eqs. (2.1.23) and (2.1.24) are given by [48],

$$I_s(z) = \frac{b_0(1-b_0)}{G(z) - b_0} I_p(0), \qquad (2.1.30)$$

$$I_s(z) = \frac{b_0(1-b_0)}{G(z) - b_0} I_p(0), \qquad (2.1.31)$$

where $G(z) = \exp[(1-b_0)(g_0 z)]$ is the overall gain, $g_0 = g_B I_p(0)$ is the SBS small signal gain, $b_0 = I_s(0)/I_p(0)$ is the pump-to-Stokes power conversion efficiency. Eqs. (2.1.30) and (2.1.31) describe the variations of the pump and Stokes intensities along the length of fibre. Due to pump depletion, the net gain is considerably smaller than without depletion. For example, if $b = I_s(L)/I_p(L) = 0.01$, then about 70% of pump power is transferred to Stokes power. The power transfer occurs most efficiently within the first 20% of the fibre length. The rest of the fibre length, though still have some contribution, does not contribute to the SBS process as significantly as the first 20% of the fibre length. This was observed experimentally by Eichler *et al* [20] (see also Section 5.3.1).

2.2 Optical Phase Conjugation

2.2.1 General Descriptions

OPC (also referred to as wavefront reversal or the generation of time-reversed wavefront), is an optical process that utilises nonlinear optical effects to reverse precisely both the direction of propagation and the overall phase factor for each plane wave in an arbitrary beam of light [43]. It can be used to remove the effects of aberrations from certain types of optical systems. OPC can be performed by various nonlinear optical methods such as holography, four-wave mixing (degenerate or non-degenerate) and stimulated scattering (Brillouin, Raman, Rayleigh-wing or Kerr) [68].

A phase conjugate mirror (PCM) is a nonlinear medium used to produce OPC and the reflected wave from the PCM that possesses all the physical properties of the pump wave is called phase conjugate wave (PCW). There are backward (degenerate and nondegenerate) and forward PCWs. Without going into details of each type of PCW, consider the general case of a plane monochromatic pump wave incidents on a PCM,

$$\mathrm{E}_p(\mathrm{r},t) = \mathrm{E}_p(\mathrm{r})\exp(-i\omega t) = \mathrm{A}(\mathrm{r})\exp(i\mathrm{k}_p \bullet \mathrm{r})\exp(-i\omega t)\,, \qquad (2.2.1)$$

where A(r) is the real amplitude function, $\mathrm{k_p} = 2\pi / \lambda_\mathrm{p}$ is the wave vector, ω is the angular frequency. The reflected wave from the PCM is the complex conjugate of Eq. (2.2.1),

$$\mathrm{E_R}(\mathrm{r},t) = a\mathrm{E_P^*}(\mathrm{r})\exp(-i\omega t) = a\mathrm{A}(\mathrm{r})^*\exp(-i\mathrm{k_p}\bullet\mathrm{r})\exp(-i\omega t), \tag{2.2.2}$$

where $0 \le a \le 1$ is the amplitude reflection constant of the PCM. Now, consider taking the complex conjugate of the time-reversed pump wave (i.e. transforming $t \to -t$),

$$\begin{aligned}(\mathrm{E_p}(\mathrm{r},-t))^* &= (\mathrm{E_p}(\mathrm{r})\exp(i\omega t))^* \\ &= \mathrm{A}(\mathrm{r})^*\exp(-i\mathrm{k_p}\bullet\mathrm{r})\exp(-i\omega t), \\ &= \frac{1}{a}\mathrm{E_R}(\mathrm{r},t)\end{aligned} \tag{2.2.3}$$

or,

$$\mathrm{E_R}(\mathrm{r},t) = a(\mathrm{E_p}(\mathrm{r},-t))^*. \tag{2.2.4}$$

Note that $\mathrm{A}(\mathrm{r})^* = \mathrm{A}(\mathrm{r})$ because A(r) is real. Eq. (2.2.4) suggests that the reflected wave from the PCM is the time-reversed complex conjugate of the pump wave. Physically it means that the reflected wave from the PCM is indeed a PCW, which is an exact replicate of the pump wave. The time-reversed transformation illustrates that the PCW can be thought of as the pump wave travels in time-reversed backward direction.

The correction of phase aberration can be exemplified by assuming the pump wave passes through an aberrator [47],

$$\mathrm{E_p'}(\mathrm{r},t) = \mathrm{A}(\mathrm{r})\exp[i(\mathrm{k_p}\bullet\mathrm{r} + \phi(\mathrm{r}))]\exp(-i\omega t), \tag{2.2.5}$$

where $\phi(\boldsymbol{r})$ is the phase function describing the aberration influence on the wavefront from the aberrator. If the pump wave is reflected by an ordinary plane mirror, after double pass through the aberrator the pump wave is given by,

$$\mathrm{E_p'''}(\mathrm{r},t) = a_m\mathrm{A}(\mathrm{r})^*\exp[i(-\mathrm{k_p}\bullet\mathrm{r} + 2\phi(\mathrm{r}))]\exp(-i\omega t), \tag{2.2.6}$$

where a_m is the is the amplitude reflection constant of the mirror. The aberration is doubled because the phase function is doubled. If the ordinary mirror is replaced by a PCM, after two passes the pump wave is,

$$\begin{aligned} \mathrm{E}_{\mathrm{p}}'''(\mathrm{r},t) &= a\mathrm{A}(\mathrm{r})^{*}\exp[i(-\mathrm{k}_{\mathrm{p}}\bullet\mathrm{r}-\phi(\mathrm{r}))]\exp(i\phi(\mathrm{r}))\exp(-i\omega t) \\ &= a\mathrm{A}(\mathrm{r})^{*}\exp(-i\mathrm{k}_{\mathrm{p}}\bullet\mathrm{r})\exp(-i\omega t) \\ &= a\mathrm{E}_{\mathrm{p}} \end{aligned} \quad , \qquad (2.2.7)$$

where $\exp[i(-\mathrm{k}_{\mathrm{p}}\bullet\mathrm{r}-\phi(\mathrm{r}))]$ describes the reflected wave from the PCM and $\exp(i\phi(\mathrm{r}))$ describes the phase of the pump wave after second pass to the aberrator. The phase aberration due to the aberrator is cancelled out (removed) and the final reflected wave indeed has the same properties as the pump wave, i.e. the PCW.

2.2.2 OPC by SBS

OPC can be achieved by a number of nonlinear techniques such as stimulated scattering and wave mixing, and this Section describes specifically the OPC process induced by using the SBS technique. OPC by SBS can be described as the selectively enhanced amplification of the components of the backscattered Stokes wave, the components that acquired maximum amplification are indeed the exact phase conjugate of the pump wave [67]. SBS is initiated by spontaneously generated Stokes wave and initially it contains all the possible spatial components. These spatial components have all the phase information of the pump wave, and are Fourier transformed into amplitude information (spatial intensity distribution). This Fourier transformation can be achieved by using a positive lens. At the focal point of the lens, the spatial components are transformed into their dual domain, such that the Fourier spectra provide the necessary information to reproduce the incident pump wave. The Fourier components of the pump wave that gained the maximum amplification are those whose intensity distributions correlate the best with the non-uniform gain distribution. These amplified components have the phases that match with the phases of the pump wave components, which are indeed the phase conjugate components of the pump wave. Generally OPC by SBS is produced under a focused pumping condition, which can be accomplished by placing a positive lens in front of the

SBS cell. The focused pump wave is required by the OPC process, which is needed in order to produce the Fourier transformed components and intense light source.

From another perspective of looking at OPC by SBS, consider the intensity equation for the Stokes wave given by Eq. (2.1.18) with $I_p = \left|\boldsymbol{E}_{\boldsymbol{p}}(\boldsymbol{r})\right|^2$ and $I_s = \left|\boldsymbol{E}_{\boldsymbol{s}}(\boldsymbol{r})\right|^2$. We change Eq. (2.1.18) into a power equation by taking $P_p = \int I_p dA$ and $P_s = \int I_s dA$, it becomes [62],

$$\frac{dP_s}{dz} = -g_B \frac{P_p P_s}{A} \frac{\langle I_p I_s \rangle}{\langle I_p \rangle \langle I_s \rangle}, \tag{2.2.8}$$

where $A = \int dA$ and $\langle I_{p,s} \rangle = \int \frac{I_{p,s}}{A} dA$ is the normalized cross correlation function of the pump and Stokes intensities. From Eq. (2.2.8) we see that the power gain experienced by the Stokes wave depends not only on the total power of the pump wave, but also on the degree of correlation between the pump and Stokes wave intensity distributions. The correlation function is largest if the Stokes wave correlates completely with the pump wave (i.e. perfect OPC), which gives the maximum amplification and suppresses all other partially correlated and uncorrelated Stokes wave components. This is considered an ideal case for OPC, because it is very difficult to obtain perfect OPC in actual experiments due to experimental uncertainties, fluctuations, noise and the properties of the SBS medium.

It is interesting to note that there is a conceptual model of OPC by SBS proposed recently based on the idea of holography by Gabor [68]. In this model, the aberrated pump wave after passing through the aberrator can be expressed as a superposition of an undisturbed part and a disturbed part,

$$\begin{aligned} \tilde{E} &= E_1 + E_2 \\ &= A_1 \exp(i\phi_1) + A_2 \exp(i\phi_2) \\ &= \exp(i\phi_1)[A_1 + A_2 \exp(i(\phi_2 - \phi_1))] \end{aligned}, \tag{2.2.9}$$

where subscripts 1 and 2 represent the undisturbed and disturbed parts of the transmitted wave respectively, A is the amplitude function and ϕ is the phase function. The two waves

E_1 and E_2 interfere with each other in the SBS medium and create an induced volume holographic grating due the electrostriction. Only the undisturbed pump wave E_1 is strong enough to fulfil the SBS threshold requirement and generate an initial backscattered wave E_3 that exhibits a regular wavefront as the wave E_1. As E_3 passes through the grating region, a diffracted wave E_4, which is the phase conjugate replicate of the disturbed pump wave E_2, is created. Both E_3 and E_4 experience amplification together because they have the same scattering frequency. In the case of SBS, $\omega_{pump} \approx \omega_{Stokes}$, it is a nearly degenerate quasi-collinear four-wave mixing process.

The quality of OPC may be described in term of phase conjugate fidelity, defined as [61],

$$F^2 = \frac{\left|\int E_s(\mathrm{r}) E_p(\mathrm{r}) dxdy\right|^2}{\int \left|E_s(\mathrm{r})\right|^2 dxdy \cdot \int \left|E_p(\mathrm{r})\right|^2 dxdy}, \tag{2.2.10}$$

where $0 \le F \le 1$. For perfect OPC, F = 1 and F = 0 means random scattering. This is a cross-correlation function that measures the degree of "likeness" between the pump and backscattered Stokes waves. The correlation function F could be measured by a technique called "power (or energy)-in-the-bucket" (see Section 3.3.2). We explain this conceptually without going into the details of mathematics. Quantitatively, F can be expressed as,

$$F^2 \approx \frac{\left(I_{sp} A_{sp}\right)^2}{I_s A_s \cdot I_p A_p} = \frac{P_{sp}^2}{P_s \cdot P_p}, \tag{2.2.10b}$$

where I, A, P, is the intensity, cross-section area, and power of the light beams respectively. Since for perfect OPC the pump and Stokes are exactly the same, so the bottom part of the equation becomes $P_s = P_p = P$. We can obtain it by measuring the power of the reflected (Stokes) beam. Alternatively we can measure the power of the pump beam if we can achieve 100% SBS, that is, the entire pump beam is converted into Stokes beam and no energy is being lost. The coupled power P_{sp} can be obtained by measuring its Fourier transformed counterpart, and this is effectively the same as measuring the far-field power of the return (Stokes) beam, and Eq. (2.2.10b) becomes,

$$F = \frac{P_{sp}}{P} = \frac{P_{Stokes,\,far-field}}{P_{Stokes}}. \qquad (2.2.10c)$$

Therefore, the phase conjugate fidelity can be obtained conveniently by measuring the power (or energy) of the return beam.

2.2.3 OPC by SBS in Optical Fibres

This Section specifically describes OPC in optical fibres, which is similar but somewhat different from that in the open cells, because of different boundary conditions, and that the light is guided inside the optical fibres. It is known that OPC can only be achieved in multimode fibres because they allow non-uniform and aberrated pump beam as needed. However, SBS can still be achieved in single-mode fibres. The following treatment is based on Ref. [46], no formal derivations are given and only the more useful results are quoted. Assuming no pump depletion and the phonon lifetime is much shorter than the variations in the intensities of other waves, the electric field equation for the Stokes wave $\boldsymbol{E_s}$ is given by [46],

$$(-\nabla^2 + \frac{\varepsilon}{c^2}\frac{\partial^2}{\partial t^2})\boldsymbol{E}_s = -\frac{1}{c^2\varepsilon_0}\frac{\partial^2}{\partial t^2}\boldsymbol{P}_{NL}, \qquad (2.2.11)$$

where ε is the dielectric permittivity of the material (ε_0 in free space) and c is the speed of light. $\boldsymbol{P}_{NL} = i\varepsilon_0\chi^{(3)}\boldsymbol{E}_p\boldsymbol{E}_p\boldsymbol{E}_s$ is the nonlinear polarization where $\chi^{(3)}$ is the third order nonlinear susceptibility and $\boldsymbol{E_p}$ is the pump wave electric field. Further assuming that the pump and Stokes waves are plane waves, the wave amplitudes only change along the propagation direction, and using the slowly varying amplitudes approximation (i.e. $\left|\frac{d^2\hat{E}_s(z)}{dz^2}\right| << \left|k_s\frac{d\hat{E}_s}{dz}\right|$), Eq. (2.2.11) can be reduced to,

$$\frac{d\hat{E}_s(z)}{dz} = \frac{k_s}{2\varepsilon}\chi^{(3)}\left|\hat{E}_p\right|^2\hat{E}_s, \qquad (2.2.12)$$

and the solutions to this Stokes field equation are,

$$\hat{E}_s(z) = \hat{E}_s(0)\exp\left[(\frac{k_s}{2\varepsilon}\chi^{(3)}\left|\hat{E}_p\right|^2 z)\right], \tag{2.2.13}$$

and

$$I_s(z) = I_s(0)\exp(g_B I_p z) \tag{2.2.14}$$

Eqs. (2.2.13) and (2.2.14) are the electric field and intensity of the Stokes wave respectively. I_p is the intensity of the pump wave and g_B is the Brillouin gain coefficient.

From linear algebra, a function can be decomposed as a linear combination of the sum of a set of orthogonal (or orthonormal) basis, by using methods such as the Gram-Schmidt orthogonalisation. Similarly, the available paths that the light can travel inside the fibre are described by the solutions of the approximated wave equation Eq. (2.2.12). The solutions are indeed the electric fields of the light wave, with the modes (bound and unbound) being the orthogonal basis. Thus, the pump and Stokes waves can be decomposed as the sum of all available modes [46, 89],

$$E_p = \sum_l \hat{E}_{p,l}(z)\, f_l(x,y)\exp(i\beta_l z), \tag{2.2.15}$$

and

$$E_s = \sum_m \hat{E}_{s,m}(z)\, f_m(x,y)\exp(-i\beta_m z) \tag{2.2.16}$$

where the functions $f_{l,m}(x,y)$ specify the dependence of the field of a given mode on the transverse coordinates and $\beta_{l,m}$ is the propagation constant of the mode. The normalisation condition is $\int f_m(x,y)\, f_l^*(x,y)dxdy = \delta_{lm}$, where the integration is performed over the cross-section area of the fibre. Substituting Eqs. (2.2.15) and (2.2.16) into Eq. (2.2.12) and applying previous assumptions and approximations, the expression for the amplitudes of the modes of the Stokes wave is,

$$\sum_m \left[\beta_m f_m(x,y)\exp(-i\beta_m z)\frac{d\hat{E}_{s,m}(z)}{dz} - \frac{\omega^2}{2c^2}\chi^{(3)}\hat{E}_{s,m}(z)\,|E_p|^2\, f_m(x,y)\exp(-i\beta_m z)\right] = 0 \tag{2.2.17}$$

Multiplying the equation by f_l^*, integrating over the area and include normalisation condition, a set of fundamental differential equations that describes the variation of the amplitudes of the modes of the Stokes wave is,

$$\frac{d\hat{E}_{s,l}(z)}{dz} = \frac{\omega^2}{2\beta_l c^2}\chi^{(3)}\sum_m \hat{E}_{s,m}(z)\exp[-i(\beta_m - \beta_l z)]\iint |E_p|^2 f_m f_l^* dxdy\,, \qquad (2.2.18)$$

l = 0, 1, 2, …, N the number of available modes in the fibre. Consider the case for only one Stokes mode $E_{s,1}$ in the fibre and all other modes have zero amplitudes, Eq. (2.2.18) becomes,

$$\frac{d\hat{E}_{s,1}(z)}{dz} = \frac{\omega^2}{2\beta_1 c^2}\chi^{(3)}\hat{E}_{s,1}(z)\iint |E_p|^2 |f_1|^2 dxdy\,. \qquad (2.2.19)$$

The mode overlap integral in Eq. (2.2.19) shows that even for single-mode pumping there appears a mode overlap inside the fibre, because the highest gain is experienced by the Stokes mode that coincides with the pump. The mode overlap integral essentially describes how well can the Stokes wave traverses with the same paths as the pump wave inside the fibre. In other words, this integral determines the "degree of likeness" that the Stokes modes match with the pump modes. Eq. (2.2.19) only describes one mode, which is the case for single-mode fibre. From the equation, it shows that it is possible to have OPC in single-mode fibres. But the degree of OPC is not significant because it does not allow non-uniform intensity distribution to be conveyed, except the intensity distribution of the fundamental mode (e.g. Gaussian distribution). To show that OPC can be achieved in multimode fibres, we introduce one more Stokes mode $E_{s,2}$ the equation becomes,

$$\begin{aligned}\frac{d\hat{E}_{s,1}(z)}{dz} = \frac{\omega^2}{2\beta_1 c^2}\chi^{(3)}\Big[&\hat{E}_{s,1}(z)\iint |E_p|^2 |f_1|^2 dxdy \\ &+ \hat{E}_{s,2}(z)\exp[i(\beta_1 - \beta_2)z]\iint |E_p|^2 f_1 f_2^* dxdy\Big]\end{aligned}\,, \qquad (2.2.20)$$

and similar expression for $E_{s,2}$. We then have two coupled equations (one for $E_{s,1}$ and one for $E_{s,2}$) for the Stokes modes amplitudes. But the coupling term between different modes

(second term in Eq. (2.2.20)) can be dropped, as it does not contribute significantly to the overall Stokes modes amplitudes. This is valid provided that most of the pump wave is essentially converted into Stokes wave. Thus, we have two independent equations for the Stokes modes amplitudes. With the exception that when the pump wave consists of the same modes as the Stokes wave, then the pump wave amplitude in Eq. (2.2.20) can be expressed as,

$$\begin{aligned}\left|E_p\right|^2 \sim \left|E_{p,1}\right|^2 + \left|E_{p,2}\right|^2 + \hat{E}_{p,1}\hat{E}_{p,2}^{*} f_1 f_2^{*} \exp(i(\beta_1 - \beta_2)z) \\ + \hat{E}_{p,2}\hat{E}_{p,1}^{*} f_2 f_1^{*} \exp(i(\beta_2 - \beta_1)z)\end{aligned}. \qquad (2.2.21)$$

In the case of matched phase relationship between modes, the Stokes wave consists of the same modes as the pump wave, which is indeed the phase-conjugated wave. This mechanism ensures the preferential amplification and the highest gain of the phase-conjugated Stokes wave over all other waves of different phase relationships. It should be noted that, similar to the case for open cells, the gain of the phase-conjugated Stokes wave is at least twice (i.e. $\propto e^{20}$) that of any other possible Stokes wave (i.e. $\propto e^{10}$), making the intensity of the non-phase-conjugated Stokes wave appreciably lower [45]. The Stokes wave intensity for steady state SBS in open cells are given in Eqs. (2.1.20) and (2.1.29), with the condition that the constant is in the range between 20 – 30 (the exact value depends on different SBS cases and on different researchers). This means in order to produce phase-conjugated Stokes wave the constant has to be at least 20. When the difference between the modal overlap integrals, and the frequencies of pump and Stoke waves are taken into account, the solution of the Stokes wave having the highest gain is not a perfect phase-conjugate replica of the pump wave.

Chapter 3

3 Experimental Setup

This Chapter describes the experimental setup for the SBS experiments and diagnostics for the SBS characteristics: SBS threshold energy, SBS reflectivity, fidelity, spatial and temporal behaviour of the Stokes pulse. The methods and practices of taking measurements are included. The experimental and diagnostic setups described are the same for both open cells and optical fibres unless otherwise stated.

3.1 Experimental Parameters for Measurements

In conducting experimental research, SBS process can be characterised by the following experimental parameters: SBS threshold energy (or power), SBS reflectivity, phase conjugate fidelity, Brillouin gain, polarisation, far-field beam patterns (spatial intensity distribution), temporal distribution, spatial frequencies of aberrations, Brillouin shift (frequency difference between pump wave and Stokes wave), Brillouin and pump linewidth (coherence length), and SBS transmission characteristics.

This research concentrated on the investigation of the threshold energy, SBS reflectivity and phase conjugate fidelity. They are the three most important and fundamental parameters which describe the performance of SBS process. The threshold energy is the minimum energy required to initiate the SBS process, defined to be the pump energy at which the SBS reflectivity is 2% [61]. It is often desirable to lower the threshold energy, so that SBS can be performed in more applications that only have low-energy pump

sources. Reflectivity is the fraction of how much the pump wave is generated into Stokes wave and scattered backward by SBS process. High reflectivity represents efficient SBS process because most of the pump wave is converted into Stokes wave. Fidelity is a measure of the fraction of backscattered wave that can resemble and retrace the original pump wave after passing twice through an aberrator [69]. Unit fidelity represents complete OPC and that the aberrated beam can be effectively restored to its original state.

3.2 Main setup

In this Section the main experimental setup, each individual optical component and their purposes are described in detail. In addition, some performance tests on the pump laser are also included in order to obtain optimal operating conditions. The schematic diagram of the main setup is shown in Fig. 3.1.

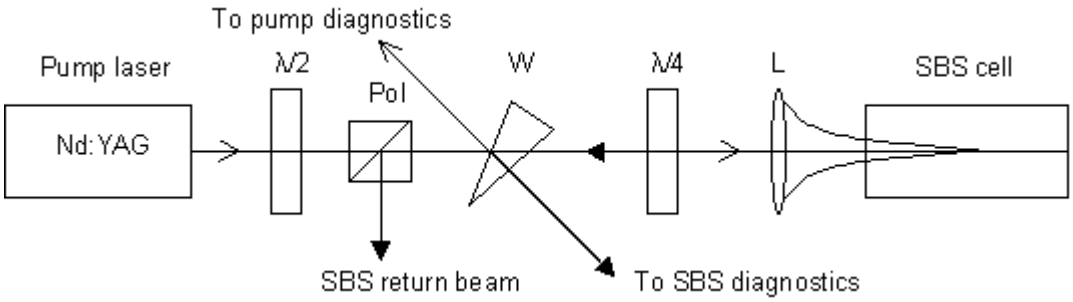

FIGURE 3.1 SCHEMATIC DIAGRAM OF THE MAIN EXPERIMENTAL SETUP. λ/2 = HALF WAVE PLATE, POL = BREWSTER POLARISER, W = WEDGE, λ/4 = QUARTER WAVE PLATE, L = 12CM POSITIVE LENS.

3.2.1 Pump Laser and its Performance Tests

All SBS experiments were performed using a Q-switched, pulsed Nd:YAG laser (Spectra-Physics, Quanta-Ray GCR-16) as the pump source. It operated at 1064nm wavelength, with a pulse width of around 25ns, and the pulse repetition frequency (PRF) between 1 – 3Hz. It was observed that the pulse width decreases monotonically with increasing pump energy (Fig. 3.2). The pulse width stayed at about 20ns once the pump energy was above 95mJ, which was the shortest pulse width achievable for this laser.

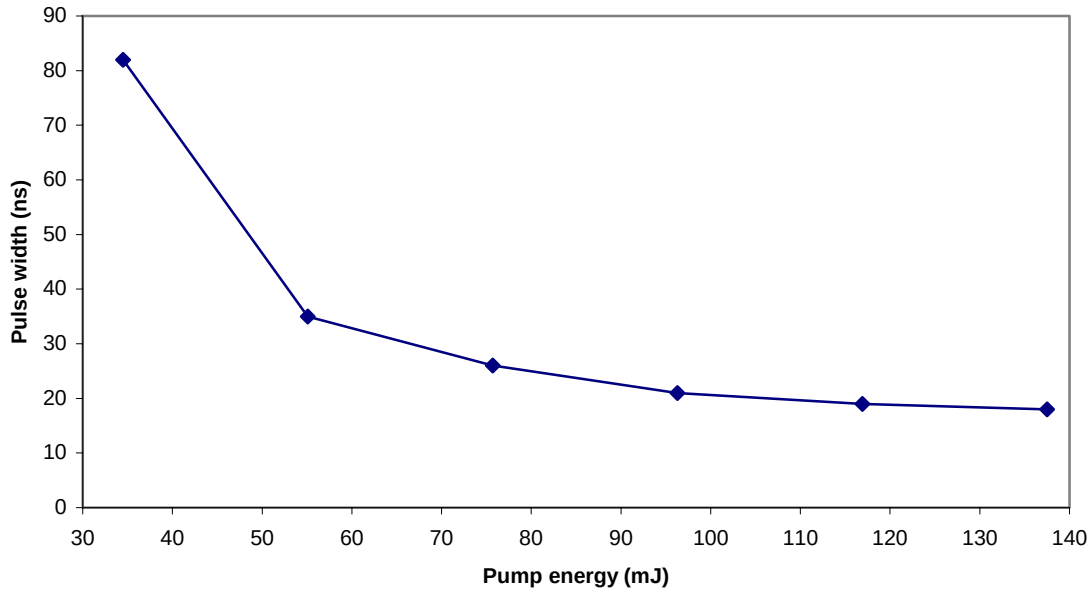

FIGURE 3.2 PULSE WIDTH OF PUMP VS ENERGY.

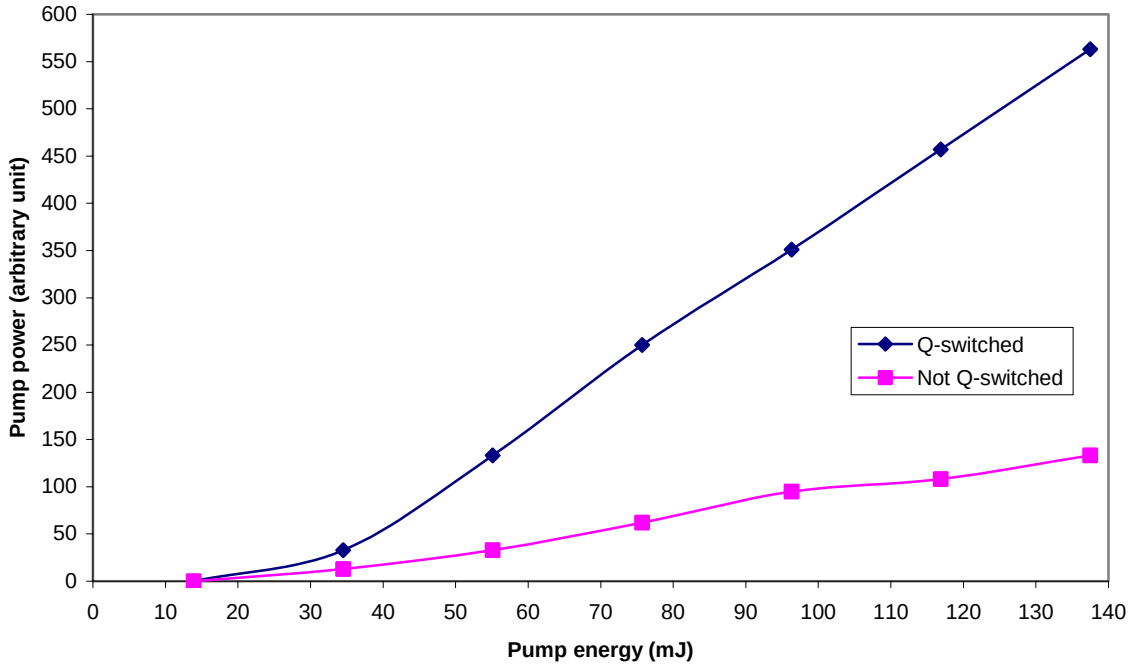

FIGURE 3.3 COMPARISONS OF PUMP POWERS (UNCALIBRATED) VS. PUMP ENERGIES BETWEEN Q-SWITCHED AND NON-Q-SWITCHED OPERATIONS.

Q-switching operation was necessary in order to increase the pump power (Fig. 3.3), and hence to acquire the desired pulse width (Fig. 3.2). Fig. 3.3 shows that the Q-switched output was able to increase the overall pump power, or equivalently reduce the pump pulse

width (i.e. pulse duration), by more than an order of magnitude compared to non-Q-switched output. The vertical axis shows the uncalibrated power measured using a power meter. It should be noted that increasing the laser power was referring only to doing experiments in SBS open cells. In the case of SBS in optical fibres, the laser needed to operate at very low energy levels (~10μJ). Therefore, in order to maintain a short pulse width, neutral density (ND) filters were used to attenuate the pump energy down to the required energy levels. Fig. 3.4 shows the pump laser pulse profiles in various operating conditions under the same input energy to the laser.

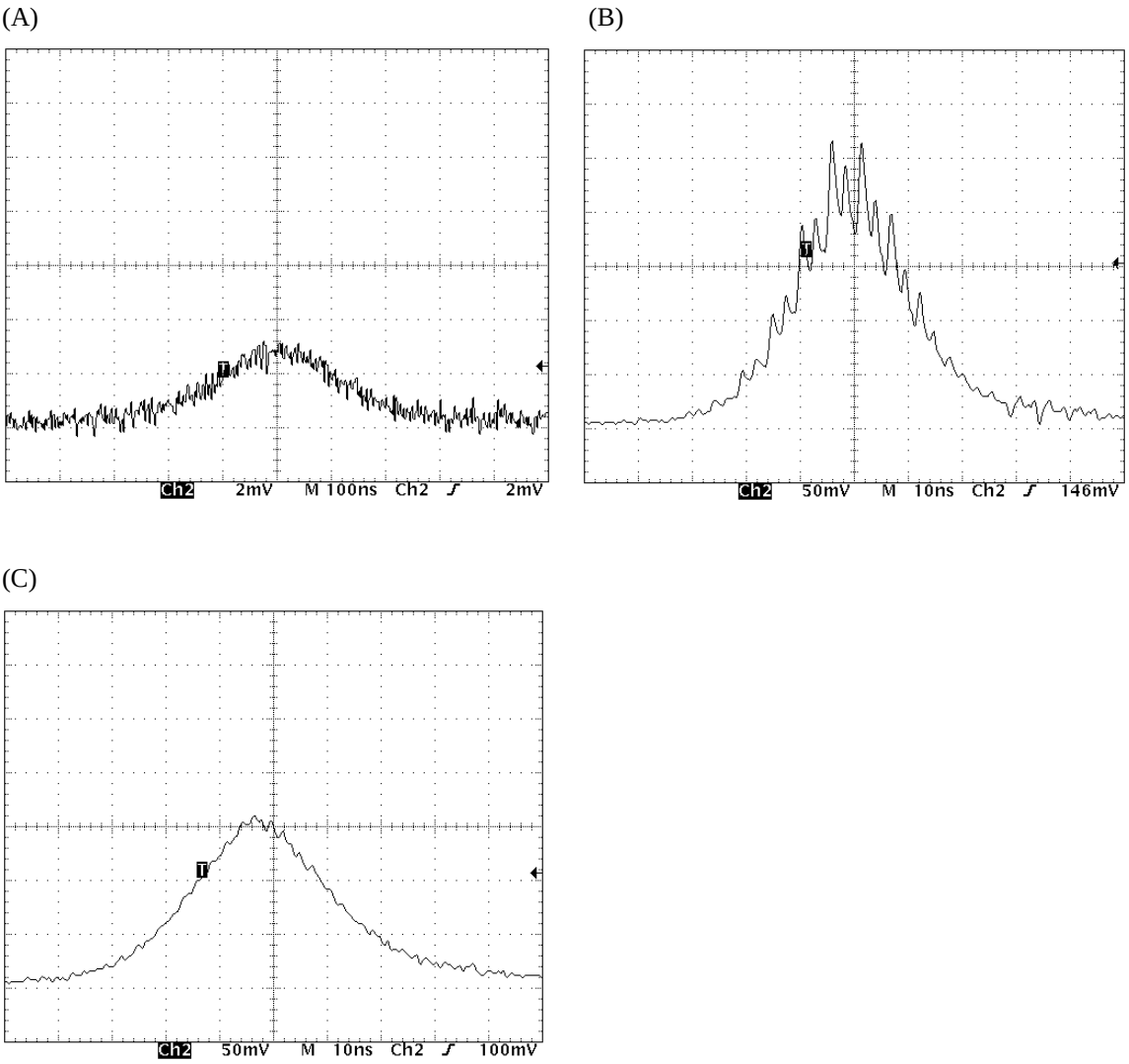

FIGURE 3.4 PUMP PULSE PROFILES IN VARIOUS OPERATING CONDITIONS UNDER THE SAME INPUT ENERGY TO THE LASER: (A) NON-Q-SWITCHED, (B) Q-SWITCHED BUT NOT INJECTION SEEDED, (C) Q-SWITCHED AND INJECTION SEEDED. NOTE (A) WAS IN DIFFERENT TIME (HORIZONTAL) AND AMPLITUDE (VERTICAL) SCALES.

Fig. 3.4 (A) shows a non-Q-switched pump pulse. As can be seen, the pump pulse was very noisy and had low output power. When the laser was running in Q-switched and free-running (no injection seeding) mode, the pump pulse was in multi-longitudinal mode and had temporal fluctuations (Fig. 3.4 (B)). According to manufacturer's specifications, when the laser operates such operating mode, the pulse has a linewidth of $1cm^{-1}$ (30GHz), corresponded to a coherence length of 10mm. On the other hand, when the laser operates in Q-switched mode and in conjunction with an injection seeder (Spectra-Physics, Model 6300), the output pluse has a linewidth of $0.003cm^{-1}$ (90MHz), corresponded to a coherence length of about 3.3m. The injection seeder was a Nd:YAG laser capable of providing 0.5W narrow bandwidth, cw power output. Single longitudinal mode operation and faster Q-switch pulse build-up were enabled by injection seeding process (Fig. 3.4 (C)). Therefore, Q-switched and injection seeded pump source was used in all experiments. The output laser beam was horizontally polarised.

3.2.2 Other Optical Components

Two 1064nm coated (for maximum reflection in the infrared wavelength region) beam steering mirrors were used to manoeuvre the pump beam and bring it down from the height of the laser system output to a comfortable height (10 cm) above the optical table for convenience. There was a polarisation rotation of the laser beam introduced by the two out of plane mirrors. It was found that the laser beam was vertically polarised after the two steering mirrors.

A combination of a Brewster polariser and a half wave ($\lambda/2$) plate were used as a variable attenuator, to adjust the amount of pump energy entering the SBS cell. It was found that this method of changing the energy level was much more stable and reliable than by adjusting the energy output directly from the laser system. But there was a drawback, the available pump energy range was limited by the combination of the polarization rotation from the $\lambda/2$–plate and the polariser. The pump energy range was measured to be about 45mJ. It was observed that there was an optical feedback to the laser due to Fresnel reflection from the front surface of the $\lambda/2$–plate ($R_{Fresnel} = \sqrt{n-1/n+1} \approx 4.1\%$ for $n = 1.506$ at 1064nm), because it was not AR-coated at 1064nm. Thus it was tilted slightly to avoid reflected light going back to the laser cavity.

The Brewster polariser was set at Brewster angle (~57°), such that the transmitted light was greater than 99% p-polarised (horizontally polarised) and reflected light was greater than 95% s-polarised (vertically polarised). When the $\lambda/2$–plate was rotated to different angles, the light changed into different polarisation states by retardation of one of the wave components of the pump beam, while allowing only the p-wave component to be transmitted through the polariser. Hence, the transmitted light was horizontally polarised, and the amount of pump energy emerged from the polariser could be controlled by varying the polarisation of the incoming light.

A wedge was used to divert and reduce the energy of the laser beams to be analysed. It was measured that the wedge allowed 97.2% transmission and 2.8% reflection of the laser beam. The SBS diagnostics was set upon the reflected positions from both sides of the wedge to analyse the pump and Stokes beams. The SBS diagnostics setup is discussed in the Section 3.3.

A quarter wave ($\lambda/4$) plate was placed after the wedge to isolate the Stokes beam from back-propagating into the laser cavity. It changes a linearly polarised beam into a circularly polarised beam by retarding the phase of one of the wave components by $\pi/2$. Hence, when horizontally polarised pump beam passed through the $\lambda/4$–plate, it changed into right circularly polarised beam. The Stokes beam from the SBS cell was then left circularly polarised, because SBS does not phase-conjugate polarisation and behaves like an ordinary mirror. When the Stokes beam passed back through the $\lambda/4$–plate, it changed into vertically polarised beam. This Stokes beam was then coupled out by the Brewster polariser. The $\lambda/4$–plate was set at a particular position to maximise the polarisation (maximum polarisation extinction ratio) such that the Stokes beam was polarised vertically and to minimise optical feedback into the laser cavity. Since the $\lambda/4$–plate was not AR-coated for 1064nm, it was slightly tilted to avoid Fresnel reflection.

An aberrator made of a microscope cover slip heated up and deformed by a welding torch was placed before the SBS cell focussing lens. It was used to aberrate (or distort) the wavefront (or phase-front) of the pump beam, such that beam restoration by OPC could be realised by observing the degree of phase-conjugation of the Stokes beam. In conducting

experiments, both unaberrated pump beam (without aberrator inserted) and aberrated pump beam (with aberrator inserted) were used, in order to compare the effects and differences of OPC by the two different pump conditions. Upon diagnosing and comparing the aberrated beam with its original pump beam, it was measured that the beam quality was 1.32 by using the "energy-in-the-bucket" technique (see Section 3.3.2 for the description of this technique), while the beam quality of the original pump beam was arbitrarily defined to be 1. As will be mentioned in Section 3.3.2, the actual beam quality of the pump beam does not necessarily have to be 1. This was merely a measure of the aberration of the pump beam caused by the aberrator, and to determine how well could the OPC restore the aberrated pump beam.

The SBS experiments were performed with two SBS liquids: Fluorinert and Acetone; and in two waveguides: SBS open cells and multimode optical fibres. When SBS liquids were studied, an open cell was used to contain the liquids; whereas no open cell was needed when multimode optical fibres were studied. The SBS cell was held upright on the side of the optical table. It was a 10.3cm long plastic tapered test tube, filled with the two SBS liquids. In addition, a 60cm long SBS cell filled with Freon-113 was used to further investigate the suspected effects of pulse compression and sharp-rise observed in Fluorinert and Acetone. When SBS experiments were done with optical fibres, the fibres were coiled around a cylindrical object with a diameter of 8.5cm, which was sufficiently larger than the minimum coiled diameter (~3cm) at which the bending loss becomes dominant and increases the SBS threshold [73]. Although Ref. [73] was referring to fused-silica capillary tubes, but it still gives a good indication of the minimum coiled diameter allowed for optical fibres without any noticeable bending loss. Due to the time constraints of doing experiments, the only parameter varied was the length of the optical fibres, varied from 1m to 4m in steps of 1m.

A positive focussing lens (plano-convex lens, f = 11cm, 1064nm AR-coated) was placed 4cm above the surface of the SBS liquids, which was the optimal distance to produce efficient SBS process for yielding the highest reflectivity and fidelity [70]. We verified the optimal distance experimentally by varying the separation between the positive lens and the entrance of the open cell. This positive lens was used to focus the pump beam into the open cell, and this focussing effect was necessary to initiate the SBS and OPC processes [62]. The choice of the focal length of the lens was not restricted. According to Kuo *et al*

[70] the SBS threshold energy is nearly independent of the focal lengths of the lenses provided the pump laser operates at single mode. The Q-switched pump laser operated in single-longitudinal mode at most of the time, except in some occasional pulse-to-pulse variations where the laser was in multi-longitudinal mode. The positive lens was placed in the orientation that the flat side was facing towards the focal point. It was found that if the orientation was placed in the wrong way, that is, the curved side faced towards the focal point, the beam quality factor of the pump beam (M^2) could degrade rapidly due to spherical aberration, a fourth order phase distortion. The M^2 value increases as $(w/w_q)^4$, where w is the beam spot size, $w_q \equiv \left(\frac{f^3 \lambda}{2^{3/2} \pi C_{4f}} \right)^{1/4}$ is the critical width, f is the focal length of lens, λ is the pump wavelength and C_{4f} is the quartic aberration factor [74]. Although OPC is capable of compensating such aberration, but it is still preferable to minimise any known and external factor that can affect the measurements.

3.3 Diagnostics setup

This diagnostic part of the setup was used to analyse the pump and Stokes beams, as well as to study the SBS characteristics and performance. It consisted of two pyroelectric energy detectors (Molectron, J25) connected to a joulemeter/ratiometer (Molectron, JD2000), and two silicon photodetectors (Electro-optics Technology, ET2000) connected to a 400MHz digital oscilloscope (Tektronix, TDS 380). The energy detectors were used to measure the energies of the laser beams, and the photodetectors were used to measure the peak powers as well as to monitor the temporal profiles of the laser beams. All detectors were located at the reflected positions of the wedge. The pyroelectric energy detectors convert signal energy into heat and then generate measurable currents in the pyroelectric element. When connected to the joulemeter, this signal current is integrated in a capacitive load to produce a voltage proportional to the signal energy, and the output reading is readily shown on the display. For the joulemeter used, the voltage responsivity is $R_v = \alpha R_I / C_E$, where R_I is given in units of the charge received (and converted from optical current) per unit optical energy (V/J), α is the absorption coefficient, R_I is the current responsivity and C_E is the load capacitance). The minimum detectable energy of the joulemeter was about 40μJ. According to manufacturer specification, the

photodetectors had a rise-time of less than 200ps and a cut-off frequency of greater than 1.5GHz. However, the measurements were limited by the bandwidth of the oscilloscope used, which had a maximum bandwidth of 400MHz. Due to the small sensing area ($0.006mm^2$) of the photodetectors, the laser beams could be mislocated and the beam diameter could be too large to focus down to such a small area. The photodetectors might not detect the same part of the pump and Stokes beams, or the entire beams, leading to incorrect readings. A focusing lens was not used because the focused laser beam had a very high power that would certainly damage the photodetectors. Instead, a diffuser made of sandblasted aluminum sheets was placed at about 1cm before each photodetector, which caused the reflected beam to have uniform irradiance by diffuse reflections. Then the entire laser beam could be detected, and the photodetectors would not be sensitive to the incident angle of the laser beam. However, only a few percent of the laser power was detected by the photodetectors, because the acceptance angle of the sensing area was very small. In doing SBS experiments in optical fibres, due to the very small signal powers, the sandblasted aluminum sheets were removed and replaced by positive lenses to focus the laser beams directly to the photodetectors.

3.3.1 SBS Reflectivity Diagnostics Setup

Experimentally the SBS reflectivity is given by,

$$R_{SBS,E} = \frac{E_{STOKES,NF}}{E_{PUMP,NF}} \tag{3.3.1}$$

or

$$R_{SBS,P} = \frac{P_{STOKES,NF}}{P_{PUMP,NF}},$$

where $E_{PUMP,STOKES,NF}$ is the near-field energies of the pump and Stokes beams, and $P_{PUMP,STOKES,NF}$ is the near-field peak powers of the pump and Stokes beams. SBS reflectivity is simply a measure of how much the pump beam is converted into the Stokes beam. The SBS threshold energy is defined to be $R_{SBS} \approx 2\%$ [61].

From the SBS reflectivity diagnostics setup (Fig. 3.5), ED1 and PD1 were used to detect the pump beam properties (energy, peak power and temporal profile) while ED2 and PD2 the Stokes beam properties. Thus, when measurements were taken, SBS reflectivity was obtained by,

$$R_{SBS,E} = \frac{ED2}{ED1} \tag{3.3.2}$$

or

$$R_{SBS,P} = \frac{PD2}{PD1}.$$

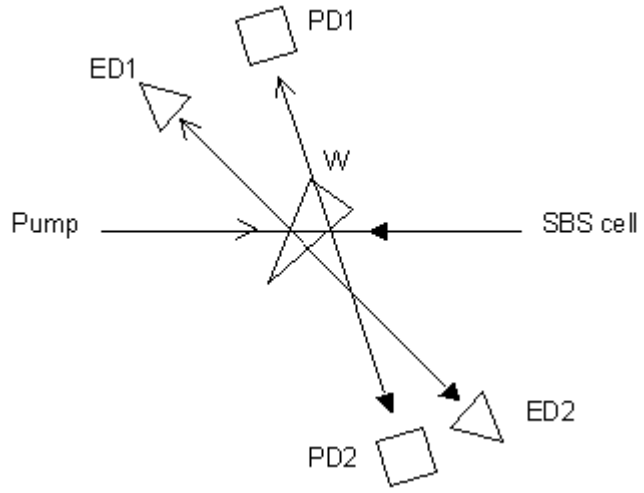

FIGURE 3.5 SCHEMATIC DIAGRAM OF THE DIAGNOSTICS OF SBS REFLECTIVITY. ED = ENERGY DETECTOR, PD = PHOTODETECTORS, W = WEDGE.

3.3.2 Phase Conjugate Fidelity Diagnostics Setup

Fidelity measurements were carried out using a diagnostics setup called the "energy (or power)-in-the-bucket" technique [69] because of its simplicity and accuracy (Fig. 3.3). In this technique, it compared the far-field energy (or power) of the phase conjugate beam detected by ED3 (or PD3), with the near-field energy (or power) of the phase conjugate beam detected by ED2 (or PD2). The fidelity is then given by the ratio of these two energies (or powers) divided by the pinhole transmission factor. With this technique, perfect OPC has a fidelity of unity. Experimentally the fidelity is given by,

$$F_{SBS,E} = \frac{E_{STOKES,FF}}{E_{STOKES,NF} \times T} \tag{3.3.3}$$

or $$F_{SBS,P} = \frac{P_{STOKES,FF}}{P_{STOKES,NF} \times T},$$

and $$T = \frac{E_{PUMP,FF}}{E_{PUMP,NF}} = \frac{P_{PUMP,FF}}{P_{PUMP,NF}}, \quad (3.3.4)$$

where $E_{PUMP,STOKES,NF}$ is the near-field energies of pump and Stokes beams, $E_{PUMP,STOKES,FF}$ is the far-field energies of pump and Stokes beams passed through a pinhole, P is the peak power measurement, and T is the pinhole transmission factor. The pinhole transmission factor is a measure of the beam quality of the pump beam, while the fidelity measures how well the Stokes beam resembles (or phase-conjugates) the pump beam. In other words, OPC does not actually improve the quality of the pump beam if it is already distorted before entering an aberrator. The best that OPC can do is to replicate the original state of the pump beam after it has double passed the aberrator. In principle, the technique works even if the M^2 factor (beam quality factor with reference to a perfect Gaussian beam) does not equal to one, which was the case in our experiments. As long as the pinhole transmission factor is measured experimentally with the pump beam used, and the pinhole diameter is chosen to contain the pump energy confined within the first Airy disc of its far-field diffraction pattern, then the M^2 factor of the pump beam is unimportant. In such case though, the beam quality factor will be arbitrarily defined to a particular value, and the far-field to near-field energy ratio of the return signal (Stokes beam after double passed the aberrator) is then compared against this defined value from the pump beam, and the ratio would yield the fidelity of the return signal.

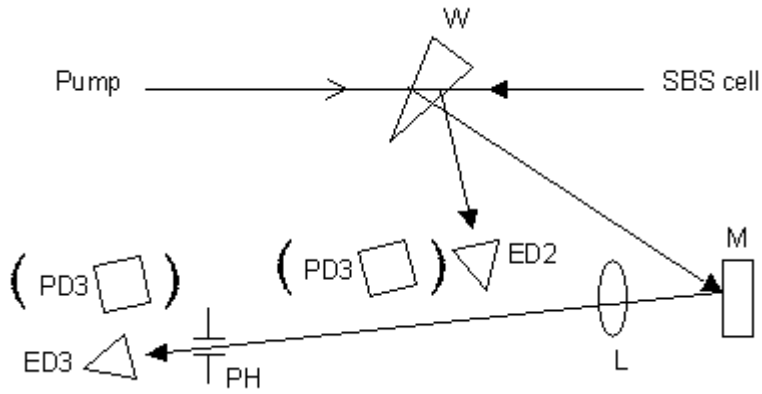

FIGURE 3.6 SCHEMATIC DIAGRAM OF THE DIAGNOSTICS OF PHASE CONJUGATE FIDELITY – THE "ENERGY-IN-THE-BUCKET" TECHNIQUE. FOR POWER MEASUREMENTS, REPLACE ENERGY DETECTORS WITH PHOTODETECTORS. ED = ENERGY DETECTOR, PD = PHOTODETECTOR, W = WEDGE, M = MIRROR, L = 1.15M POSITIVE LENS, PH = 0.40MM PINHOLE.

When measurements were taken experimentally, the fidelity was obtained by,

$$F_{SBS,E} = \frac{ED3}{ED2 \times T} \tag{3.3.5}$$

or

$$F_{SBS,P} = \frac{PD3}{PD2 \times T},$$

where T was defined in Eq. (3.3.4). The energy (or power) ratio readings had to be taken simultaneously because of pulse-to-pulse variations of the pump beam. For energy measurements, this was done by using the joulemeter/ratiometer to obtain the ratio directly. For power measurements, only the peak of the pulse was taken for each reading.

A positive lens (plano-convex lens, f = 1.15m) was used to produce the far-field pattern of the Stokes beam and focus it into the pinhole. The diameter of the pinhole had to be very small with small acceptance angle. Therefore, a long focal length lens was used to converge the beam slowly into the pinhole. The pinhole diameter was chosen such that it allowed approximately 84% of the total energy of the pump beam to pass through, which is the amount of energy contained in the first Airy disc of the far-field pattern for a top-hat intensity distribution. Hence the transmission factor should be 0.84. The first Airy disc is the zeroth order circular bright spot in the Fraunhofer diffraction pattern. The actual pump beam had a super-Gaussian intensity distribution, which was similar but not quite the same as the top-hat intensity distribution. Therefore, the actual transmission factor was

measured from the pump beam with different combinations of focal lengths and pinhole diameters at different separations (Fig. 3.7). From the results, a combination of a 1.15m focal length lens and a 0.40mm diameter pinhole was chosen, with a transmission factor of 0.83. This combination was chosen to allow a slowly converging beam (i.e. longer focal length needed), and was the closest to the ideal value for the top-hat intensity distribution (0.84), because it was the more similar profile to the super-Gaussian intensity distribution of the pump beam.

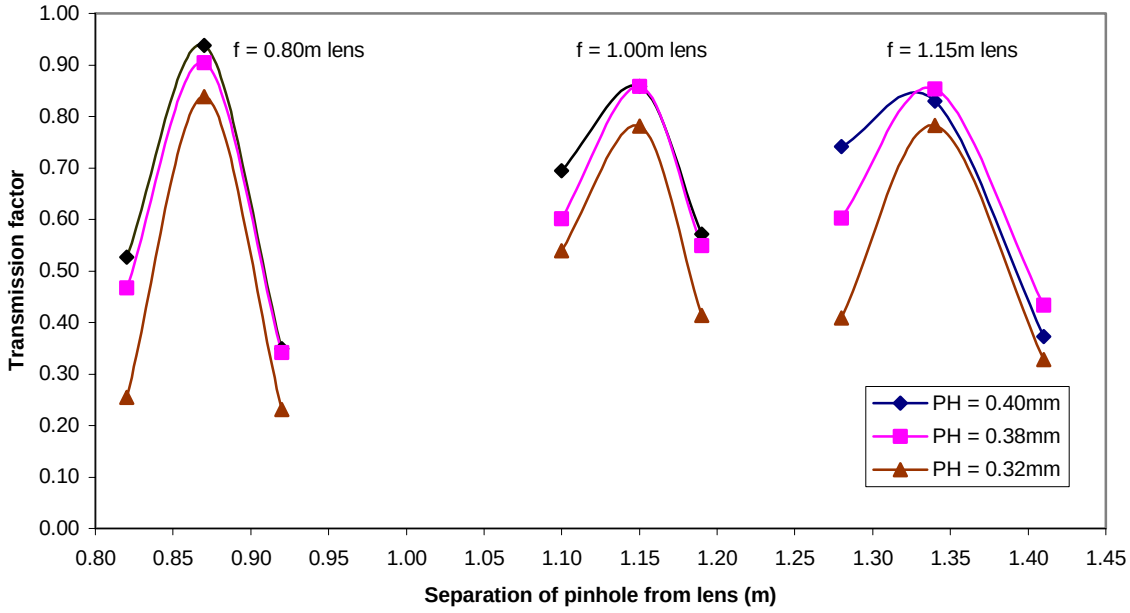

FIGURE 3.7 PINHOLE TRANSMISSION FACTORS FROM DIFFERENT COMBINATIONS OF FOCAL LENGTHS AND PINHOLE DIAMETERS AT DIFFERENT SEPARATIONS. DOTS ARE EXPERIMENTAL DATA; LINES ARE HIGH ORDER POLYNOMIAL CURVE FITS OF THE DATA POINTS.

It is interesting to note that the maximum transmission (i.e. smallest beam waist) shown in Fig. 3.4 was not at the focal plane of the lens, but rather it was slightly further away from the focal plane of the lens, and this separation increased with focal length. This indicated that the pump beam was diverging. If a collimated beam is incident upon a converging lens, the smallest beam waist will be at or near the focal plane. But if the beam diverges, it is focused further from the focal plane of the lens.

3.4 Measurement Methods

When conducting the experimental measurements, each configuration was repeated at least two times under the same experimental conditions, in order to obtain more reliable, consistent and accurate results. For SBS reflectivity experiments, the energy and power measurements were taken simultaneously from the same pump source. While for fidelity experiments, energy and power measurements were done separately because of the way the experimental setup was.

Calibrations were done before and after each measurement. The purposes were: (1) to calibrate (i.e. to normalise) the detectors, and (2) to ensure the experimental conditions were the same and consistent throughout each measurement. In some cases, when the calibration factors differed noticeably (greater than 10%), the whole measurement was discarded and taken again. This was mainly due to the instability of the pump beam at high output power and the contamination of the SBS liquids by dust particles when operated in a prolonged period of time.

Temporal profiles of pump and Stokes pulses were recorded during the SBS reflectivity and fidelity experiments. There were two purposes: (1) to observe and compare the temporal behaviour of the pulses, and (2) to ensure the pump beam operated in optimal condition (i.e. single longitudinal mode with minimum fluctuations). When the pump beam was not in single longitudinal mode, the corresponding energy and power data were discarded. It was observed that whenever the pump beam was not in a single longitudinal mode, optical breakdown was observed. This was due to the sudden increase in peak power to enable the ionisation of the molecules of the SBS liquids around the focal region (See Section 4.5 for more detail descriptions). This resulted in poor and degraded OPC, which gave the unreliable and inaccurate data. It should be noted that optical breakdown only occurred in liquids, not in optical fibres. Optical breakdown occurred much more frequently in Acetone than in Fluorinert. The data of Fluorinert with optical breakdown could be removed promptly, but the data of Acetone were more difficult to remove due to high frequency of occurrences. Therefore, data with optical breakdown were included in the results for Acetone.

Two types of measurements were used in conducting SBS experiments: energy (time-averaged) and power (time-resolved) measurements. When the pump pulse width (τ) is comparable to the phonon lifetime (τ_p) of the SBS materials, both energy and power measurements are valid and legitimate, and they should have similar results in terms of behaviour and output readings. But for longer pump pulse ($\tau > \tau_p$), it is preferable to employ power measurement for more realistic results. This is because for a pump pulse, only the portion above the SBS threshold contributes to the SBS process for the generation of Stokes return pulse. If energy measurement was used, then the total energy of the entire pulse (including the portion that did not contribute to the SBS process) was taken and compared against the total energy of the Stokes pulse. This would give a lower reflectivity and/or fidelity ratio (because the pump energy below SBS threshold was also included). On the other hand, energy measurement is preferred for shorter pump pulse ($\tau < \tau_p$), because the bandwidth of each pulse to be measured could be too large (i.e. the pulse duration is too short) to be resolved accurately even by using fast oscilloscopes. In doing SBS experiments, both energy and power measurements were taken in SBS cells. This was to compare the same results against two different types of measurements and to justify if the results were reliable and consistent. Only power measurements were taken in optical fibres experiments because the Stokes signals were below the actual minimum energy sensitivity (~40μJ) of the joulemeter.

In observing the temporal pulse profiles by using photodetectors and oscilloscope, because the two photodetectors were connected to two coaxial cables of different lengths, there was a time delay introduced by this length difference. The two pulses shown on the captured images was not the actual time delay between the two pulses. Therefore, synchronisation measurement was done to determine the actual time delay between the photodetectors. In doing so, the two coaxial cables were connected to a common output of a fast pulse generator (Tabor, 8600) to produce square pulse signals, and were observed by an oscilloscope. The two synchronised square pulse signals from a common output to the photodetectors are shown in Fig. 3.8. It was measured from the oscilloscope that the signal sent to Channel-2 (Ch2) led the signal sent to Channel-1 (Ch1) by 2.31ns. That is, in all the captured images for pump and Stokes pulses, the Stokes pulse led the pump pulse by 2.31ns. Likewise, in the captured images for near- and far-fields Stokes pulses, the far-

field pulse led the near-field pulse by 2.31ns. Since this cable length difference was fixed for all experiments, this time delay remained the same for all measurements.

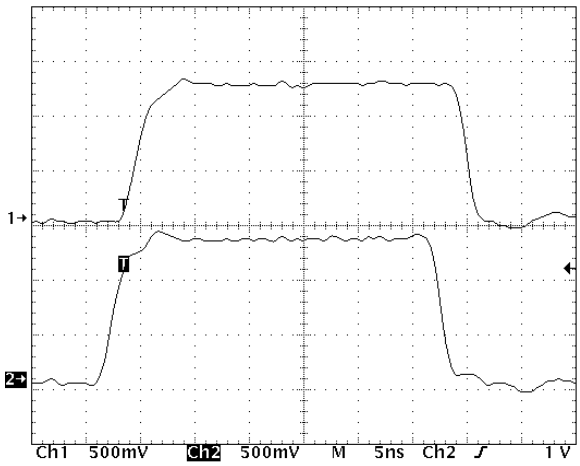

FIGURE 3.8 SYNCHRONISATION MEASUREMENT TO DETERMINE THE TIME DELAY BETWEEN TWO SIGNALS RECEIVED FROM THE PHOTODETECTORS TO THE OSCILLOSCOPE.

Chapter 4

4 SBS Experiments in Open Cells

This Chapter presents the results obtained from using SBS open cells. Fluorinert and Acetone were used as the SBS liquids to investigate the time-averaged and time-resolved SBS reflectivity and fidelity, as well as the Stokes pulse temporal behaviour. The properties of the SBS cell, the SBS liquids, and the observations of phase correction, optical breakdown and pulse compression are also included. *The SBS experiments in test tubes served as preliminary tasks for doing experiments in optical fibres, in order to understand the SBS characteristics and performance, and to gain enough laboratory skills in conducting SBS experiments.* Therefore, characterisations of the two chosen SBS liquids (Fluorinert and Acetone) did not go into great details, and only simple analyses were carried out.

4.1 Properties of SBS Cell

An SBS cell is a container, such as a glass tube or a metal pipe, that is used to contain the SBS liquid. The container we used for SBS cell was a 10mL plastic test tube, with 1.5cm in diameter and 10.3cm in length. As mentioned in Chapter 3, the test tube was held vertically upright on the side of the optical table and was not sealed. When the test tube was not used, it was covered by a cap. The advantage was that it eliminated the potential damage to the sealed window due to intense focussing of the pump beam, so that the optimal separation between the front face of the cell and the focal plane could be achieved easily. But the disadvantage was that it allowed for accidental contamination including

dust particles to be immersed into the liquids, and the evaporation of the liquids during measurements.

The effective interaction length (L_{eff}) is the length for which the pump beam travels inside a material of SBS gain, G, to have sufficient gain above the threshold intensity (I_{th}) to initiate the SBS process. For the steady-state SBS, the relationship is given by [61]: $GI_{th}L_{eff} = k$, where k is a constant in the range between 20 – 30. Thus, if the SBS cell has a length shorter than L_{eff}, there will be no SBS process to occur. Munch *et al* [72] observed that there are three factors affecting the L_{eff}, and found experimentally the minimum L_{eff} to initiate the SBS process. This is the shorter of the cell length (L_{cell}), three times the coherence length (l_c) or five times the Rayleigh range (Z_R) of the pump beam. The cell we used has a length of 10.3cm. The linewidth of the pump laser was about 0.003cm^{-1} (90MHz), corresponded to a coherence length of about 3.3m ($l_c = c/\Delta\nu = 1/\Delta\delta$, where c is the speed of light, $\Delta\nu$ and $\Delta\delta$ are the linewidth in Hz and wave-number respectively). The Rayleigh range is given by $Z_R = n\pi w_p^2/\lambda_p$, where n is the refractive index of material, w_p is the pump beam waist radius, λ_p is the pump wavelength. For n = 1.276, $w_p = 0.05$mm, and λ_p = 1064nm, the Rayleigh range Z_R = 9.4mm. The corresponding effective interaction lengths are given in the Table 4.1. The shortest effective interaction length was 47mm, which was contributed from the Rayleigh range of the pump beam. Thus, as long as the SBS cell is not shorter than five times the Rayleigh range, the choice of the cell length is unimportant and does not affect the initiation of the SBS process, hence the threshold energy.

TABLE 4.1 EFFECTIVE INTERACTION LENGTHS FOR SBS PROCESS.

Parameter	L_{eff} (mm)
L_{cell}	103
$3\times l_c$	9900
$5\times Z_R$	47

The choice of SBS liquids was determined by their high Brillouin gain coefficients, high refractive indices and small absorption coefficients [27, 73, 74]. Of such SBS liquids considered, many of them are toxic and/or hazardous to the environment, such as CS_2, CH_4, $TiCl_4$, CCl_4, toluene, benzene and etc. Thus, Fluorinert and Acetone were chosen to

be the SBS liquids for our experiments. Both liquids are relatively non-toxic, non-hazardous and easy to handle under standard laboratory procedures, while retaining good SBS characteristics.

4.2 Using Fluorinert

Fluorinert (3M, FC-75), according to manufacturer specifications, is a clear, colourless, odourless, inert and fully-fluorinated electronic liquid. It is thermally and chemically stable, compatible with materials such as metals and plastics, and is practically non-toxic [75]. It is used in many electronic applications including vapour phase soldering and thermal management, heat transfer, electronics testing and inert reaction media. Fluorinert has many good SBS related properties, such as excellent optical quality, low absorption from ultraviolet to infrared region, high optical breakdown threshold, good thermodynamic properties, and good chemical stability [76]. Table 4.2 lists the physical properties and Table 4.3 lists the SBS related properties of Fluorinert FC-75.

TABLE 4.2 PHYSICAL PROPERTIES OF FLUORINERT FC-75 AT 25ºC. FROM REF. [75].

Main component	C_8F_{18}
Average molecular weight	420
Density (kg/m^3)	1.77
Boiling point (ºC)	102
Pour point (ºC)	-88
Critical pressure ($\times 10^6$ Pa)	1.60
Specific heat (J/kg K)	1046
Thermal conductivity (W/m K)	0.063
Expansion coefficient (10^3/K)	1.4
Sound velocity (m/s)	563
Dielectric strength (MV/m)	15.7
Refractive index (at 546nm)	1.276

TABLE 4.3 SBS RELATED PROPERTIES OF FLUORINERT FC-75 AT 25ºC AND 1064NM. FROM REFS. [76, 77].

Brillouin gain factor (cm/GW)	4.7
Absorption coefficient ($\times 10^{-6}$ cm^{-1})	2.8
Optical breakdown threshold (GW/cm^2)	100 – 130

Brillouin frequency shift (GHz)	1.36
Hypersound velocity (m/s)	563
SBS threshold energy (mJ) (18ns pulse)	3.4
SBS steady-state threshold (kW)	190
Brillouin linewidth (MHz)	420
Phonon lifetime (ns)	0.78

4.2.1 SBS Reflectivity of Fluorinert

As mentioned in Section 3.3.1, the SBS reflectivity determines how much of the pump wave is converted into Stokes wave and scattered backward by SBS process. Therefore, high reflectivity indicates good SBS performance. Figs. 4.1 and 4.2 show respectively, the energy and peak power reflectivities of Fluorinert using unaberrated (without aberrator) and aberrated (with aberrator) pumps, as a function of threshold energy ratio. Unfortunately, the uncertainties for each energy or power reading were not recorded when taking the reflectivity measurements. However, it was estimated, from the figure, that the uncertainties (standard errors) were ~3% of the measured energy reflectivity, and ~10% of the measured power reflectivity. Each data point corresponded to the average of six pulses, and each reflectivity and fidelity measurement was performed three times to ensure reproducibility. The time-averaged threshold energy for unaberrated pump beam was 4.2mJ ($R_{SBS} \approx 2.3\%$), compared to the published value of 3.4mJ by Yoshida *et al* [76]. This suggested that the lower threshold energy could be due to some experimental variations from ours, namely they used ultra-filtered Fluorinert, shorter pump pulse width (pulse width of 10ns) and different experimental layout. Note that all of the measured SBS threshold values were obtained by energy measurements (i.e. not by power measurements).

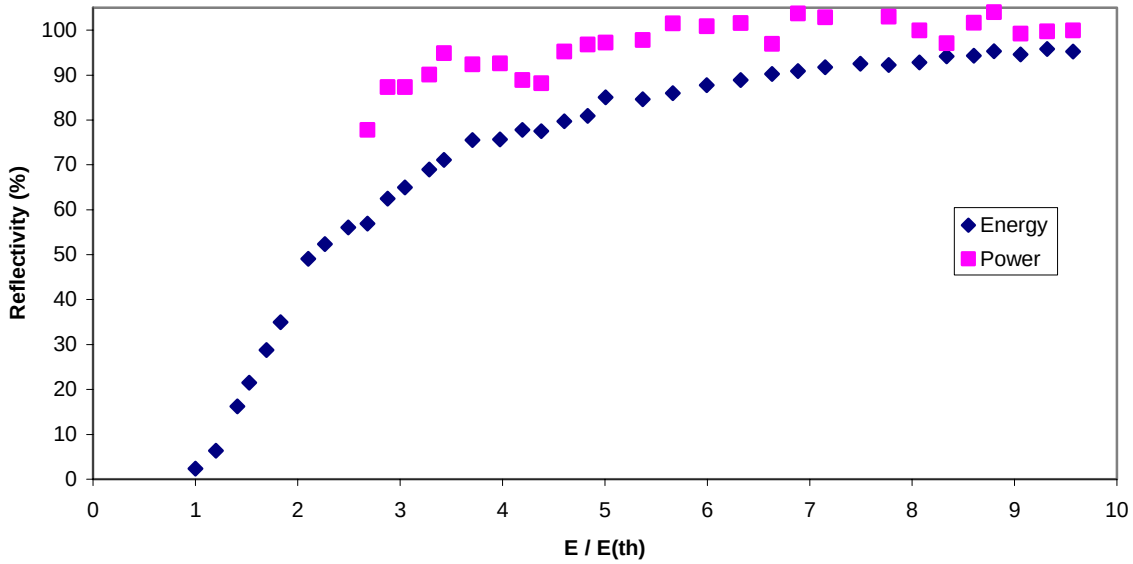

FIGURE 4.1 REFLECTIVITY VS THRESHOLD ENERGY RATIO OF FLUORINERT WITHOUT ABERRATOR. EACH DOT REPRESENTS AN AVERAGE OF 6 PULSES.

From Fig. 4.1, the energy reflectivity by unaberrated pump increased monotonically and rapidly soon after threshold was reached. The rate of increase slowed down after four times the threshold energy and reached up to a maximum reflectivity of 95%, compared to its maximum value of 98% with ultra-filtration [76]. By comparing with other well-known SBS materials from published results, Fluorinert yielded the highest time-averaged reflectivity, among them were N_2 [71], CH_4 [71], SF_6 [78], Freon-113 [27] and CS_2 [37].

In contrast, the peak power reflectivity reached above 85% at just about three times the threshold energy, increased slowly and reached up to the maximum close to 100% at about seven times the threshold. It stayed at around 90 – 100% thereafter at higher pump energies. The higher than 100% data points were due to measurement uncertainties. By observation from the graph, the peak power reflectivity had more frequent and larger uncertainties than energy reflectivity. This was due to the pulse-to-pulse variations of the peak powers of the pump pulses during measurements, and thus to the corresponding peak powers of Stokes pulses. The properties of pump wave (pump energy, intensity, pulse width, transverse and longitudinal modes, wavelength and etc) and acoustic wave of the SBS material (phonon lifetime, gain coefficient, absorption coefficient, sound velocity, optical breakdown threshold and etc) had direct influence to the generation of Stokes wave, because it is the interaction between the pump and acoustic waves that determines the properties of the Stokes wave. It should be noted that optical breakdown did not

contribute to the power reflectivity uncertainties, because the data were discarded promptly whenever optical breakdown occurred. This can be justified by the fact that the energy and power reflectivities were taken simultaneously and that energy reflectivity was very high and well behaved with very small uncertainties. Optical breakdown was occasionally observed in all experiments, and a more detail discussion is included in Section 4.5.

For the SBS reflectivity by an aberrated pump (i.e. with aberrator inserted), as shown in Fig. 4.2, the threshold energy was 6.6mJ ($R_{SBS} \approx 1.7\%$), which was about 2.5mJ higher than that without the aberrator. The energy reflectivity curves behaved very similarly for both with and without aberrator, except the former had a lower maximum reflectivity of about 80% at 6 times the threshold. From the graph, the energy reflectivity had very small uncertainties and had well predicted behaviour even by the aberrated pump beam. As pointed out by Schelonka *et al* [69], the reflectivity (not necessarily the fidelity) depended only on the focal intensity, regardless of whether the beam was aberrated or simply reduced in power. This suggested that the aberrator indeed reduced the focal intensity of the pump beam, therefore, an increase in the SBS threshold energy and a reduction in overall reflectivity when compared with the aberrator removed. The same happened for the peak power reflectivity, with the maximum reflectivity lowered to about 90% compared to near 100% for without the aberrator. The maximum reflectivity was reached at merely two times the threshold energy, then stayed in the 80 – 90% range with small uncertainties at higher energy levels.

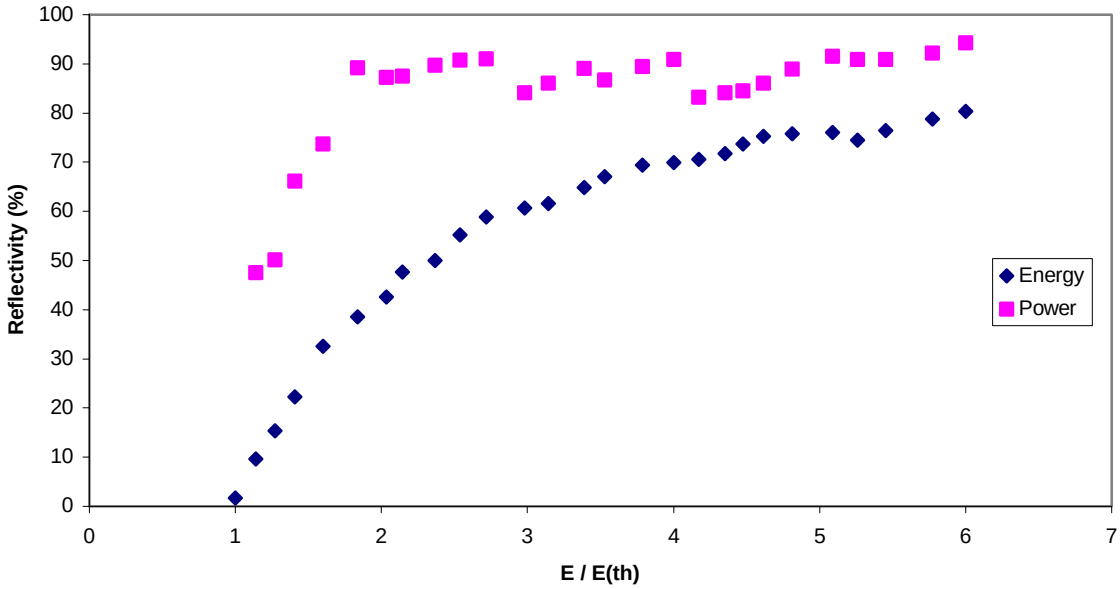

FIGURE 4.2 REFLECTIVITY VS THRESHOLD ENERGY RATIO OF FLUORINERT WITH ABERRATOR. EACH DOT REPRESENTS AN AVERAGE OF 6 PULSES.

In both cases with and without aberrator, the trends of both energy and power reflectivities curves were very similar. The peak power reflectivity had consistently higher values (about 10 – 20%) than the energy reflectivity, but the gap became slightly smaller at higher pump energy levels. As mentioned in Section 3.4, for pump pulse that is comparable to the phonon lifetime of Fluorinert, both energy and power measurements would have similar behaviour and reflectivity ratios, although the peak power reflectivity was slightly higher than energy reflectivity.

The temporal profiles of the Stokes pulses were recorded for unaberrated and aberrated pump beams (Figs. 4.3 (A) and (B)). The Stokes pulse of the unaberrated pump was quite similar to its pump pulse, that both have Gaussian-like shapes (Fig. 4.3 (A)). But the Stokes pulse had a more steep and linear leading edge (due to SBS threshold) than the pump pulse, together with a slowing decreasing tailing edge, which was a typical averaged (by diffuse reflection) Stokes pulse profile. The Stokes pulse of the aberrated pump shown in Fig. 4.3 (B) had a steeper and sharper rising part, and longer trailing part. The peak power was lower compared to that of the unaberrated pump. In both cases, the Stokes pulses had shorter pulse widths compared to the pump pulse width, which was a typical characteristic of Stokes pulse.

The “temporal fidelity”, defined to be the phase conjugate fidelity in time domain to determine the degree of temporal fluctuations of the Stokes pulse [36] was indeed very good. It was observed that optical breakdown and pump beam at multi-longitudinal mode were the two main factors for poor temporal fidelity. When the pump beam was in single longitudinal mode, its corresponding Stokes beam was also in single longitudinal mode with smooth Gaussian-like shape. But when the pump beam was in multi-longitudinal mode, its corresponding Stokes beam not only had the same number of modal peaks, but with optical breakdown occurred.

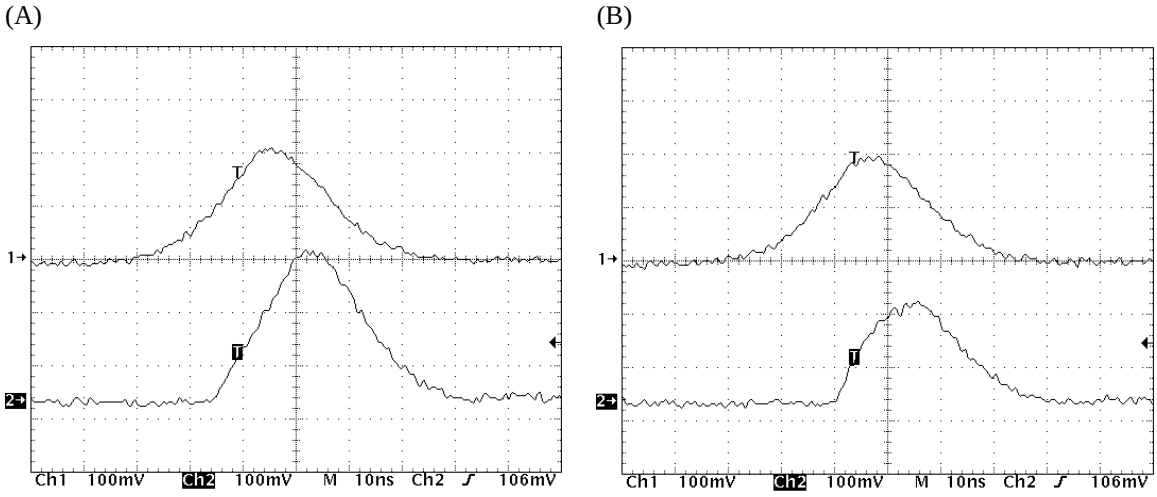

FIGURE 4.3 TEMPORAL PROFILES OF PUMP AND STOKES PULSES OF FLUORINERT WITHOUT (A) AND WITH (B) ABERRATOR INSERTED. CH1 = PUMP PULSE, CH2 = STOKES PULSE. CH1 LAGGED CH2 BY 2.31ns.

4.2.2 Phase Conjugate Fidelity of Fluorinert

Fluorinert, a heavy fluorocarbon liquid, has been shown to be an excellent SBS liquid for OPC according to the published data [76, 77]. These data agreed with our findings. For both energy fidelity and peak power fidelity, ratios near unity were achieved. The peak power fidelity is measured to be the instantaneous peak amplitude of a pulse observed from the transient digitiser. This is somewhat different from the averaged power fidelity, in which it measures the averaged power of the entire pulse. There are two points to note: (1) both the energy fidelity and peak power fidelity measurements presented in this Chapter were, strictly speaking, measurements of spatial fidelities. We did not analyse the temporal fidelities. However, the fidelity in time domain did have indirect influence on the spatial fidelity, which can be justified by the fact that “bad” pump pulse shape (i.e. multi-

longitudinal pump laser mode) almost always produced low reflectivity and poor fidelity. (2) the threshold was taken to be the energy at which OPC was initiated by SBS process, not necessarily the same as SBS reflectivity threshold. Generally, fidelity threshold is higher than reflectivity threshold, because the former measures the phase conjugated Stokes beam while the latter simply measures the backscattered Stokes beam from the SBS medium. As mentioned in Section 2.2.2, the generation of phase conjugated Stokes beam requires selectively enhanced amplification of the Stokes beam. The components that acquired maximum amplification are those that correlate the best with the non-uniform gain distribution, and hence the phase conjugated Stokes beam is generated. This selective amplification process requires higher intensity to produce the non-uniform gain distribution, and therefore, higher threshold is required for fidelity than reflectivity. Fig. 4.4 shows the energy fidelity by both unaberrated pump (no aberrator) and aberrated pump beams (with aberrator) as a function of threshold energy ratio. Each data point represents an average of 30 pulses. The error bars represent the measurement uncertainties, which are the standard deviations of the 30 pulses taken for each data point. The threshold energy by unaberrated pump was 5.5mJ ($F_{SBS} \approx 49\%$) and by aberrated pump was 8.7mJ ($F_{SBS} \approx 35\%$), a difference of 3.2mJ. It was difficult to measure the threshold once OPC was initiated. This was due to the sudden steep jump of the fidelity ratio soon after threshold was reached that made the threshold measurements difficult. As in most cases for the fidelity in different SBS materials, the fidelity usually reached its maximum immediately after the threshold and up to about three times the threshold.

With the unaberrated pump beam, the energy fidelity climbed rapidly to a maximum of around 100% at about 2.5 times the threshold, and stayed in the range between 90 – 100% at up to 10 times the threshold. Initially the measurement uncertainties were quite large at low energies, but decreased with increased energy levels. From the trend of the curve, the energy fidelity had a tendency to stay constant with increasing pump energy. It is interesting to note that there are divided opinions in whether the fidelity stays, increases or decreases with increasing pump energy, all according to their published experimental findings. Some researchers found fidelity increases with pump energy [69, 80], while others found fidelity decreases with pump energy [71, 79]. But there is no simple answer to such argument because there are many factors involved in the measurements that can

affect the fidelity, such as focussing and cell geometries, SBS materials, competing nonlinear effects, pump source conditions, and experimental setups.

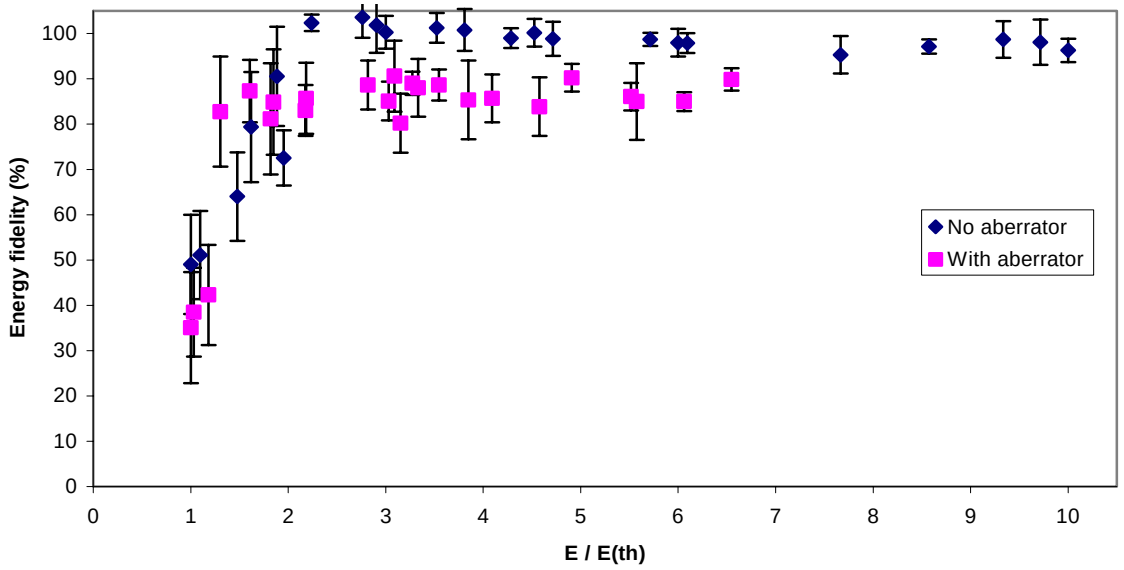

FIGURE 4.4 ENERGY FIDELITY VS THRESHOLD ENERGY RATIO OF FLUORINERT. E_{TH} (NO ABERRATOR) = 5.5MJ, E_{TH} (WITH ABERRATOR) = 8.7MJ. EACH DOT REPRESENTS AN AVERAGE OF 30 PULSES. ERROR BARS ARE MEASUREMENT UNCERTAINITES.

With the aberrated pump beam (Fig. 4.4) the energy fidelity jumped from about 35% near threshold up to 80% with a mere increase of 1mJ of pump energy. The fidelity stayed at around 80 – 90% for higher pump energies, though with greater fluctuations. The overall uncertainties were larger than that by the unaberrated beam, especially at low energies. The fidelity was lower than that by an unaberrated pump beam. The reasons for the lower fidelity could be due to the degree of phase distortion of pump beam by the aberrator. If the degree of phase distortion of the pump beam is high, its far-field pattern at the SBS interaction region could have separated, unrelated and distinct intensity peaks. There is only little correlation between each intensity distribution, and each one of them is transferring the individual amplitude information back to their own phase counterparts. Then the overall reconstruction of the phase information of the Stokes beam could be incomplete and cannot resemble the pump beam completely. This is called partial or incomplete phase conjugation, which leads to lower fidelity than that by an unaberrated pump beam. Experimentally, the amount of energy contained within the first Airy disc in the far-field (~84% of total energy) would be less for the Stokes beam by an aberrated pump beam than that by an unaberrated beam due to the separated, unrelated and distinct

far-field intensity peaks produced, and hence yielded lower fidelity. It was measured that the aberrator decreased the amount of energy that can be transmitted through the pinhole (which allowed ~84% of total energy to be transmitted), with the ratio of the transmitted energy of aberrated to unaberrated pump beam being 0.572. This showed that the aberrator caused the far-field intensity peaks of the pump beam to be distributed non-uniformly and laid outside the first Airy disc. This caused lesser amount of energy to be confined in this region, and hence lower fidelity as described above. This non-uniformly distributed far-field pattern by the aberrator can be seen in Fig. 4.14 (B) of Section 4.4.

There were several causes of uncertainties in fidelity measurements, including pulse-to-pulse variation, noise in the electronics of equipments and spatial variation in SBS reflectivity. Pulse-to-pulse variation was due to the instability of the pump beam, which in turn had more possibilities of causing it. We managed to minimise the instability by using the variable attenuator (Brewster polarisar and λ/2-plate) to adjust the pump energy. We also maintained to restrict the usage time of the laser from prolonged period of time, in order to avoid possible instability from the electronics of the laser system. There were always some inherit noise associated in the electronics of the detecting equipments. This was especially apparent for the joulemeter as it had nonzero background readings even after calibration. But it was later found that the nonzero background noise was due to one of the joulemeter probes not properly grounded. Spatial variation of reflectivity could be caused by the instability of the pump beam. That is, each pump pulse was not “hitting” at exactly the same interacting location to initiate SBS process. There might be local density variations at different interacting locations, either due to optical breakdown, micro-particles present or inhomogeneities in the SBS liquid, which resulted in the fluctuations of the SBS reflectivity. This could reduce the stability of the phase conjugated beam because essentially it was the reflected Stokes beam from the SBS cell that was phase conjugating the pump beam.

The power fidelities by unaberrated (no aberrator) and aberrated (with aberrator) pump beams as a function of threshold energy ratio are shown in Fig. 4.5. The power fidelity threshold for unaberrated pump was 5.6mJ ($F_{SBS} \approx 95\%$) and for aberrated pump was 6.8mJ ($F_{SBS} \approx 78\%$), with a difference of 1.2mJ. For the unaberrated pump beam, the peak power fidelity reached a very high value of above 90% immediately after the threshold,

and stayed in the range of 90 – 100% at higher energies. The measurement uncertainties were larger than that in energy fidelity, the "amount" of uncertainties (i.e. the length of the error bar) was quite constant at about 8 – 10%. Although the measurements had relatively high uncertainties, the overall fidelities were indeed very high, indicated that Fluorinert was capable of producing high quality phase conjugated Stokes pulses.

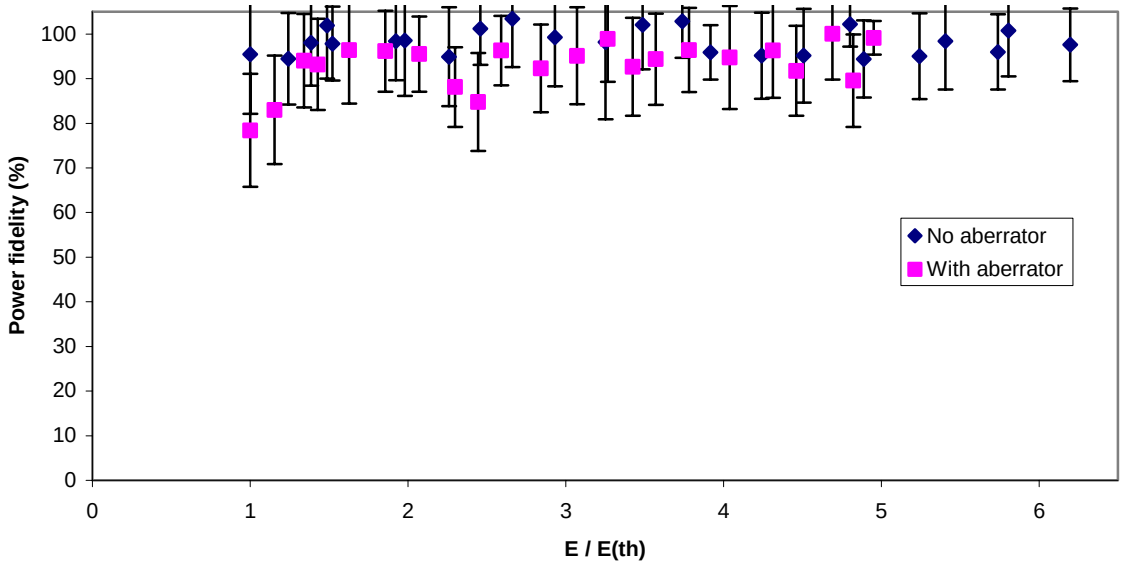

FIGURE 4.5 PEAK POWER FIDELITY VS THRESHOLD ENERGY RATIO OF FLUORINERT. E_{TH} (NO ABERRATOR) = 5.6MJ, E_{TH} (WITH ABERRATOR) = 6.8MJ. EACH DOT REPRESENTS AN AVERAGE OF 30 PULSES. ERROR BARS ARE MEASUREMENT UNCERTAINITES.

With the aberrated pump beam, it also yielded a very high peak power fidelity. It reached to a maximum of above 90% at 1.5 times the threshold and stayed at around 85 – 100% afterward. There were some data points appearing to be over 100% due primarily to the measurement uncertainties. The peak power fidelity by both unaberrated and aberrated pump beams exhibited moderate uncertainties, which can be explained by the same arguments as given for uncertainties in energy fidelity. It was observed from the temporal profiles of the pump and Stokes pulses in the oscilloscope, that the major contributing factor to the measurement uncertainties was due to pulse-to-pulse variations of the pump beam. It was the peak amplitudes of the pump and Stokes pulses that were being recorded in each reading, and each pump pulse peak variation influenced directly the peak and quality of the corresponding phase conjugated Stokes pulse.

Since both unaberrated and aberrated pump beams turned out to have very high peak power fidelities, this exhibited the high capability and quality of instantaneous resemblance of the pump beam by the phase conjugated Stokes beam. This showed that Fluorinert not only yielded high reflectivity, but also good fidelity, which is a very good candidate when choosing the SBS materials in important applications that required fast, instantaneous response and perfect OPC with high reflectivity, such as phase conjugate oscillators.

The typical near-field and far-field temporal profiles of the Stokes pulses by unaberrated and aberrated pump beams are shown in Fig. 4.6, in which the time-resolved behaviour of the phase conjugated Stokes pulse can be examined. The horizontal scale shows the time, and vertical scale the amplitude of the pulses. Near-field Stokes pulse is simply the backscattered pulse from the SBS cell, while the far-field Stokes pulse is the backscattered pulse that was focussed by a positive lens and passed through a pinhole. The near-field temporal profiles (Ch1 (upper trace) of Fig. 4.6) for unaberrated and aberrated beams showed very similar shapes, indicating that the aberrator did not alter the temporal profiles of the phase conjugated Stokes pulse much. The only apparent difference is that the aberrated Stokes pulse had a slightly steeper rising edge and lower peak power, which can be seen more clearly in their corresponding enlarged far-field temporal profiles (Ch2 (lower trace) of Fig. 4.6). One thing worth noting is that the very high spatial fidelities achieved for both unaberrated and aberrated pump beams may have resulted partly from the high temporal fidelities, that is, very little temporal fluctuations besides measurement uncertainties. It is known that poor temporal fidelity leads to degradation of the Stokes beam and hence a reduction in SBS reflectivity and efficiency of OPC [36]. The temporal profiles of pump and Stokes pulses in Figs. 4.3 and 4.6 showed that the pulses had very steady and well behaved temporal profiles, and hence very high energy and power fidelities.

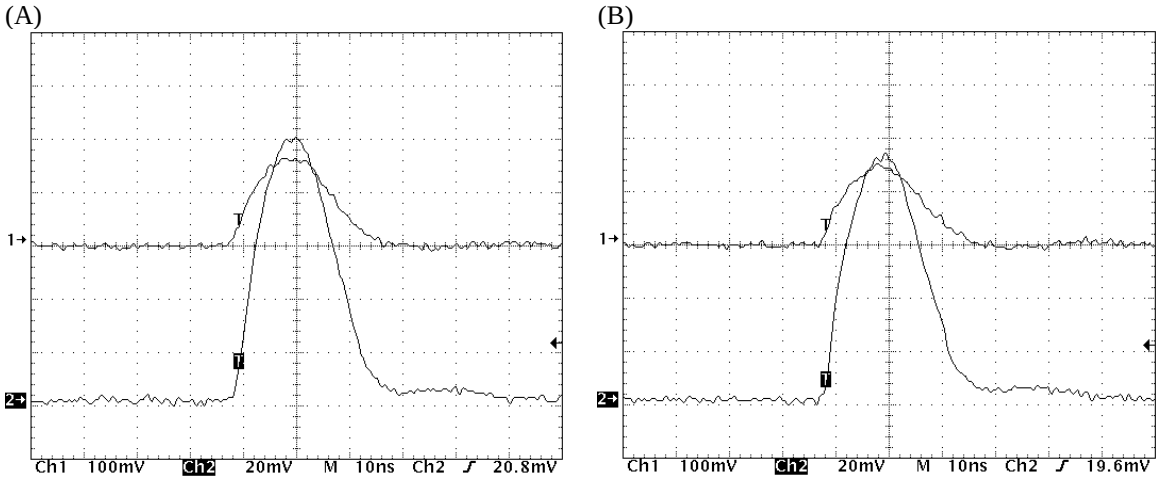

FIGURE 4.6 TEMPORAL PROFILES OF STOKES PULSES OF FLUORINERT WITHOUT (A) AND WITH (B) ABERRATOR INSERTED. HORIZONTAL SCALE SHOWS THE TIME, VERTICAL SCALE SHOWS THE AMPLITUDE. CH1 (UPPER TRACE) = NEAR-FIELD STOKES PULSE, CH2 (LOWER TRACE) = FAR-FIELD STOKES PULSE. CH1 LAGGED CH2 BY 2.31ns.

4.3 Using Acetone

Acetone (Merck, 1.00022.0500) has the chemical formula of CH_3COCH_3, is a clear, colourless, odorous, volatile and highly flammable liquid. Most Acetone produced is used to make other chemicals for making plastics, fibres and drugs [81]. It is also used to dissolve other substances, remove grease stains and nail varnishes. Acetone has been widely used as a SBS medium because of high reflectivity and good fidelity. Table 4.3 lists the physical properties and Table 4.4 lists some SBS related properties. Besides CS_2, Acetone has the highest Brillouin gain coefficient among many common SBS liquids.

TABLE 4.4 PHYSICAL PROPERTIES OF ACETONE AT 20ºC. FROM REF. [82].

Main component	CH_3COCH_3
Average molecular weight	58.08
Density (g/mL)	0.7844
Boiling point (ºC)	56.29
Vapour pressure ($\times 10^6$ Pa)	0.791
Specific heat (J/kg K)	1046
Thermal conductivity (W/m K)	0.063
Expansion coefficient (10^3/K)	1.4
Viscosity (centipoises)	0.36
Dielectric constant (MV/m)	20.7 (at 25ºC)
Refractive index	1.3587

TABLE 4.5 SBS RELATED PROPERTIES OF ACETONE AT 1064NM. FROM REFS. [44, 61, 62].

Brillouin frequency shift (GHz)	4.6
Hypersound velocity (m/s)	1170
Brillouin linewidth (MHz)	180
Brillouin gain factor (cm/GW)	20
Phonon lifetime (ns)	2

4.3.1 SBS Reflectivity of Acetone

Fig. 4.7 shows the energy and power reflectivities of Acetone by an unaberrated (without aberrator) pump beam as a function of threshold energy ratio. The time-averaged threshold energy was 5.9mJ ($R_{SBS} \approx 1.7\%$). The energy reflectivity increased monotonically and slowly, and reached to a maximum value of about 70%. In comparing with the energy reflectivity of Fluorinert, Acetone had higher threshold energy and lower maximum reflectivity value, as well as a non-typical growth trend. A typical reflectivity curve would look like the one found in Fluorinert. No further investigations were carried out, but possible reasons are given later in this Section.

The power reflectivity had higher ratios than the energy reflectivity. It had a maximum of about 95% with some uncertainties. As mentioned, when taking the average of the data, each individual reading was not recorded. Therefore, the actual measurement uncertainties in reflectivities were not known. The trends of the energy and power reflectivity curves were remarkably similar in terms of the rate of increase and stability, and had a fairly constant difference of about 20%. This shows a clear distinction between energy and power measurements, that the former measured the entire pulse while the latter measured the peak power of the pulse. This implies that the pump was having a constant pulse width throughout the experiments for Acetone, and that the pulse width was considerably larger than the phonon lifetime of Acetone (see Section 3.4).

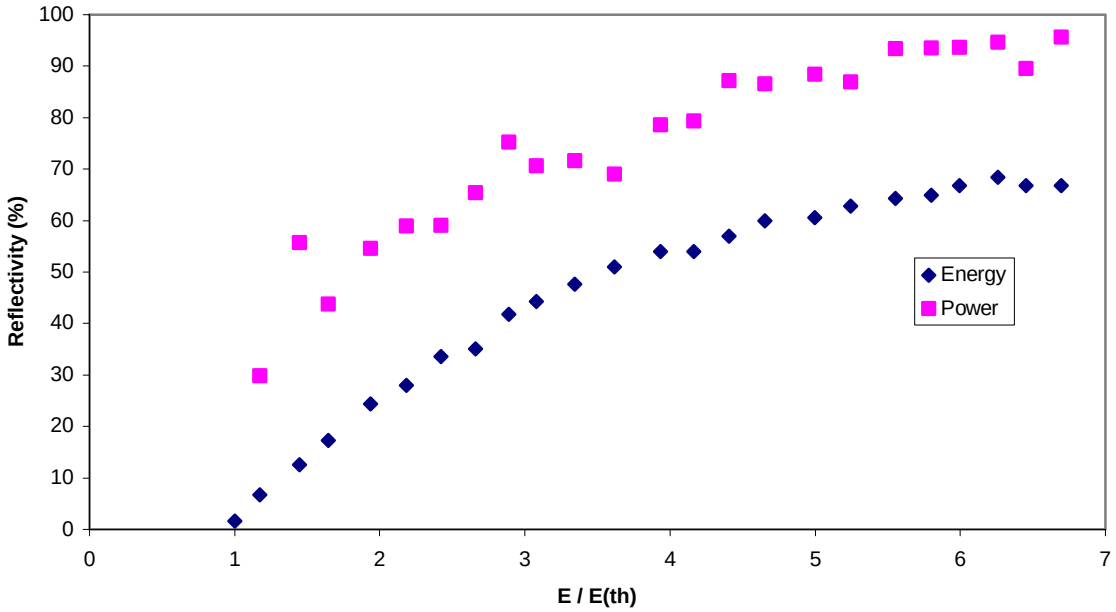

FIGURE 4.7 REFLECTIVITY VS THRESHOLD ENERGY RATIO OF ACETONE WITHOUT ABERRATOR. EACH DOT REPRESENTS AN AVERAGE OF 6 PULSES.

Fig. 4.8 shows the energy and power reflectivities of Acetone by an aberrated (with aberrator) pump beam as a function of threshold energy ratio. The time-averaged threshold energy was 6.6mJ ($R_{SBS} \approx 1.8\%$). The maximum energy reflectivity was about 62%, which was considerably lower than that for Fluorinert. Also the rate of increase was slow, with a mere 30% reflectivity at 3 times the threshold, and up to about 60% reflectivity at 7 times the threshold. As will be seen in the next Section, that Acetone yielded reasonably high energy and power fidelities, although the reflectivity was only moderately high.

Initially, the power reflectivity increased slowly, only 10% at about 1.5 times the threshold. But it then increased more rapidly to around 70% at 4 times the threshold, and reached to a maximum of about 90%. The measurement uncertainties were larger than that that in energy reflectivity. The power reflectivity of Acetone by aberrated pump beam was indeed very high, although not as high as measured in Fluorinert. The aberrator lowered the energy reflectivity due to reduction in focal intensity and localised individual intensity peaks, but it did not affect the power reflectivity that much. This would be interesting to have a deeper investigation on the influence on the degree of pump aberration to the energy and power reflectivities in terms of temporal fluctuations and pulse characteristics. This is known that it is possible in optical fibres to have very high fidelity while having only moderate reflectivity [20], which also happened in our findings in Acetone. Our

results showed that, in general, aberrated pump beam had lower reflectivity than unaberrated pump beam, but the fidelity seemed to be less affected. That is, the differences in the fidelities for aberrated and unaberrated pump beams were smaller than that in reflectivities. We did not conduct the reflectivity and fidelity experiments in time domain, because it would take a fair amount of additional works, and we did not have sufficient time to do so. But this would be valuable to know the effects of the temporal fluctuations, temporal pulse characteristics and degree of aberration of pump beam to the overall SBS reflectivity and fidelity.

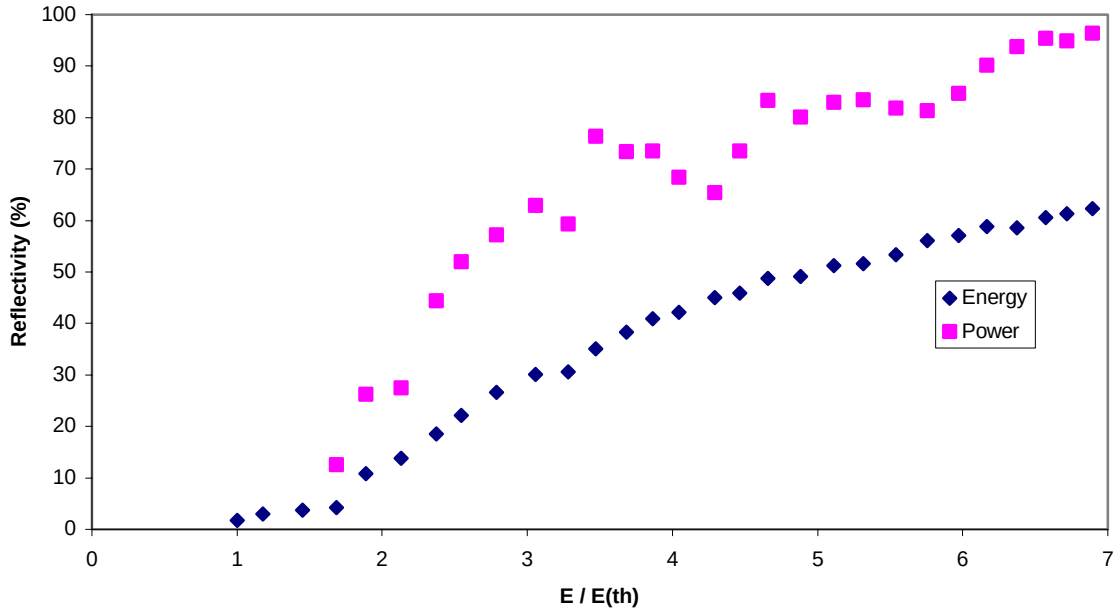

FIGURE 4.8 REFLECTIVITY VS THRESHOLD ENERGY RATIO OF ACETONE WITH ABERRATOR. EACH DOT REPRESENTS AN AVERAGE OF 6 PULSES.

Both energy and power reflectivities increased more slowly and had lower maxima than that of Fluorinert, which seemed to be a bit unusual. This was because Fluorinert had a steady-state Brillouin gain factor of 4.7cm/GW [77], about 4 times less than that of Acetone, which was 20cm/GW [62]. Thus, under the same experimental conditions and available pump power, Acetone should have higher reflectivity than Fluorinert, which was clearly not the case we observed. As mentioned in Section 3.4, the readings with optical breakdown were inevitably included in the results of Acetone due to the very frequent occurrences of optical breakdown appeared in Acetone. But the data with optical breakdown were not included in Fluorinert.

The possible reasons could be due to intrinsic and extrinsic influences. Intrinsic factors include physical and chemical properties, molecular composition, and SBS responses to the SBS materials that cannot be changed or altered easily. On the other hand, extrinsic factors include micro-particles presence in liquid, evaporation of the liquid, measurement uncertainties, and systematic errors that can be minimised or eliminated experimentally. In particular, the two extrinsic factors were discussed below: (1) the Acetone was used directly from the manufactured container without filtration. There could have some micro-particles such as dust and impurities present in the liquid. Since those micro-particles had different chemical composition from Acetone, they absorb the pump energy and dissipate heat differently, which in turn caused an increase in the energy and heat locally around the micro-particles. This results in the lowering of the optical breakdown threshold (of pure Acetone), and increased the SBS threshold. This caused the reflectivity not as high as Acetone supposed to have. In comparing with Fluorinert, it was evident that Acetone had much more occurrence of optical breakdown observed. The optical breakdown in Fluorinert could likely be caused by strong heating and photo-ionisation (see Section 4.5), more than due to heat absorption by impurities. (2) the evaporation rate of Acetone was moderately fast. It was observed that after one complete measurement (about 45 – 60 minutes) the liquid evaporated as much as 1.5mL. The problem of liquid evaporation was that it altered the focusing condition for optimal SBS process. According to Kuo *et al* [70] for a short SBS cell, if the separation between the front face of the SBS cell and the effective focal length of the focussing lens inside the cell (L_R) is outside the so-called maximum reflectivity region ($L_{R,max}$), then the SBS reflectivity reduces significantly. The maximum reflectivity region is the length L_R at which it yields the maximum SBS reflectivity. For example, for a 20cm cell, $L_{R,max}$ is between 2 – 6cm. The shorter the cell length, the shorter the $L_{R,max}$. Therefore, when the liquid is evaporated, the separation between front face of the cell and effective focal length of the lens is shortened, and so the SBS reflectivity is reduced. This was verified experimentally. Different L_R was attempted to locate the optimal separation for the most efficient SBS process, and observed that the SBS reflectivity varied with L_R. Apart from that, other assumptions mentioned above could not be justified experimentally. No further experimental investigations were carried out, because the original purposes of performing SBS experiments in open cells were only to gain solid experience, and to understand the basic characteristics and performance of the chosen SBS liquids.

The temporal profiles of the pump and Stokes pulses are given in Fig. 4.9. The Stokes pulses for both unaberrated and aberrated pump beams were remarkably similar both in shape and width. They were also very similar to the Stokes pulses produced in Fluorinert. The figure showed that the amplitude of the Stokes pulses for the unaberrated pump beam was very high, indicated that good power reflectivity was achieved for Acetone.

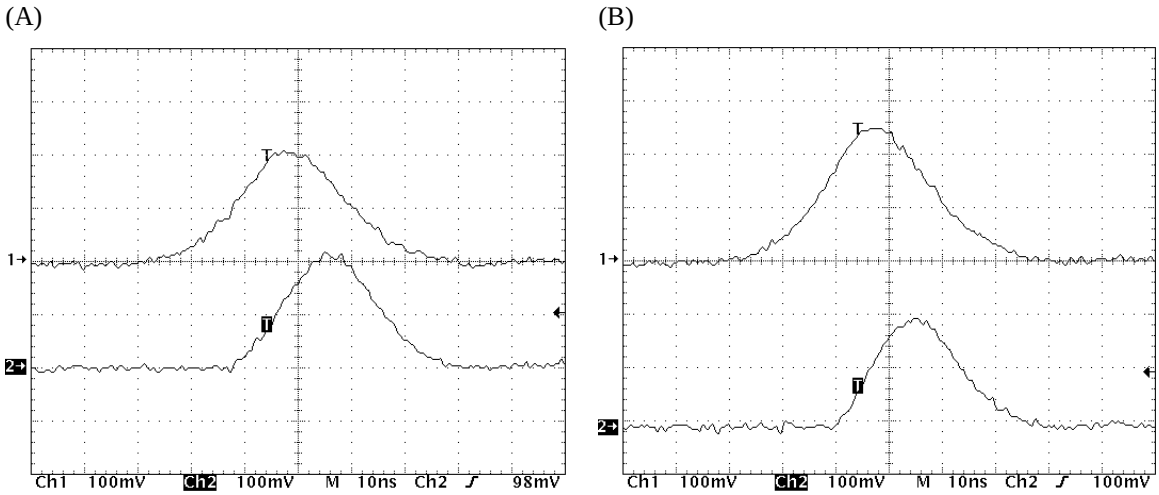

FIGURE 4.9 TEMPORAL PROFILES OF PUMP AND STOKES PULSES OF ACETONE WITHOUT (A) AND WITH (B) ABERRATOR INSERTED. CH1 = PUMP PULSE, CH2 = STOKES PULSE. CH1 LAGGED CH2 BY 2.31ns.

4.3.2 Phase Conjugate Fidelity of Acetone

Fig. 4.10 shows the energy fidelities of SBS using Acetone by unaberrated (no aberrator) and aberrated (with aberrator) pump beams, as a function of threshold energy ratio. The threshold energy was 9.0mJ ($F_{SBS} \approx 32\%$) for unaberrated and 10.2mJ ($F_{SBS} \approx 41\%$) for aberrated pump beams, a difference of 1.2mJ. The threshold energies were higher than that for Fluorinert (5.5mJ for unaberrated and 8.7mJ for aberrated pump beams). One possibility of higher threshold energy could be due to the low reflectivity at low pump energies, causing higher energy required to get OPC into action. Recall from Figs. 4.7 and 4.8 that at around 9 – 10mJ of pump energy, the energy reflectivity was about 15% for unaberrated pump and only 4% for aberrated pump beams. Thus, higher threshold energy was required to produce the phase conjugated Stokes beam, because of the low energy reflectivity at such energy levels.

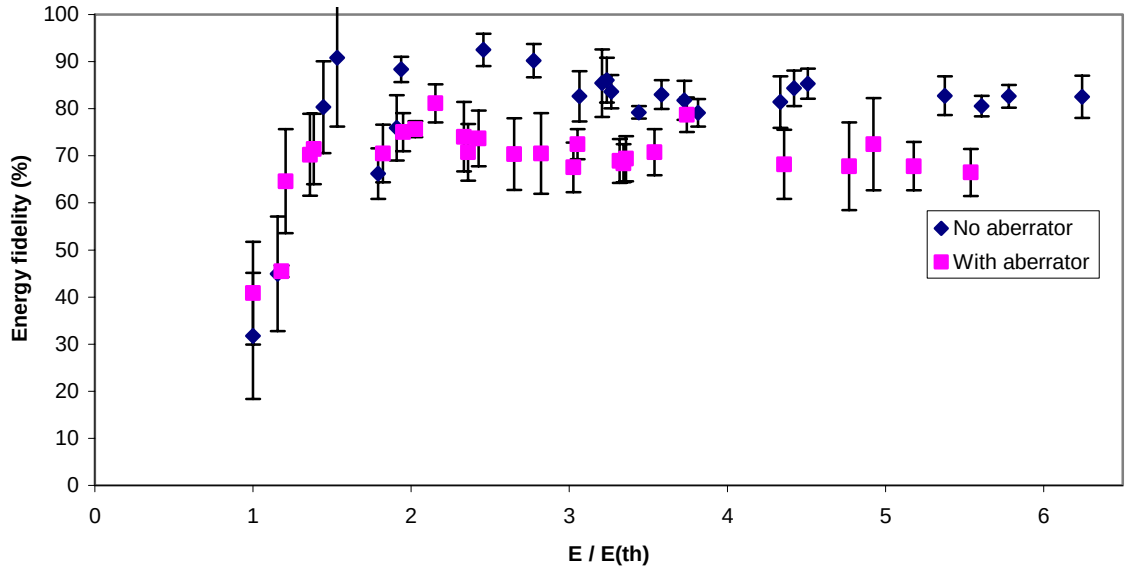

FIGURE 4.10 ENERGY FIDELITY VS THRESHOLD ENERGY RATIO OF ACETONE. E_{TH} (NO ABERRATOR) = 9.0MJ, E_{TH} (WITH ABERRATOR) = 10.2MJ. EACH DOT REPRESENTS AN AVERAGE OF 30 PULSES. ERROR BARS ARE MEASUREMENT UNCERTAINITES.

From Fig. 4.10, both unaberrated and aberrated pump beams established average fidelity of around 30 – 40% at threshold, jumped steeply to their respective maxima (90% for unaberrated and 75% for aberrated pump beams) at around 2 times the threshold. Both pump beams behaved similarly in the following ways: (1) they had large scatters of data points initially but reduced with increased pump energies; (2) they stayed at their respective maximum fidelities once the maximum ratios were reached; (3) they had a consistent difference in fidelity ratio of about 10%; and (4) the trends of both fidelity curves showed very similar phase conjugate response from both pump beams. As we know, the fidelity is a measure of how well the Stokes beam can restore to the original quality of the pump beam when it passed through an aberrator. Therefore, when comparing with the energy fidelity between Acetone and Fluorinert (Fig. 4.4), it showed that Acetone yielded a lower overall fidelity, this implies that Acetone cannot restore the aberrated pump beam as good as it can for Fluorinert.

Fig. 4.11 shows the peak power fidelities of Acetone by unaberrated (no aberrator) and aberrated (with aberrator) pump beams as a function of threshold energy ratio. The threshold energy for unaberrated pump was 6.1mJ ($F_{SBS} \approx 66\%$) for unaberrated and 7.5mJ ($F_{SBS} \approx 73\%$) for aberrated pump beams, a difference of 1.4mJ. The overall

uncertainties were higher than that in energy fidelity, with the "amount" of uncertainties was quite constant at about 8 – 10%. As can be seen, the peak power (time-resolved) measurements of the SBS threshold values and maximum fidelity ratios were comparable to those of Fluorinert, even though Acetone had relatively lower energy fidelities than Fluorinert. This immediately gives four interesting observations: (1) the peak power fidelities behaved alike regardless of the choice of SBS liquids; (2) the "amount" of uncertainties were almost the same for both liquids, which was about 8 – 10% in average; and (3) the peak power fidelities by both unaberrated and aberrated pump beams were very good and almost identical. Both pump beams reached above 90% at merely 1.5 times the threshold and stayed in the range between 90 – 100% thereafter with some measurement uncertainties.

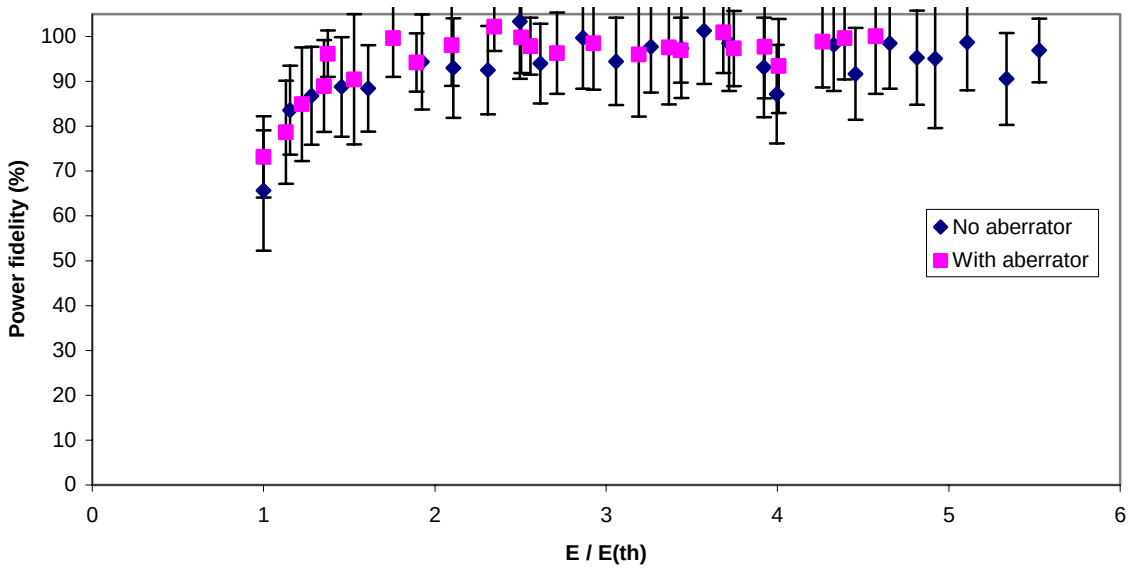

FIGURE 4.11 POWER FIDELITY VS THRESHOLD ENERGY RATIO OF ACETONE. E_{TH} (NO ABERRATOR) = 6.1MJ, E_{TH} (WITH ABERRATOR) = 7.5MJ. EACH DOT REPRESENTS AN AVERAGE OF 30 PULSES. ERROR BARS ARE MEASUREMENT UNCERTAINITES.

While there was a constant difference of about 10% in energy fidelities between unaberrated and aberrated pump beams, there was not much difference in power fidelities between both pump beams. This behaviour was also observed in Fluorinert (Fig. 4.5). Although no experimental justification was made, we suspect that was due to the way the measurements were made and the pulse width of the pump pulse. As mentioned in Section 3.4, when the pump pulse width is larger than the phonon lifetime of the SBS material, it may be more accurate to use peak power (time-resolved) measurements, such that the

"unused" part of the pump pulse would not be included to the overall reflectivity and fidelity results. By the "unused" part, we mean the early part (more than phonon lifetime) of the temporal part of the pulse that is below the SBS threshold, which does not contribute to the initiation of SBS process. Nevertheless, the similarity in peak power fidelities by unaberrated and aberrated pump beams showed that the good aberration restoration of the aberrated beam to the original pump beam was achieved.

The near-field and far-field temporal profiles of the Stokes pulses by unaberrated and aberrated pump beams are given in Fig. 4.12. The horizontal scale shows the time, and vertical scale the amplitude of the pulses. Note the difference in the amplitude (vertical) scale of Ch2. For the unaberrated pump beam (Fig. 4.12 (A)), the near-field and far-field Stokes temporal profiles were very similar, although the latter had lower peak power. With the aberrated pump beam, the Stokes profiles (both near-field and far-field) for Acetone and Fluorinert (Fig 4.6 (B)) were surprisingly similar if not identical, even for their corresponding sharp-rise leading edges.

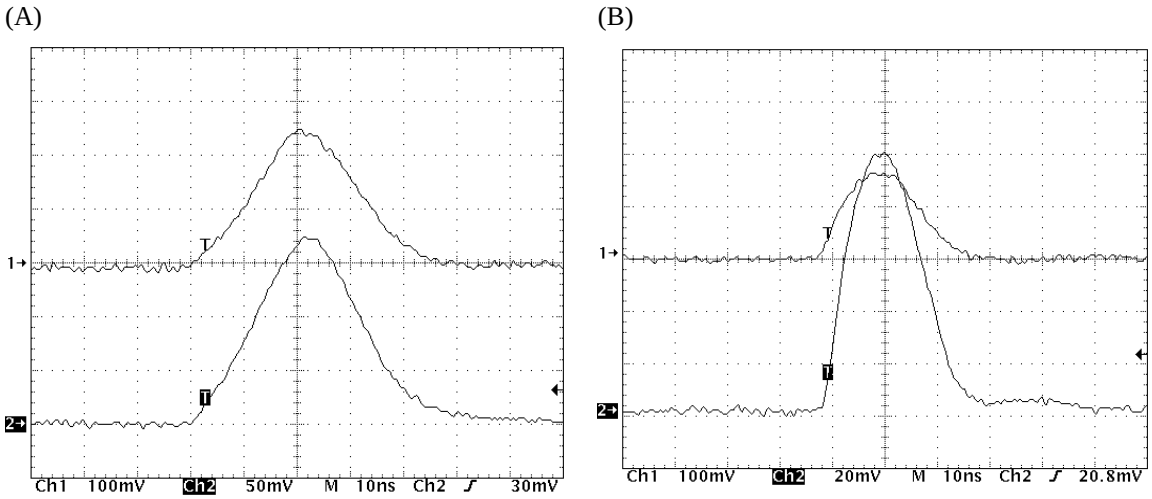

FIGURE 4.12 TEMPORAL PROFILES OF STOKES PULSES OF ACETONE WITHOUT (A) AND WITH (B) ABERRATOR INSERTED. HORIZONTAL SCALE SHOWS THE TIME, VERTICAL SCALE SHOWS THE AMPLITUDE. CH1 (UPPER TRACE) = NEAR-FIELD STOKES PULSE, CH2 (LOWER TRACE) = FAR-FIELD STOKES PULSE. CH1 LAGGED CH2 BY 2.31ns. NOTE THE DIFFERENCE IN AMPLITUDE (VERTICAL) SCALE OF CH2.

4.4 Phase Correction of an Aberrated Beam

OPC by SBS has proven to be a simple and effective way of restoring the pump beam after double passing an aberrator. This is the main reason that this technique was employed in many high power solid-state MOPA laser systems. Phase correction of the aberrated (phase-distorted) beam was observed and is shown in Figs. 4.13 and 4.14, although the phase conjugated beam did not perfectly resemble the original pump beam.

Fig. 4.13 shows the near-field patterns of the pump and Stokes beams. The figure shows the 3-D plots of the detected pump beam intensity distributions as a function of the transverse position. The axes labelling and scales were not shown in the plots, but they were all have the same scales. Also, the position and configuration of the CCD camera was fixed throughout the measurements. Due to the saturation of the CCD camera, the top parts of the images were truncated. Fig. 4.13 (A) shows the intensity distribution of the pump beam, which showed that it was partially aberrated even before passing an aberrator. Fig. 4.13 (B) shows the pump beam aberrated by an aberrator, in which more irregular intensity distributions can be seen. Fig. 4.13 (C) shows the mirror reflected beam after passing through the aberrator twice. Clearly the degree of aberration was increased noticeably, and there were more individual intensity spikes present. Fig. 4.13 (D) shows the near-field pattern of the Stokes beam reflected from a PCM after double passing the aberrator. Apart from local individual intensity irregularities, the near-field distribution did resemble (though not much) to the original pump beam with lower intensity. By comparing with Figs. 4.13 (A) and (D) we see that some phase correction was achieved by OPC using SBS. The corresponding far-field patterns of the original pump beam (Fig. 4.14 (A)) and the reflected Stokes beam (Fig. 4.14 (B)) also showed this similarity.

Fig. 4.14 shows the far-field beam patterns of the pump and Stokes beams. The figure shows the 2-D contour plots of the detected pump beam intensity distributions as a function of the transverse position. The axes represent the transverse position, and the intensity given by different grey scale levels. Brighter (or whiter) levels represent higher intensity and vice versa. Note that the images were not recorded simultaneously with the near-field beam patterns shown in Fig. 4.13. However, since the experimental setup and conditions were the same, apart from pulse-to-pulse variations, it can be thought of as they are relating to each other. Fig. 4.14 (A) shows the far-field pattern of the pump beam,

which appeared to be a single peak in the first Airy disc. The peak was inclined to one side and the distribution was not quite uniform, as would be expected for a diffraction limited beam. By referring to its near-field pattern (Fig. 4.13 (A)) it is clear that the pump beam was not diffraction limited. Fig. 4.14 (B) shows the far-field pattern of the aberrated pump beam, and that there were a few peaks and were not evenly distributed. The pump beam was distorted (Fig. 4.13 (B)) and its far-field pattern was not a single peak confined in the first Airy disc. We also expect the amount of intensity fell within the first Airy disc to be less that that with a diffraction limited pump beam, because some of the intensity peaks were outside the Airy disc region. Fig. 4.14 (C) shows the far-field pattern of the reflected beam by a mirror, after passing through an aberrator twice. The spatial distribution of the pump beam was doubly distorted, and so its far-field peaks scattered around non-uniformly. Finally, Fig. 4.14 (D) shows the far-field pattern of the Stokes beam reflected from the PCM after passing through an aberrator twice, which showed a sharp single intensity peak similar to the one in Fig. 4.14 (A). This suggests that the phase conjugated Stokes beam had, at least partially, corrected the phase aberration introduced by the aberrator, that is, partially resembled to the pump beam (Fig. 4.13 (D)).

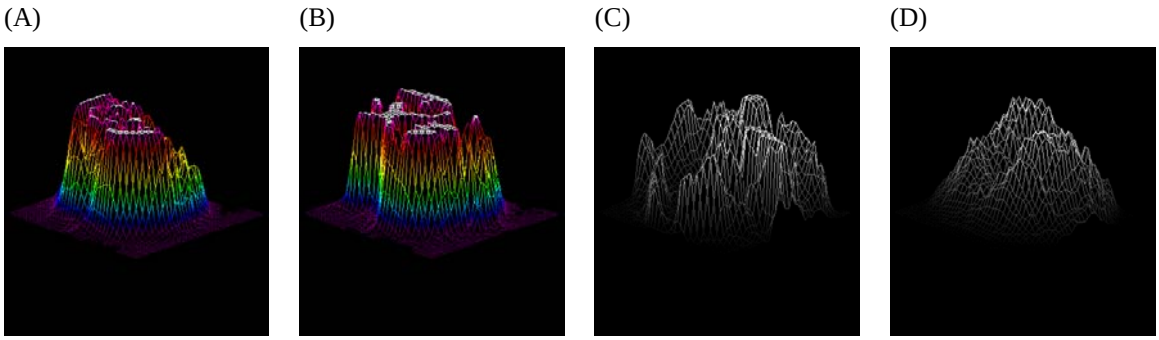

FIGURE 4.13 NEAR-FIELD PATTERNS OF THE (A) PUMP PULSE, (B) ABERRATED PUMP PULSE, (C) RETURN PULSE FROM MIRROR, (D) STOKES PULSE.

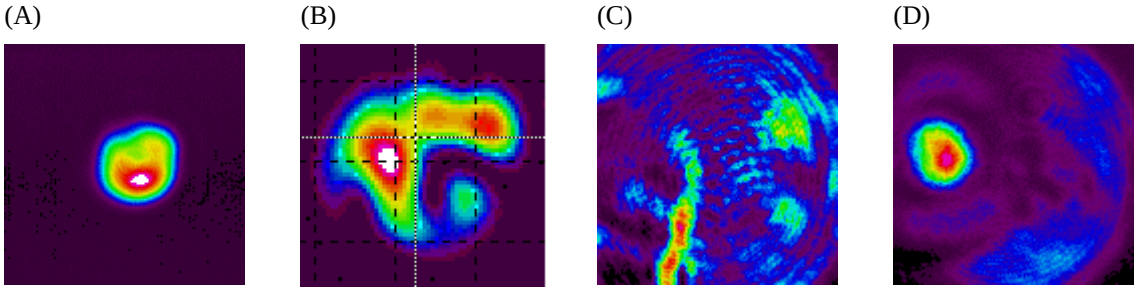

FIGURE 4.14 FAR-FIELD PATTERNS OF THE (A) PUMP PULSE, (B) ABERRATED PUMP PULSE, (C) RETURN PULSE FROM MIRROR, (D) STOKES PULSE.

4.5 Optical Breakdown

There are two main reasons causing optical breakdown: (1) excessive intensity of the pump beam (greater than 10^{10}W/cm^{2}s) caused strong heating and photo-ionisation via multi-photon excitation; (2) impurities and micro-particles present inside the SBS liquid [27, 61]. Excessively high intensity can be achieved easily by focussing the short pulse pump beam. When photo-ionisation occurs, electrons are freed from the molecules, hot plasmas and new chemical species are formed due to the dissociation of the molecular structures of the liquid. These plasmas screened and shortened the effective interaction length, absorb the pump beam more rapidly and strongly, and hence degrade the SBS reflectivity and fidelity.

When impurities and micro-particles are present in the SBS liquid, they do not have the same properties as the SBS liquid, and do not contribute constructively and usefully to the SBS process, which degrade the overall SBS performance. This resulted in an increase in the SBS threshold energy, reduction in SBS reflectivity and fidelity performances. In addition, they can decrease the breakdown threshold by a few orders of magnitude. Generally they can be removed by purification and ultra-filtration. Since complete characterisations of the SBS liquids were not the main objective of this research, they were used directly and did not undergo purification and filtration. During our experiments, optical breakdown were observed in both liquids near the focal region of the focussing lens. Both possibilities mentioned contributed to this phenomenon because: a high energy (> 100mJ) and short pulse (~25ns) pump beam being was used and being focussed by a

short focal length lens (f = 11cm) before entering the SBS cell. Also, the SBS cell had an open entrance without any window sealed, which allowed micro-particles such as dust to get in. Optical breakdown can be identified by the visible sparks, bubble formations around the focal region, and audible sparking noises could be heard. It should be noted that, whenever there occurred an optical breakdown, the pump beam was almost always operating at multi-longitudinal mode.

4.6 Pulse Compression

Pulse compression is the phenomenon when the width of the generated Stokes pulse is narrower than its pump pulse. The energy in the latter part of the pump pulse is converted and contributed to the compressed Stokes pulse by the mirror formed from the phonon envelope to reflect and compress this Stokes pulse. It is the result of strong gain saturation of the pump pulse by the leading edge of the counter-propagating and strong SBS reflectivity growing Stokes pulse [26, 28]. Pulse compression is an important application of SBS that is employed in pulse shaping and narrowing, in order to obtain the desired pulse shape and width for other applications, while retaining the aberration correction ability. To produce significant pulse compression, the cell length must be at least half the spatial length of the pump pulse [28], which is about 3.8m for our 25ns pump pulse width.

The mechanism of pulse compression is the interaction between the pump and Stokes pulses, and the seeding process of the travelling Stokes pulse. When the pump pulse is focussed into a long cell, the Stokes pulse is generated as usual. As the Stokes pulse travels backward, the leading edge of the Stokes pulse acts as a seed for further acoustic wave, because of the standing wave that is generated by the interference of the pump and Stokes pulses inside the cell. The centre of reflection of the grating moves towards the entrance face of the cell, compressing the part of the pump pulse that is still coming in and this results in the overall pulse compression of the pump pulse. The compression efficiency depends on the electrostrictive response time of the material. That is, the rate at which the centre of reflection of the grating can follow the leading edge of the Stokes pulse [84].

Damzen *et al* [30] suggested a few configurations to produce effective pulse compression. The first method is to use a tapered waveguide. It provides total internal reflection along the walls of the tubing, relatively low-loss propagation and large acceptance angle. The second method is to focus the pump beam with long focal length lenses into an open cell. Distinct pulse shortening and peaking of the leading edge of the pump pulse were achieved. The third method is to employ a two-cells generator-amplifier arrangement, which is an effective and convenient way of producing pulse compression and pulse width as short as 1ns was obtained.

The observations of sharp-rise effect and relaxation oscillation of the Stokes pulse are typical dynamical behaviour of pulse compression, which was also reported by Devrelis [27]. The sharp-rise effect is the sudden and steep rise of the leading edge of the Stokes pulse, may or may not be due to pulse compression. Relaxation oscillation in SBS is due to the energy interchange between the pump and Stokes fields, via the continuous process of increase and reduction of the gains between these two fields [36]. In order to investigate these behaviour caused by pulse compression, a longer SBS cell (60cm in length and 3.5cm in diameter) filled with Freon-113 ($C_2Cl_3F_3$) was used, as it was readily available in the laboratory. Although, the cell was not long enough to produce effective pulse compression and its associated behaviours, but it still gave some insights of what the Stokes pulse behaved in a moderately long cell. The end surfaces of the cell were cleaned and polished to remove any dirt adhered on the surfaces, which could cause optical damage when focussed beam was used. The experimental and diagnostics setups were described in Chapter 3. The cell was laid horizontally on the optical table to allow horizontal movements of the cell. A long focal length lens (plano-convex lens, f = 100cm) was used as the focussing lens. Figs. 4.15 (A) – (L) show the evolution of the Stokes pulse temporal profile as a function of the distance from the front face of the cell to the effective focal plane of the lens ($D_{front\text{-}focal}$). The shortest allowable $D_{front\text{-}focal}$ was 5cm. If the distance was shorter than that, the intensity of the focussed beam could exceed the damage threshold of the front window. This could damage the window and unable to initiate SBS, because most of the energy would be deposited onto the window. On the other hand, the longest $D_{front\text{-}focal}$ was near to the far end face of the cell, which was about 60cm. Sharp-rise effect started at $D_{front\text{-}focal}$ = 11cm (Fig. 4.15 (B)) and became more apparent at $D_{front\text{-}focal}$ = 25cm (Fig. 4.15 (D)). As the $D_{front\text{-}focal}$ increased, the portion of the sharp-rise in the leading edge of the pulse became larger also (Fig. 4.15 (F)). Relaxation oscillation started

to occur at $D_{front\text{-}focal}$ = 42cm (Fig. 4.15 (G)), about two third of the cell length. As the $D_{front\text{-}focal}$ increased further, the profile of the Stokes pulse no longer appears to be a smooth Gaussian shape, although the "envelope" of the Stokes pulse still shown to be a truncated quasi-Gaussian shape (Figs. 4.15 (J) – (L)). Fig. 4.15 (K) showed a typical Stokes pulse with relaxation oscillation [36]. When the effective focal plane was near the end face of the cell, the leading edge of the Stokes pulse had the largest sharp-rise. It appeared to be a magnified version of the damped oscillation, similar to the one produced in the laser resonator (Fig. 4.15 (L)). This observation is in agreement with the numerical model developed by Afshaarvahid *et al* [36], that the fluctuations and relaxation oscillation of the Stokes pulse are influenced by the immersion length and pulse compression.

In conclusion, no apparent pulse compression was observed because the SBS cell was not long enough to provide sufficient spatial length for the pump pulse to be compressed. However, both sharp-rise effect and relaxation oscillation were observed. But due to the time available, no further investigation was carried out to explain these phenomena.

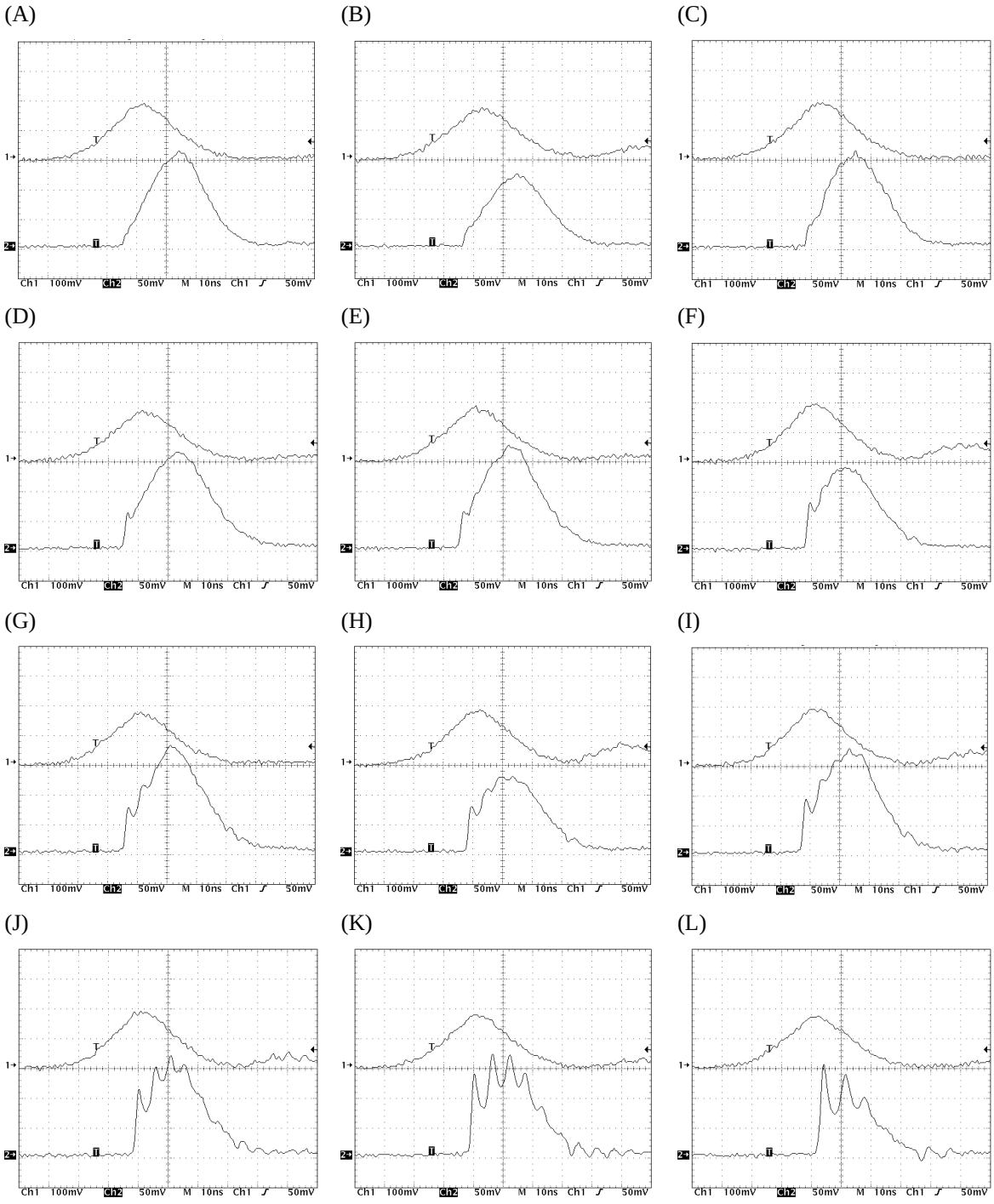

FIGURE 4.15 EVOLUTION OF STOKES PULSE TEMPORAL PROFILE AS A FUNCTION OF THE DISTANCE FROM FRONT FACE OF SBS CELL TO EFFECTIVE FOCAL PLANE OF THE LENS: (A) 5CM, (B) 11CM, (C) 16CM, (D) 25CM, (E) 35CM, (F) 37CM, (G) 42CM, (H) 46CM, (I) 51CM, (J) 54CM, (K) 56CM, (L) 60CM. CH1: PUMP PULSE, CH2: STOKES PULSE. CH1 LAGGED CH2 BY 2.31ns.

Chapter 5

5 SBS Experiments in Multimode Optical Fibres

The Chapter presents the results from using multimode optical fibres as the SBS medium, which includes the observations and investigations of SBS threshold reduction, SBS reflectivity, and Stokes and transmitted pulses dynamical behaviour. Initially it was planned to include both reflectivity and fidelity measurements, using fibres with different core diameters, and to test the fibres lengths with wider choices. But due to the very limited time available, only the peak power reflectivity, and pulse dynamical behaviour were performed. The results obtained were preliminary, and measurements were taken only once for each configuration. Therefore, we cannot claim the results are repeatable and reliable, and more quality results are needed in order to understand and explain completely the SBS characteristics and performance in optical fibres. Nevertheless, the preliminary results presented here provide a good pathway to pursue further research in SBS using optical fibres.

5.1 Properties of Optical Fibres

SBS process can occur in single-mode optical fibres as it involves only the initiation and generation of Stokes beam from the pump beam. However, OPC cannot occur in single-mode fibres because they could not confine and guide the non-uniform, aberrated pump beam as needed for OPC experiments [46]. The reason is that the single-mode fibres do not allow mode selection and distribution of the aberrated pump beam inside the fibre core apart from the fundamental mode. The aberrated pump beam can be thought of as an optical image, which can be expressed as the sum of the bound and unbound modes of the

fibre [89]. For single-mode fibre, since it can only accommodate the fundamental mode, all higher order modes are excluded, making the modal decomposition not energy conserved, and hence could not perform OPC. Therefore, multimode optical fibres were used to investigate the SBS and phase conjugate abilities in optical fibres. The fibres used were germanium-doped silica core, concentric glass cladding, graded index fibres with 62.5μm core and 125μm cladding diameters (Corning 62.5/125 CPC6). The fibres had a numerical aperture of 0.275 and an attenuation constant of <0.7dB/km at 1300nm wavelength [88]. The lengths of the fibre used ranged from one to four meters. Table 5.1 gives the SBS related properties of typical silica fibres.

In order to couple the pump beam into the fibre core efficiently, a specially designed fibre holder was made to provide four degrees of freedom. Different focal length lenses were tested to obtain the highest laser-to-fibre coupling efficiency. It was found that using a positive achromatic lens (biconvex, f = 10cm) yielded a very good coupling efficiency, which was measured to be 82%.

TABLE 5.1 SBS RELATED PROPERTIES OF SiO_2 (FIBRE) AT 1.55μM. FROM REF. [46, 48, 61].

Brillouin frequency shift (GHz)	11.2
Hypersound velocity (m/s)	5960
Brillouin linewidth (MHz)	69.2
Brillouin gain factor (cm/GW)	5
Phonon lifetime (ns)	4.6
Refractive index	1.46

It was observed that the pump conditions were crucial in obtaining SBS in fibres. Two conditions were required: (1) pump pulse width needed to be ≥25ns, and (2) the pump needed to operate in single longitudinal mode. When the pump pulse width was less than 25ns, no SBS was observed and the pump pulse simply transmitted through to the end of the fibre. We did not know the reason. From both the published results [20, 21, 23, 46] and our observation, the optimal pump pulse width was around 30ns. When the pump was not in single longitudinal mode, there was either no or only very weak Stokes pulse generated and had large variations in terms of pulse temporal profile and peak power. In the case of single longitudinal mode operation, SBS threshold depended on the ratio between the pump and Brillouin linewidths. If the pump linewidth becomes small compared to

Brillouin linewidth, the interaction length in fibre is no longer limited by the coherence length of the pump laser [20].

Fresnel reflections from the ends of the fibre were observed when the pump was below SBS threshold. Fig. 5.1 (A) shows the Fresnel reflections from both front and back ends of the fibre. The first peak was from the front end, while the second peak was from the back end of the fibre. From the Figure, the peak-to-peak separation was about 41.3ns, which was exactly the round-trip of the 4.2m fibre used. The round-trip is given by $t_r = 2nL/c$, where n is the refractive index, L is the fibre length and c is speed of light. For n = 1.46 and L = 4.2m, t_r = 40.9ns. Fig. 5.1 (B) shows the Fresnel reflection from the front face only. Note the second peak due to the back end reflection had disappeared.

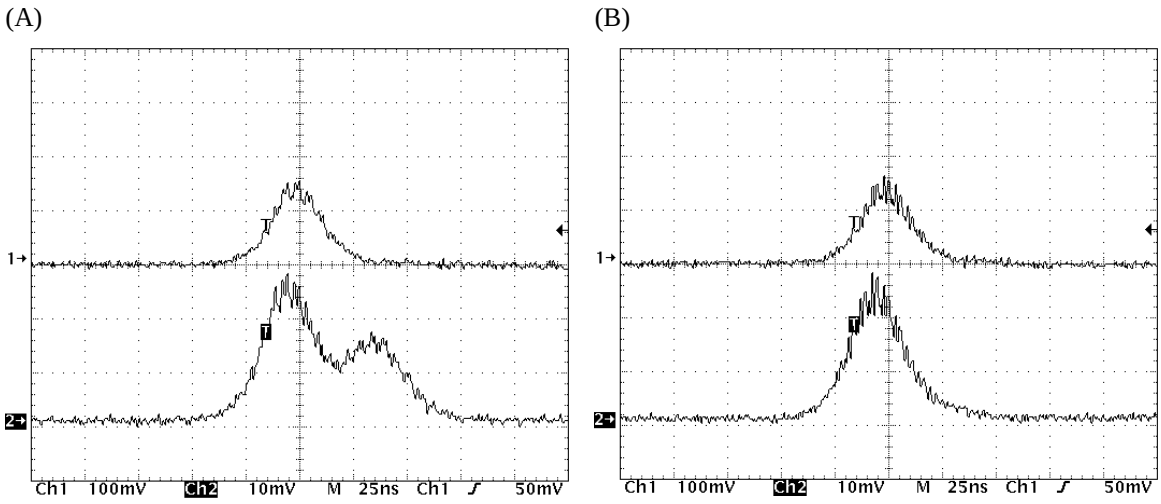

FIGURE 5.1 FRESNEL REFLECTIONS FROM BOTH ENDS (A) AND FRONT END (B) OF THE 62.5μM CORE FIBRES. CH1 = PUMP PULSE, CH2 = REFLECTED PULSE.

The Fresnel reflection had negligible influence on the SBS performance, and was suppressed once the pump was above SBS threshold, provided the ends of the fibre were flat and not damaged. If the ends of the fibre were damaged, then the back reflection could be seen at the base of the Stokes pulse, which appeared as a flat bed underneath the Stokes pulse. This was observed in some of our measurements (Fig. 5.2) when the front face of the fibre end was damaged and had a dark spot in the core when viewed under microscope. There was a very strong back reflection from the front face of the fibre, and it did not disappear even when Stokes pulse was formed, but increased linearly with the pump power. At just above SBS threshold (Fig. 5.2 (A)), the reflection from the damaged front face of the fibre was clearly seen (lower peak in Ch2) in addition to the generated Stokes

pulse (higher, narrow peak in Ch2). Comparing the Stokes pulse generated at threshold from a normal flat front face (Fig. 5.2 (B)), the front face reflection was suppressed by the much higher power Stokes pulse. At higher pump level, the reflection from the damaged front face can still be seen at the base of the Stokes pulse (Fig. 5.2 (C)). But for the Stokes pulse from the flat front face fibre without damage, the front face reflection had totally disappeared (Fig. 5.2 (D)), and had negligible contribution to the overall SBS reflection compare to the SBS Stokes pulse. Damaged fibres might still be able to initiate SBS and generate Stokes pulse, but this resulted in higher SBS threshold, lower reflectivity and poor fidelity. We believe this might be one of the reasons for having peculiar results observed for SBS reflectivity as a function of fibre length, which are presented in the next section.

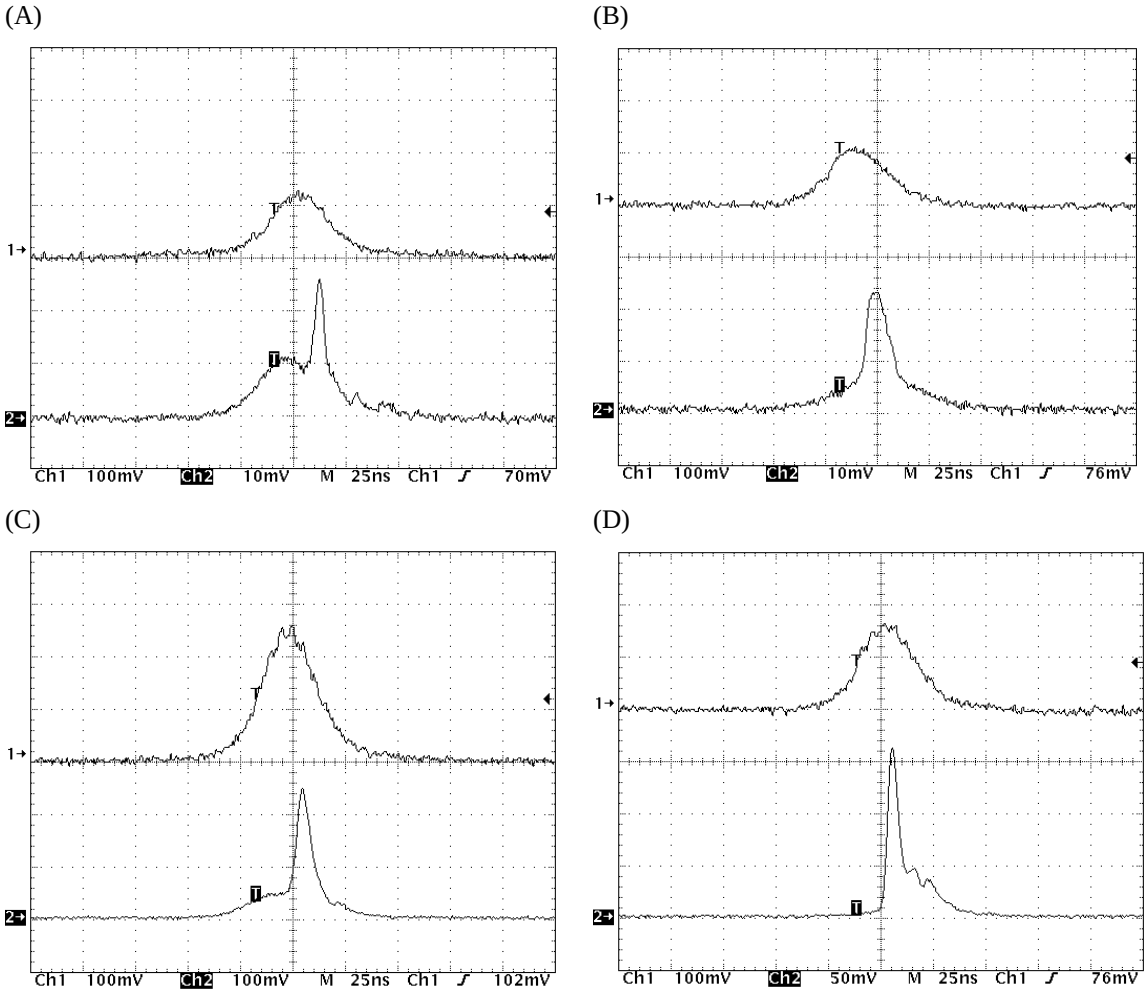

FIGURE 5.2 STOKES PULSES FROM A PARTIALLY DAMAGED FRONT FACE (A & C) AND FROM A NORMAL FLAT FRONT FACE (B & D) OF THE 62.5µM CORE FIBRES. CH1 = PUMP PULSE, CH2 = REFLECTED PULSE. CH1 LAGGED CH2 BY 2.31ns. NOTE THE DIFFERENCE IN AMPLITUDE (VERTICAL) SCALE OF CH2.

5.2 SBS Reflectivity of Optical Fibres

Fig. 5.3 shows the peak power reflectivity of fibres of various lengths using an unaberrated (without aberrator) pump beam as a function of pump energy. The lines on the graph were the curve-fits of the data points for respective fibre lengths for easier viewing only. The threshold energy and maximum peak power reflectivity respectively, for 1m fibre were 17.8μJ ($R_{SBS} \approx 6\%$) and 52%, for 2m were 16.5μJ ($R_{SBS} \approx 4\%$) and 62%, for 3m were 15.4μJ ($R_{SBS} \approx 5\%$) and 50%, and for 4m were 15.1μJ($R_{SBS} \approx 5.0\%$) and 71%. Out of all fibre lengths, the lowest threshold was 15.1μJ and the maximum peak power reflectivity of 71% occurred at 5 times the threshold, both were from the 4m fibre. Unlike the case of SBS in open cells, the pump energy range was limited by the damage threshold of the fibre, which had a much smaller range than the maximum allowable range (about 45mJ) from the experimental setup. From the graph we see that there seemed to have no direct relationship between the power reflectivity and the fibre length, although the rate of increase in reflectivities were about the same for all fibre lengths. In comparing the reflectivity with SBS liquids, fibres generally had lower reflectivity, say Fluorinert and Acetone. We had higher reflectivity than that observed by others using similar and longer fibres [20, 22, 23], but relatively less than that observed in tapered single mode fibres [21].

As stated at the beginning of the Chapter, the measurements were only taken once for each fibre length, and there could be large measurement errors in the results. Therefore, it is difficult to come up with any definite conclusions about the relationship of reflectivity and fibre length with these primitive results. However, one possible reason of having such relationship between the power reflectivity and fibre length could be related to the randomness of Stokes pulse temporal, dynamical behaviour. As will be mentioned in Section 5.3 there was a direct influence of the temporal profiles of the Stokes pulse to the power reflectivity. Two examples of unusual but typical and frequently observed Stokes pulse profiles will be explained in Section 5.3.2.

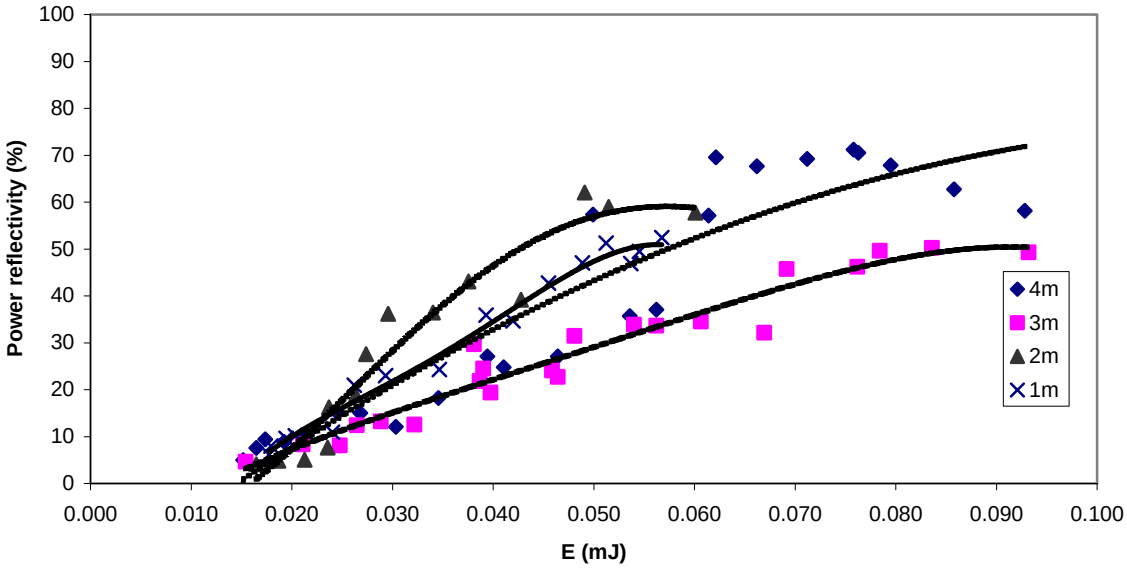

FIGURE 5.3 POWER REFLECTIVITY VS THRESHOLD ENERGY RATIO OF 62.5μM CORE FIBRE OF DIFFERENT LENGTHS WITHOUT ABERRATOR. EACH DOT REPRESENTS AN AVERAGE OF 5 PULSES. THE LINES ARE FOR EASIER VIEWING ONLY.

Fig. 5.4 shows the SBS threshold energy as a function of fibre length by an unaberrated pump beam. The theory line on the graph was based on Eq. (2.2.29), and the error bars were the measurement uncertainties. There was a 2.6μJ reduction in threshold energy from 1m to 4m long fibre. The SBS threshold decreased with increased fibre length within the uncertainty limits, except for the 4m fibre. We did not have time to investigate the cause, but the more likely reason could be some errors involved during measurements, such as large uncertainty in measurements and mistakenly moved the fibre position. There might be another reason that was related to the number of longitudinal modes of the pump interacting in the fibre. If the frequency separation of two longitudinal laser modes is large compared to the half Brillouin linewidth and a uniform energy distribution exists among all longitudinal laser modes, then the SBS threshold is directly proportional to the number of interacting laser modes [20]. But because both the separation of longitudinal laser mode and the half Brillouin linewidth were not measured, we could not justify it.

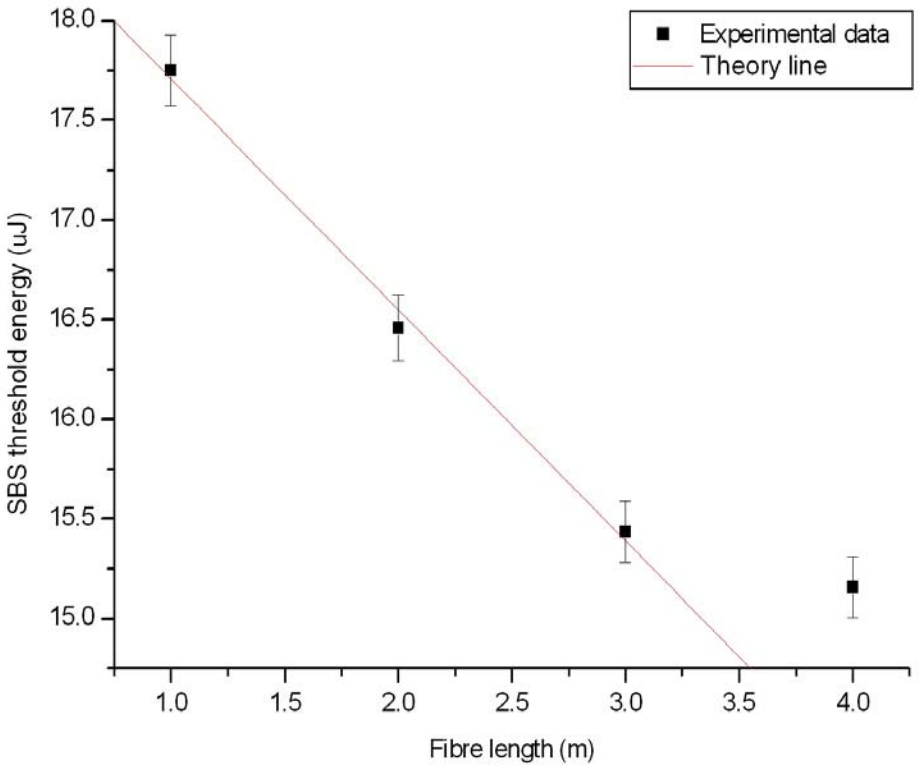

FIGURE 5.4 SBS THRESHOLD ENERGY OF 62.5μM CORE FIBRE WITHOUT ABERRATOR FOR DIFFERENT FIBRE LENGTHS. EACH DOT REPRESENTS AN AVERAGE OF 5 PULSES. THEORY LINE IS BASED ON EQ. (2.2.29).

Fig. 5.5 shows the peak power reflectivity of fibres of various lengths using an aberrated pump beam (with aberrator) as a function of threshold energy ratio. The lines on the graph were curve-fits of the data points for easier viewing only. The threshold energy and maximum peak power reflectivity respectively, for 1m fibre were 27.0μJ ($R_{SBS} \approx 4\%$) and 13%, for 2m were 19.1μJ ($R_{SBS} \approx 4\%$) and 39%, for 3m were 18.1μJ ($R_{SBS} \approx 4\%$) and 24%, and for 4m were 21.6μJ ($R_{SBS} \approx 3\%$) and 23%. From all fibre lengths measured, the lowest threshold was 18.1μJ from the 3m fibre and the maximum peak power reflectivity was 39%, occurred at about 2.5 times the threshold from the 2m fibre. The overall power reflectivities were very low for all fibre lengths. Similar to the case for unaberrated pump beam, there seemed to have no direct relationship between the power reflectivity and the fibre length. However, the power reflectivity of the 2m fibre was distinctively higher than that of other fibre lengths, while the fibres of other lengths had similar reflectivity curves.

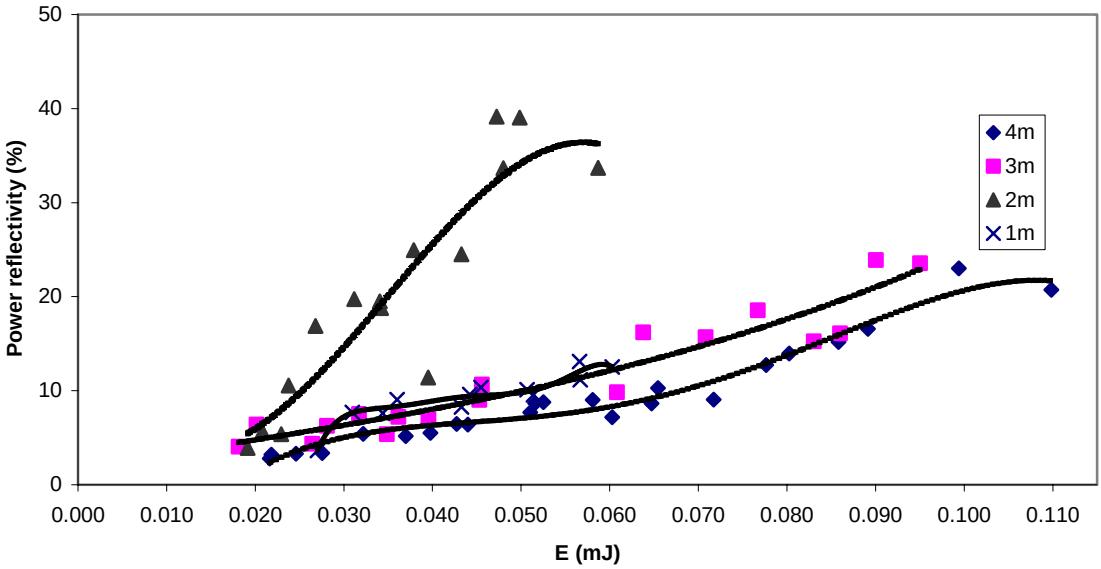

FIGURE 5.5 POWER REFLECTIVITY VS PUMP ENERGY OF 62.5μM CORE FIBRE OF DIFFERENT LENGTHS WITH ABERRATOR. EACH DOT REPRESENTS AN AVERAGE OF 5 PULSES. THE LINES ARE FOR EASIER VIEWING ONLY.

Fig. 5.6 shows the SBS threshold energy as a function of fibre length by an aberrated pump beam (with aberrator). The theory line on the graph was based on Eq. (2.2.29), and the error bars were measurement uncertainties. There was a 5.4μJ reduction in threshold energy from 1m to 3m long fibre, almost twice in the amount of threshold reduction to that by the unaberrated pump beam. From the graph we can see that the threshold energy decreased with increasing fibre length, although the threshold for the 2m was lower than expected (from theory) and for the 4m fibre was unusually higher than expected. As in the case for unaberrated pump beam (Fig. 5.4), there was not enough time to further investigate the disagreements with the theory. The possible reasons were given earlier. For both unaberrated and aberrated pump beams, they agreed (though not rigorously) with the well-known relationship, that the SBS threshold is inversely proportional to the interaction length of the SBS medium. According to Eq. (2.2.29) for optical fibres, to lengthen the interaction length is one of the easier ways to reduce the SBS threshold.

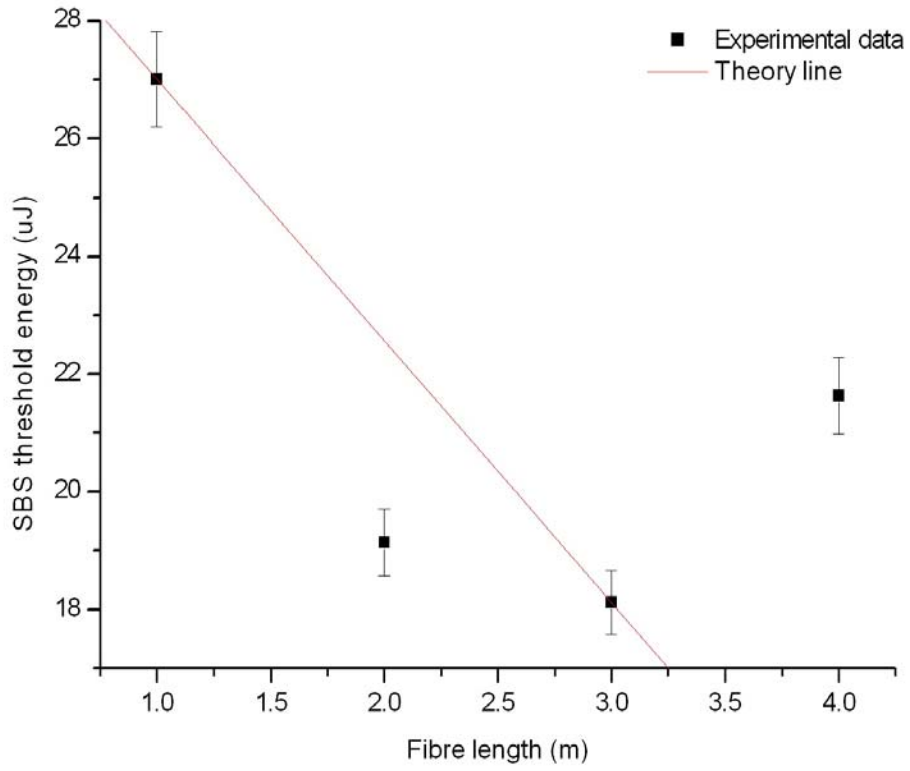

FIGURE 5.6 SBS THRESHOLD ENERGY OF 62.5μM CORE FIBRE WITH ABERRATOR FOR DIFFERENT FIBRE LENGTHS. EACH DOT REPRESENTS AN AVERAGE OF 5 PULSES. THEORY LINE IS BASED ON EQ. (2.2.29).

5.3 Pulse Dynamical Behaviour in Optical Fibres

5.3.1 General Descriptions

In most of the SBS experiments in optical fibres, the Stokes wave intensity exhibited complicated and random dynamical behaviour as a function of time. The Stokes wave can display large intensity fluctuations due to either deterministic or stochastic processes. Deterministic process exhibits the relaxation oscillations as a result of the rapid turn-on effect of the pump wave. Stochastic process is the random and spontaneous scattering that occurred to initiate the SBS process, in which case the Stokes wave inherited certain noise properties [46, 52].

In order to understand the Stokes pulse dynamical behaviour, we look at the physical picture of how the SBS process works inside the fibre. Fig. 5.7 shows schematically

typical power levels of the pump and Stokes waves inside an optical fibre [46]. The whole fibre length is conceptually divided into three regions. In Region 1 of Fig. 5.7, if the pump power is below SBS threshold, most of the power is transmitted through without noticeable pump depletion. In other words, the pump power simply transmits through the fibre with the power depletion mainly comes from the scattering and attenuation. This is the reason that SBS is not a severe problem in telecommunications, because in most cases, the transducer operates at low power levels, much lower the SBS power threshold. However, if the pump power is above the SBS threshold, depletion starts to occur as the pump wave is converted into Stokes wave. The pump power is depleted appreciably in Region 2 of Fig. 5.7, and the Stokes power increases slightly without much amplification. A final amplification of the Stokes power comparable to the pump power occurs in Region 3 of Fig. 5.7. The unconverted pump wave will be simply transmitted. The length of Region 3 depends on the phonon lifetime [46]. Agrawal [48] mentioned that most of the power transfer occurs at the first 20% of the fibre length, which can be considered as the length of Region 3. This is experimentally confirmed by Eichler *et al* [20] that only the first 2m of their 10m long fibre (i.e. 20% of fibre length) participated constructively in the SBS process.

Ref. [46] further explains the Stokes pulse dynamical behaviour as well as temporal fluctuations. The Stokes pulse temporal fluctuations arise from the fact that SBS in fibre is generated and amplified by spontaneous Stokes noise in Region 1 of Fig. 5.7, and that the Stokes pulse would inherit this random, noise-like properties. Phonon lifetime plays an important role in the dynamical behaviour of Stokes pulse. For example, in the steady amplification regime where the duration of the undepleted fraction of the pump wave is much longer than the phonon lifetime, the Stokes pulse temporal fluctuations is typically in order of four times the phonon lifetime. In the case where the undepleted fraction is shorter than the phonon lifetime, the Stokes pulse broadens and depends on the duration of undepleted fraction of pump wave and the steepness of its leading edge. On the other hand, if the pump pulse width is larger than the fibre transit time (i.e. half of the fibre round trip time), then Stokes pulse has periodic oscillations with the modulation period that is related to the fibre round trip time ($T = 2nL/c$) and phonon lifetime (τ). For $\tau/T < 0.05$ the modulation period is $2nL/c$, and the period increases as the ratio τ/T increases. The modulation becomes aperiodic when $\tau/T > 0.1$. The Stokes intensity fluctuations are

generally smaller in multimode fibres because of the averaging of intensities over different fibre modes.

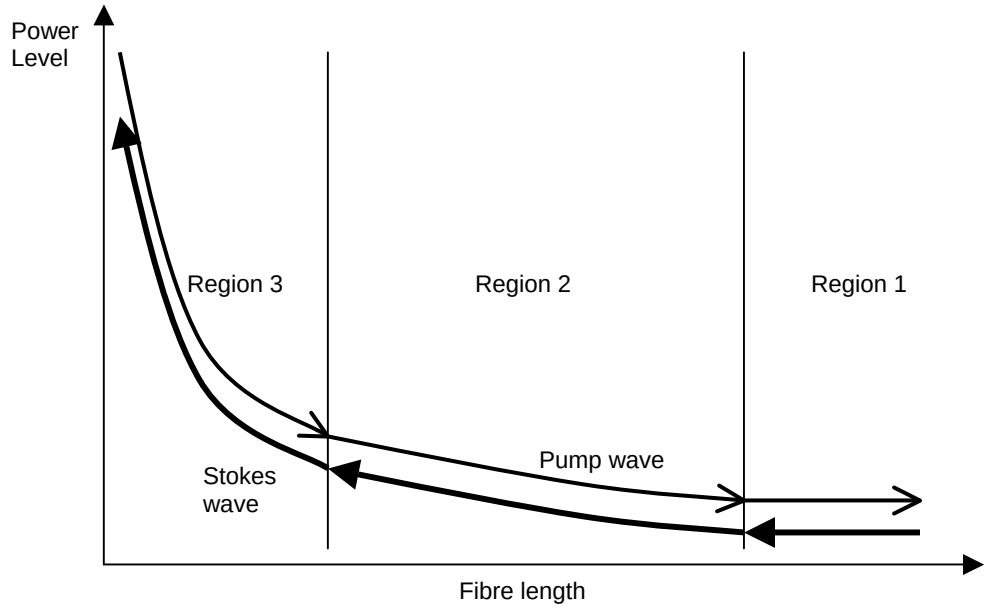

FIGURE 5.7 POWER DISTRIBUTION OF THE PUMP AND STOKES WAVES INSIDE AN OPTICAL FIBRE. FROM REF. [46].

Typical Stokes pulses taken during measurements of different fibre lengths are shown without the aberrator in Fig. 5.8 and with aberrator in Fig. 5.9. Pulse from Ch2 led the pulse from Ch1 by 2.31ns. The Stokes pulses without aberrator had random, complex temporal structures. As will be mentioned in Section 5.3.3, even when the Stokes pulses had these features, the fibre transmitted pulses did not reveal much information about the mechanism of how they were formed and behaved. The transmitted pulses appeared to be typical ones observed in ordinary SBS open cells, even when their corresponding Stokes pulses were having intensity fluctuations and/or periodic modulations. On the other hand, the Stokes pulses with aberrator appeared to have more distinct and simple features with narrowed pulse widths, and had less intensity fluctuations with time. Most of the pulses had only a single intensity peak with relaxation oscillations followed. The reason for such big difference to the Stokes pulse without aberrator was not known, as there was not enough time to carry out further investigation.

(A) 4m fibre

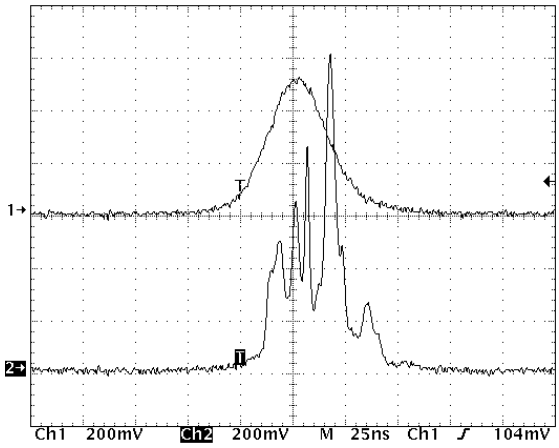

(B) 3m fibre

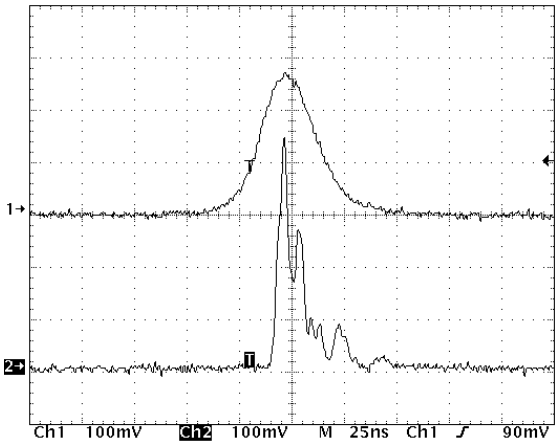

(C) 2m fibre

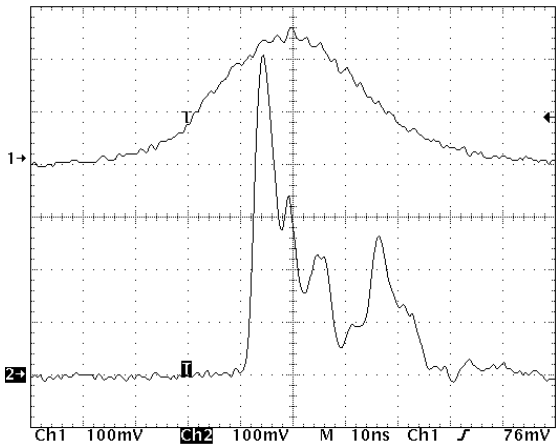

(D) 1m fibre

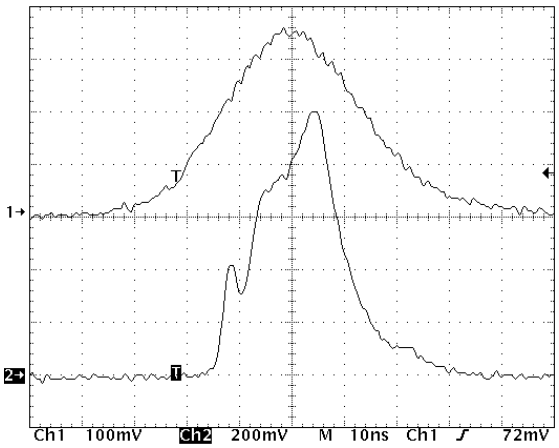

FIG. 5.8 SNAPSHOTS OF TYPICAL STOKES PULSES TAKEN DURING MEASUREMENTS OF DIFFERENT FIBRE LENGTHS WITHOUT ABERRATOR. CH1 = TRANSMITTED PULSE, CH2 = STOKES PULSE. CH1 LAGGED CH2 BY 2.31ns. NOTE THE DIFFERENCE IN TIME (HORIZONTAL) AND AMPLITUDE (VERTICAL) SCALES.

(A) 4m fibre

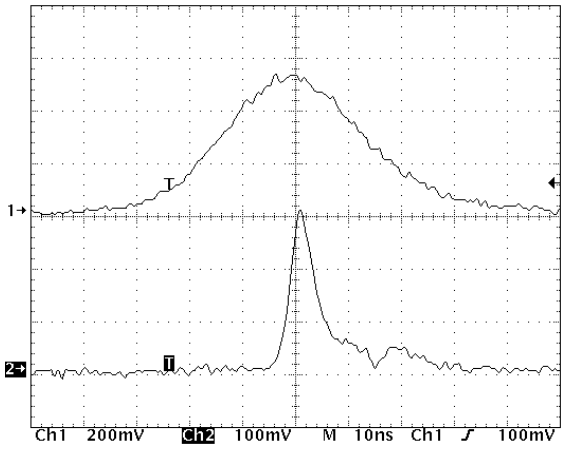

(B) 3m fibre

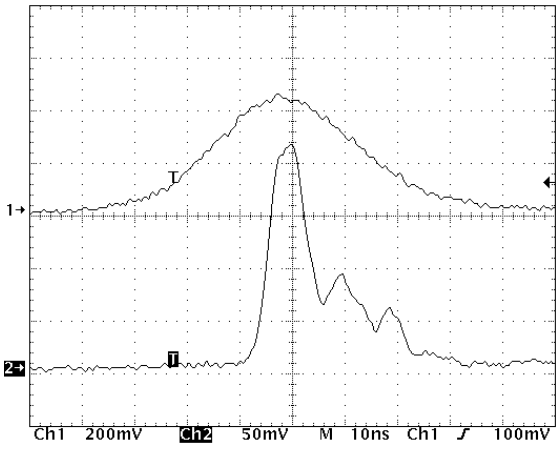

(C) 2m fibre

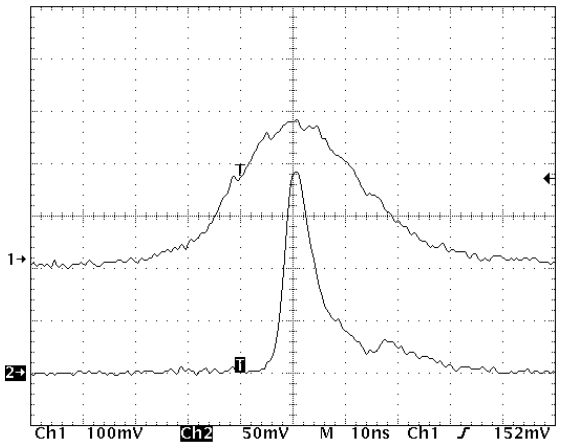

(D) 1m fibre

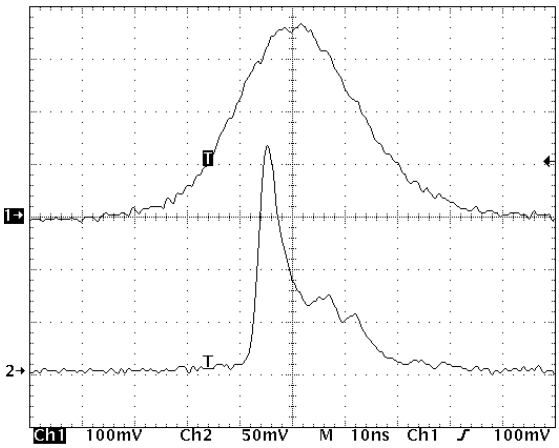

FIG. 5.9 SNAPSHOTS OF TYPICAL STOKES PULSES TAKEN DURING MEASUREMENTS OF DIFFERENT FIBRE LENGTHS WITH ABERRATOR. CH1 = TRANSMITTED PULSE, CH2 = STOKES PULSE. CH1 LAGGED CH2 BY 2.31ns. NOTE THE DIFFERENCE IN TIME (HORIZONTAL) AND AMPLITUDE (VERTICAL) SCALES.

5.3.2 Unusual Stokes Pulse Temporal Behaviour

Broadly speaking, there were two types of unusual Stokes pulse temporal behaviours observed frequently in our fibre experiments. They were unlike the Stokes pulses generated in ordinary SBS open cells, and were never observed in our open cells (test tubes) experiments. During the power reflectivity measurements, occasional individual readings reached above 90% were recorded. These readings appeared in all fibre lengths tested, and had certain Stokes pulse properties in common: (1) for a single pulse, a single distinct high peak with a series of low oscillatory peaks; (2) for a single pulse, the pulse width of the distinct high peak was highly compressed down to a few nanoseconds; (3) temporal profile of each single pulses observed successively were stochastic that they did

not follow any orderly or predictable manner, i.e., the occurrences of high reflectivity was random and independent of the amount of pump energy (provided it was above the SBS threshold).

Fig. 5.10 shows images of such unusually high power reflectivity, highly compressed Stokes pulses taken during measurements of different fibre lengths. Pulse from Ch2 led the pulse from Ch1 by 2.31ns. The average value of the peak power reflectivities was above 90%, and the average pulse width of the highest peak was around 3 – 8ns. There are relatively few published papers that specifically explained this kind of behaviour: unusually high peak power reflectivity (from a single, distinct intensity peak in each Stokes pulse) that is independent of pump power once above SBS threshold, and its associated Stokes pulse temporal behaviour in multimode optical fibre, pumped by a Q-switched, pulsed laser source. One possible reason could be the formation of a Brillouin oscillator by the end faces of the fibre under high Brillouin gain conditions, as mentioned in Ref. [52]. The Stokes wave produced in the Brillouin oscillator can exhibit random and oscillatory dynamical behaviour in the early SBS stage where it was initiated by spontaneous scattering. The build-up of Stokes energy and pump depletion inside the fibre led to pulse compression-type of mechanism, in which a highly compressed Stokes pulse with very high reflectivity was produced. But as mentioned earlier in Section 5.1 and shown in Fig. 5.1, reflections from the fibre ends were dominant only below SBS threshold, and were negligible once SBS was established. This means even though this was possible that the end faces established a Brillouin oscillator, but it could not have contributed to the generation of Stokes pulses that possessed very high power reflectivities and stochastic temporal profiles.

(A) 4m fibre

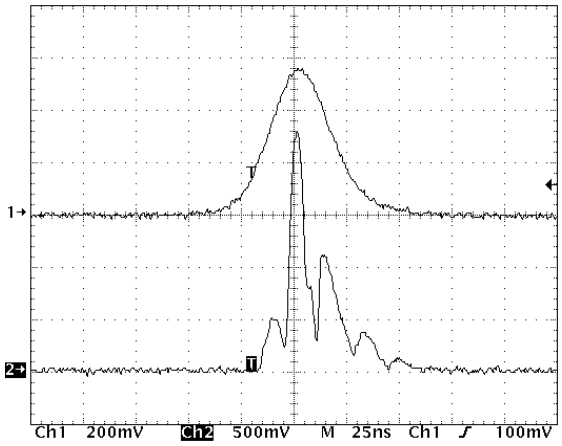

(B) 4m fibre

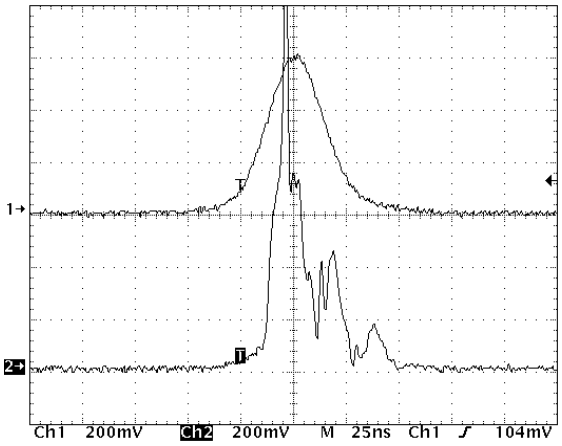

(C) 3m fibre

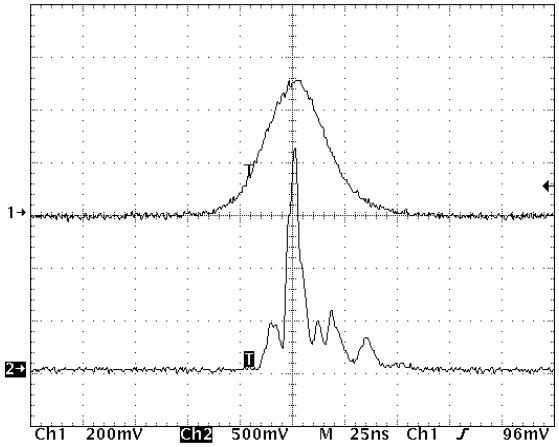

(D) 2m fibre

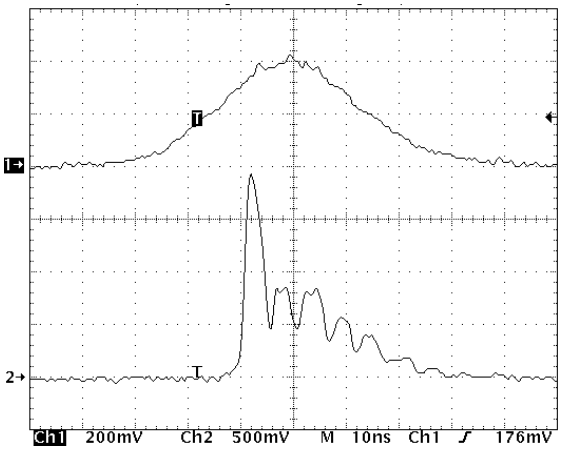

FIG. 5.10 SNAPSHOTS OF UNUSUALLY HIGH POWER REFLECTIVITY, HIGHLY COMPRESSED STOKES PULSES TAKEN DURING MEASUREMENTS OF DIFFERENT FIBRE LENGTHS. CH1 = PUMP PULSE, CH2 = STOKES PULSE. CH1 LAGGED CH2 BY 2.31ns. NOTE THE DIFFERENCE IN TIME (HORIZONTAL) AND AMPLITUDE (VERTICAL) SCALES.

In contrast to the distinct high power reflectivity and highly compressed single peaks, there was another unusual Stokes pulse temporal behaviour observed. The individual peaks of a Stokes pulse were similar in shape, intensity, width and modulated periods. Fig. 5.11 shows the images of such Stokes pulses taken during the measurements of different fibre lengths. Pulse from Ch2 led the pulse from Ch1 by 2.31ns. The figure shows that these temporal pulse profiles were independent of the pump power once the SBS process was established. Since the pump power appeared to be “shared” among the individual peaks, the average value of peak power reflectivity was less than 50%. Most explanations for this phenomenon were given in terms of periodic modulations due to finite fibre length [7, 21, 22, 46], stochastic nature of Stokes pulses in fibres [52], or a combined action of Brillouin gain and nonlinear Kerr effect [53, 85]. By measuring the separations of

successive peaks, it was found that they were separated by the amount close to the round-trip time of the fibres. For example in Fig. 5.11 (D), the 1m fibre has round-trip time of about 9.73ns, and the image showed the successive peaks had an average separation of 9.75ns. However, we also observed that not all of this kind of Stokes pulses had their peak separations equal to the round-trip time of the fibre. Nevertheless, we think the periodic modulations were the cause for such temporal behaviour. In addition, this periodically modulated Stokes pulses were different from the cases for high reflectivity and compressed Stokes pulses (Fig. 5.9), in which the separations of successive peaks were about half of the round-trip time instead of the full round-trip time. These two unusual temporal behaviours occurred less frequently in the shortest fibre (1m), in which the Stokes pulse profiles appeared to be similar to those produced in ordinary long length open cells.

(A) 4m fibre

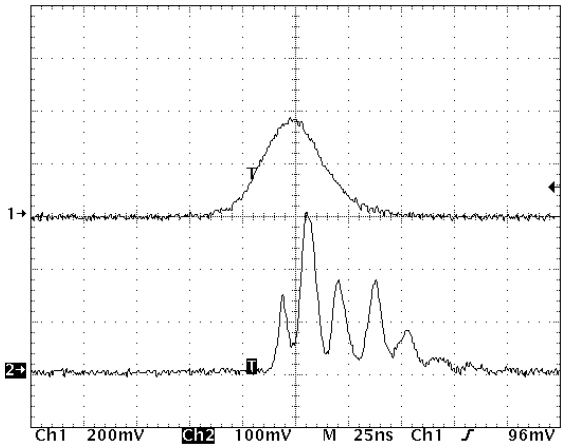

(B) 4m fibre

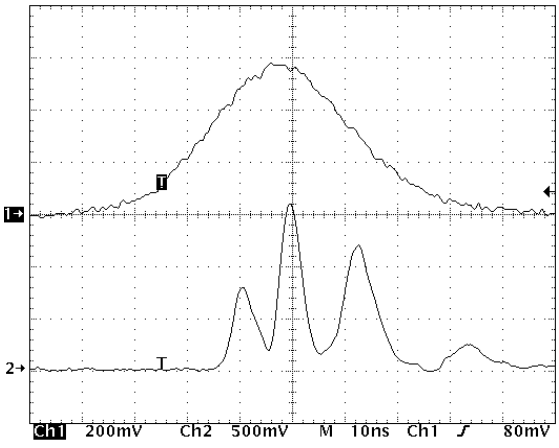

(C) 2m fibre

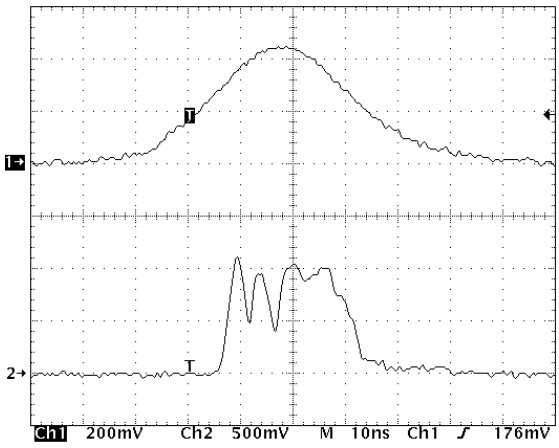

(D) 1m fibre

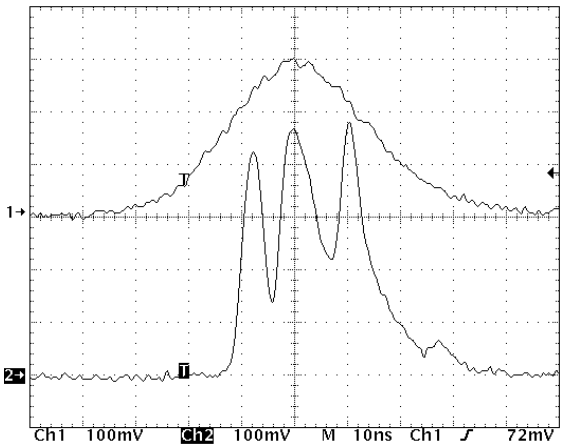

FIG. 5.11 SNAPSHOTS OF UNUSUAL, SIMILARLY MODULATED PEAKS OF THE STOKES PULSES TAKEN DURING MEASUREMENTS OF DIFFERENT FIBRE LENGTHS. CH1 = PUMP PULSE, CH2 = STOKES PULSE. CH1 LAGGED CH2 BY 2.31ns. NOTE THE DIFFERENCE IN TIME (HORIZONTAL) AND AMPLITUDE (VERTICAL) SCALES.

5.3.3 Fibre Transmitted Pulse Dynamical Behaviour

Fig. 5.12 shows images of transmitted and Stokes pulses taken during measurements of different fibre lengths. Pulse from Ch2 led the pulse from Ch1 by 2.31ns. Recall that Ch2 (Stokes pulse) was emerged from the front side of the fibre, while Ch1 (transmitted pulse) was emerged from the far end of the fibre. The apparent additional lag of the transmitted pulse was the transit time that the pump beam needed to travel through the whole length of the fibre before it reached to the photodetector at the exit of the fibre. Fig. 5.12 (A) shows a typical transmitted pulse: the leading part is similar to the pump pulse, once the SBS threshold was reached, most of the pump power was converted into Stokes pulse. This is identified in the transmitted pulse profile as a strong depletion seen in the tailing part of

the pulse, and only the non-converted portion of the pump pulse was transmitted. The corresponding Stokes pulse was a typical one produced in fibre. Fig. 5.12 (B) – (D) revealed that although the transmitted pulse profiles were typical and with some fluctuations after depletion, the corresponding Stokes pulses showed complicated structure that did not “match” the dynamical evolutions of the transmitted pulses. This raised a question of how did this random and complicated Stokes pulse structure come from and what was its mechanism. There are three possibilities: (1) the stochastic nature of the Stokes pulse that was formed in the SBS process that started off from Stokes noise, as mentioned earlier in this Section. (2) the finite fibre length and round trip time gave rise to periodic modulations and random fluctuations, which can be seen from the oscillations that appeared in the tailing parts of the transmitted pulses. (3) there might be some non-uniform, cracked or damaged spots within and along the fibre that acted like filters (as in fibre Bragg gratings) that partially blocked, leaked or reduced the amount of Stokes pulse propagating backward via total internal reflection inside the fibre. Further investigations are needed to verify these assumptions. In all three cases, the transmitted pulse was simply the unconverted or the non-participated portion of the pump pulse that was being transmitted through the fibre. Thus, they can be thought of as having separate interaction process from the pump-to-Stokes conversion process during SBS, and hence, their behaviour did not match their corresponding Stokes pulse dynamical evolution. This may be a valid assumption because the SBS process is a three wave optical parametric interaction between the pump, Stokes and acoustic waves. The transmitted wave is, strictly speaking, not involved in the SBS process, although it does reveal some of the temporal pulse dynamics and properties of the SBS process.

(A) 4m fibre

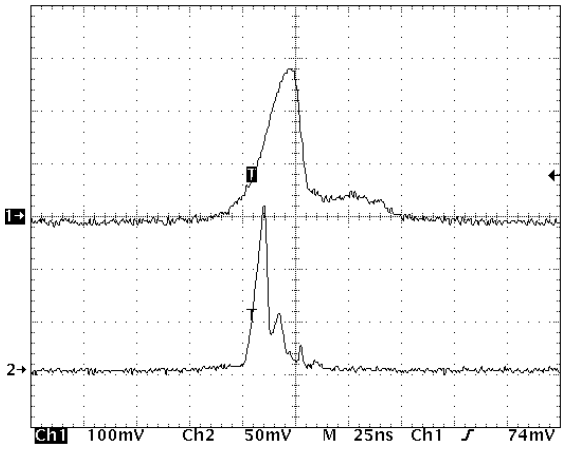

(B) 4m fibre

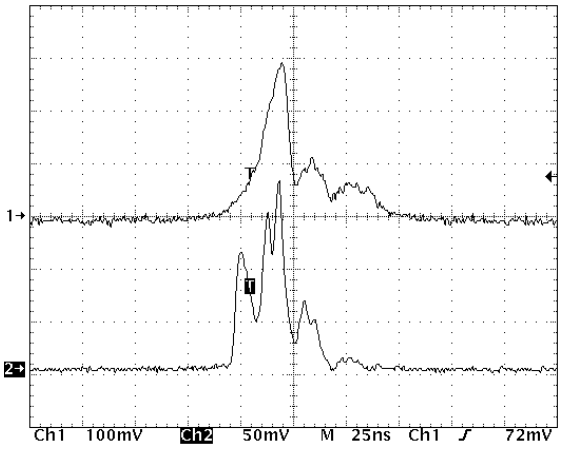

(C) 4m fibre

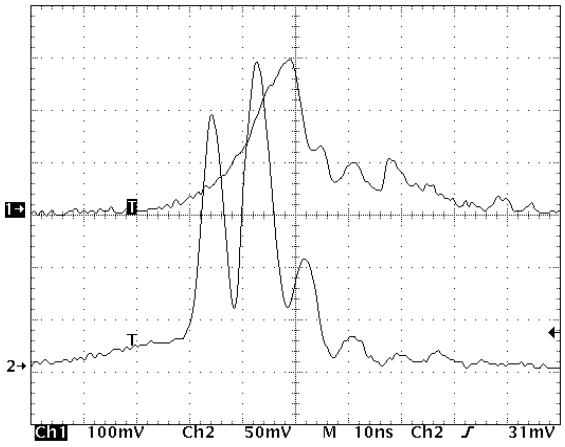

(D) 3m fibre

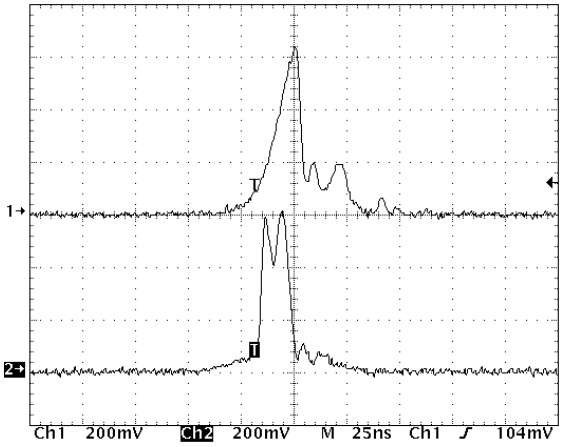

FIG. 5.12 SNAPSHOTS OF TRANSMITTED PULSES TAKEN DURING MEASUREMENTS OF DIFFERENT FIBRE LENGTHS. CH1 = TRANSMITTED PULSE, CH2 = STOKES PULSE. CH1 LAGGED CH2 BY 2.31ns. THE ADDITIONAL LAG OF THE TRANSMITTED PULSE (CH1) WAS THE TRANSIT TIME THAT THE PULSE TRAVELLED THROUGH THE WHOLE LENGTH OF THE FIBRE. NOTE THE DIFFERENCE IN TIME (HORIZONTAL) AND AMPLITUDE (VERTICAL) SCALES.

Chapter 6

6 Conclusion

6.1 Summary

The characteristics and performance of SBS in Fluorinert and Acetone have been studied through the characterisations of their SBS related properties. Fluorinert yielded the highest reflectivity and fidelity. For unaberrated pump beam, the threshold was 4.2mJ, maximum energy reflectivity was 95% and fidelity was close to 100%; whereas for aberrated pump beam, the threshold was 6.6mJ, maximum energy reflectivity was 80% and fidelity was 90%. Acetone exhibited good SBS performance with reasonably high reflectivity and fidelity. For unaberrated pump beam, the threshold was 5.9mJ, maximum energy reflectivity was about 70% and fidelity was 85%; while for aberrated pump beam, the threshold was 6.6mJ, maximum reflectivity was 62% and fidelity was 75%. These findings indicated that Fluorinert is an ideal SBS material that can be used in critical applications such as high power MOPA laser systems. As mentioned in Chapter 4, better results could be achieved if the liquids were ultra-filtered. The power reflectivity and fidelity were also studied. Generally, the power reflectivity and fidelity were higher than their energy measurements counterparts, and the measurement uncertainties were larger due to pulse-to-pulse variations in the temporal pulse profiles.

Phase correction of an aberrated beam was examined and was shown in Figs. 4.13 and 4.14. The aberrated beam was partially corrected, and the corresponding far-field patterns of the phase conjugated beam were quite similar to that of the original unaberrated beam. Optical breakdown occurred throughout the course of experiments and was mainly caused by excessive pump power and energy absorption by impurities present in the SBS

materials. Pulse compression was examined with a 60cm long SBS cell. It was observed that sharp-rise effect started when the distance between the front face of the cell and the effective focal plane was about 25cm, nearly half way of the cell. More complex structure and relaxation oscillation occurred at about 54cm and up to the whole length of the cell. But no explicit pulse compression was observed.

In contrast to SBS in Fluorinert and Acetone in open cells, optical fibres are optical light-guides where the SBS process was constrained by the physical and chemical properties of the fibres, and the light guided inside the fibres. Since the effective interaction length can be very long, the threshold can be a few orders of magnitude less than that of ordinary SBS materials in open cells. The measured lowest threshold was 15.2μJ (or 506.7W for a 30ns pulse width) obtained for the longest fibre (4m), and 17.8μJ (or 593.3W) for the shortest fibre (1m). The thresholds were 3 orders of magnitude less than that for Fluorinert or Acetone. This dramatic reduction in threshold was mainly due to the long interaction length and small interaction area of the fibres. Fibre Brillouin lasers and sensors have developed because of this advantage. Preliminary results showed that power reflectivity depended on the fibre length. The maximum power reflectivity was 70% (from the 4m fibre) for an unaberrated pump beam and 40% (from the 2m fibre) for an aberrated pump beam. The Stokes pulse temporal profiles appeared to have random, complex structures and fluctuations in intensity. The temporal structures of the Stokes and transmitted pulses were also dependent on the fibre length. The longer the fibre length, the more complex of the temporal structures. In addition, long fibres reduce the stability of fibre phase conjugators because severe depolarisation may occur [20]. Harrison *et al* [86] reported that the radiation transmitted through the fibre was totally depolarised, but the polarisation of Stokes radiation was linearly polarised. Imai *et al* [87] demonstrated that degree of polarisation of the Stokes wave is better for shorter fibres, which was measured to be above 95% in 0.5m fibres. Therefore, in applications where the SBS threshold needs to be reduced by using longer fibres, considerations need to be taken with other affecting factors such as the reflectivity, fidelity, and the spatial and temporal qualities of the Stokes wave.

6.2 Future Direction

A preliminary investigation of SBS in multimode optical fibres had performed, and there are more in-depth studies to be carried out. Ultimately, the design and construction of a distributed fibre Brillouin sensor for remote strain and temperature sensing have great potentials for military and industrial applications. Some suggestions are:

- Perform SBS (threshold, reflectivity and phase conjugate fidelity) measurements by varying the following parameters:
    - ◊ Fibre lengths – shorter (1cm to 20cm) and longer (in orders of 100m to 1km) fibre lengths;
    - ◊ Fibre core diameters – 10μm (single-mode) up to 800μm;
    - ◊ Fibre materials – glass, fused silica, polymer, and with dopants;
    - ◊ Pump conditions – pulse width, wavelength, degree of aberration, higher pulse repetition rate, and cw mode.
- Establish relationships between fibre parameters and SBS parameters – in particular, the dependence of Brillouin frequency shift to the change of refractive index of fibre under different tensions and heat conditions.
- Evaluate and conduct experiments to any SBS parameter that relate directly or indirectly to the fibre parameters, such as pump and Brillouin linewidths, polarisations of reflected and transmitted pulses.
- More in-depth investigation and explanation on the dynamical behaviour of the Stokes wave intensity and temporal profile. This can be done by conducting experiments and computational modelling.
- Methods and techniques of gathering and processing raw data obtained from the sensing elements.
- Design and construction of an optical signal analyser to analyse and demodulate the raw data obtained.
- Design, construction and implementation of a compact, lightweight and portable fibre Brillouin sensor prototype for field-testing.

Bibliography

[1] R.Y. Chiao, C.H. Townes and B.P. Stoicheff, Phys. Rev. Lett., 12, 592 (1964)

[2] R.A. Fisher (ed.), Optical Phase Conjugation, Academic Press, NY (1983)

[3] D.A. Rockwell, IEEE J. Quantum Electron., 24, 1124 (1988)

[4] J. AuYeung *et al*, IEEE J. Quantum Electron., 15, 1180 (1979)

[5] O.Yu. Nosach *et al*, Sov. Phys. JETP Lett., 16, 435 (1972)

[6] V. Wang and C.R. Giuliano, Opt. Lett., 2, 4 (1978)

[7] E.P. Ippen and R.H. Stolen, Appl. Phys. Lett., 21, 539 (1972)

[8] K.O. Hill, B.S. Kawasaki and D.C. Johnson, Appl. Phys. Lett., 28, 608 (1976)

[9] N.A. Olsson and J.P. van der Ziel, Appl. Phys. Lett., 48, 1329 (1986)

[10] C. Culverhouse *et al*, Electron. Lett., 25, 914 (1989)

[11] X. Bao, D.J. Webb and D.A. Jackson, Opt. Lett., 18, 552 (1993); Opt. Lett., 18, 1561 (1993)

[12] X. Bao, D.J. Webb and D.A. Jackson, Opt. Commun., 104, 298 (1994); Opt. Lett., 9, 141 (1994)

[13] P.C. Wait, K. De Souza and T.P. Newson, Opt. Commun., 144, 17 (1997)

[14] V. Lecouche *et al*, Opt. Commun., 168, 95 (1999)

[15] C.J. Duffy and R.P. Tatam, Appl. Opt., 32, 5966 (1993)

[16] X.S. Yao for NASA's Jet Propulsion Laboratory, Internet resource: http://www.nasatech.com/Briefs/May98/NPO20091.html

[17] N.A. Olsson and J.P. van der Ziel, J. Lightwave Technol., LT-5, 147 (1987)

[18] L. Brillouin, Ann. Phys., 17, 88 (1922)

[19] B.Ya. Zel'dovich *et al*, Sov. Phys. JETP Lett., 15, 109 (1972)

[20] H.J. Eichler, J. Kunde and B. Liu, Opt. Commun., 139, 327 (1997)

[21] A. Heuer and R. Menzel, Opt. Lett., 23, 834 (1998)

[22] C. Hanisch, A. Heuer and R. Menzel, Appl. Phys. B, 73, 851 (2001)

[23] H.J. Eichler *et al*, Opt. Commun., 208, 427 (2002)

[24] G.K.N. Wong and M.J. Damzen, J. Mod. Opt., 35, 483 (1988)

[25] G.K.N. Wong and M.J. Damzen, IEEE J. Quantum Electron., 26, 139 (1990)

[26] D.T. Hon, Opt. Lett., 5, 516 (1980)

[27] V. Devrelis, Fidelity of optical phase conjugation using stimulated Brillouin scattering, Ph.D. thesis, The University of Adelaide (1997)

[28] C.B. Dane, W.A. Neuman and L.A. Hackel, IEEE J. Quantum Electron., 30, 1907 (1994)

[29] P. Klövekorn, Time dependent nonlinear optics using a phase conjugated laser, Ph.D. thesis, The University of Adelaide (1997)

[30] M.J. Damzen and M.H.R. Hutchinson, IEEE J. Quantum Electron., 19, 7 (1983)

[31] D.A. Rockwell and C.R. Giuliano, Opt. Lett., 11, 147 (1986)

[32] M. Valley, G. Lombardi and R. Aprahamian, J. Opt. Soc. Am. B, 3, 1492 (1986)

[33] B.C. Rodgers, T.H. Russell and W.B. Roh, Opt. Lett., 24, 1124 (1999)

[34] S. Sternklar *et al*, Opt. Lett., 15, 469 (1990)

[35] S. Afshaarvahid, Transient phase conjugation using stimulated Brillouin scattering, Ph.D. thesis, The University of Adelaide (2001)

[36] S. Afshaarvahid, V. Devrelis and J. Munch, Phys. Rev. A, 57, 3961 (1998)

[37] S. Afshaarvahid *et al*, Phys. Rev. A, 64, 043803-1 (2001)

[38] M. O'Connor, A study of stimulated Brillouin scattering and its application to phase conjugate oscillators, Ph.D. thesis, The University of Adelaide (1997)

[39] I.Yu. Anikeev, Study of limiting factors and methods of optical phase conjugation by stimulated Brillouin scattering, Ph.D. thesis, The University of Adelaide (2000)

[40] M.S. Jo, B.I. Choi and C.H. Nam, Opt. & Quantum Electron., 27, 405 (1995)

[41] M.S. Mangir *et al*, Phys. Rev. Lett., 68, 1702 (1991)

[42] M.R. Osborne and M.A. O'Key, Opt. Commun., 94, 346 (1992)

[43] R.A. Fisher (ed.), Optical Phase Conjugation, Academic Press, NY (1983)

[44] W. Kaiser and M. Maier, *Stimulated Rayleigh, Brillouin and Raman spectroscopy*, in Laser Handbook, edited by F.T. Arecchi and E.O. Schulz-Dubois, North-Holland, Amsterdam (1972)

[45] B.Ya. Zel'dovich, N.F. Pilipettshii and V.V. Shkunov, Principles of Phase Conjugation, Springer-Verlag, NY (1985)

[46] M. Gower and D. Proch (ed.), Optical Phase Conjugation, Springer, Berlin (1994)

[47] G.S. He, Progress in Quantum Electronics, 26, 131 (2002)

[48] G.P. Agrawal, Nonlinear Fiber Optics 2nd Ed., Academic Press, San Diego (1995)

[49] D. Cotter, Electron. Lett., 18, 495 (1982)

[50] H.J. Eichler *et al*, Opt. Commun., 123, 412 (1996)

[51] S. Le Floch, F. Riou and P. Cambon, J. Opt. A: Pure Appl. Opt., 3, L12 (2001)
[52] A.L. Gaeta and R.W. Boyd, Phys. Rev. A, 44, 3205 (1991)
[53] H. Li and K. Ogusu, Jpn. J. Appl. Phys., 38, 6309 (1999)
[54] V.I. Kovalev and R.G. Harrison, Opt. Commun., 204, 349 (2002)
[55] A. Höök, J. Opt. Soc. Am. B, 8, 1284 (1991)
[56] G. Grosso and A. Höök, J. Opt. Soc. Am. B, 10, 946 (1993)
[57] R.H. Stolen, IEEE J. Quantum Electron., 15, 1157 (1979)
[58] V.I. Kovalev and R.G. Harrison, Phys. Rev. Lett., 85, 1879 (2000)
[59] C.N. Pannell, P.St.J. Russell and T.P. Newson, J. Opt. Soc. Am. B, 10, 684 (1993)
[60] G.P. Agrawal, Fiber-Optic Communication Systems, Wiley, NY (1992)
[61] R. Menzel, Photonics, Springer, Berlin (2001)
[62] R.W. Boyd, Nonlinear Optics, Academic Press, San Diego (1996)
[63] R.W. Boyd, K. Rzążewski and P. Narum, Phys. Rev. A, 42, 5514 (1990)
[64] G.C. Valley, IEEE J. Quantum Electron., 22, 704 (1986)
[65] L. Chen and X. Bao, Opt. Commun., 152, 65 (1998)
[66] C.L. Tang, J. Appl. Phys., 37, 2945 (1966)
[67] P.H. Hu, J.A. Goldstone and S.S. Ma, J. Opt. Soc. Am. B, 6, 1813 (1989)
[68] G.S. He and S.H. Liu, Physics of Nonlinear Optics, World Scientific, Singapore (1999)
[69] L.P. Schelonka and C.M. Clayton, Opt. Lett., 13, 42 (1988)
[70] Y.S. Kuo, K. Choi and J.K. McIver, Opt. Commun., 80, 233 (1991)
[71] J.J. Ottusch and D.A. Rockwell, Opt. Lett., 16, 369 (1991)
[72] J. Munch, R.F. Wuerker and M.J. LeFebvre, Appl. Opt., 28, 3099 (1989)
[73] D.C. Jones, M.S. Mangir and D.A. Rockwell, Opt. Commun., 123, 175 (1996)
[74] S.F. Grigor'ev, O.P. Zaskal'ko and V.V. Kuz'min, Sov. Phys. JETP, 65, 697 (1987)
[75] 3M Fluorinert Electronic Liquid FC-75 Catalog (1999)
[76] H. Yoshida *et al*, Appl. Opt., 36, 3739 (1997)
[77] V. Kmetik *et al*, Appl. Opt., 37, 708 (1998)
[78] H. Ming and H.J. Eichler, Opt. Lett., 16, 569 (1991)
[79] P. Suni and J. Falk, Opt. Lett., 12, 838 (1987)
[80] R.H. Lehmberg, Opt. Commun., 43, 369 (1982)
[81] Solvent Properties (CAS 67-64-1), Macromolecular Studies Group, Louisiana State University, Internet resource: http://macro.lsu.edu/howto/solvents/acetone.htm
[82] Mallinckrodt Baker, Inc., Material Data Safety Sheet No. A0446 (2001)

[83] E. Jakeman and K.D. Ridley, J. Opt. Soc. Am. A, 13, 2279 (1996)

[84] P. Klövekorn, Time dependent nonlinear optics using a phase conjugated laser, Ph.D. thesis, The University of Adelaide (1997)

[85] R.G. Harrison *et al*, Phys. Rev. Lett., 65, 167 (1990)

[86] R.G. Harrison *et al*, Opt. Commun., 163, 208 (1999)

[87] Y. Imai and M. Yoshida, Opt. Fibre Technol., 6, 42 (2000)

[88] Corning 62.5/125 CPC6 Multimode Optical Fibre Production Information (1998)

[89] G.J. Dunning and R.C. Lind, Opt. Lett., 7, 558 (1982)